Geological Survey of Finland

Bulletin 350

Interpretation of aerogeophysical anomalies of Southwestern Tanzania

by Isaac Marobhe

INTERPRETATION OF AEROGEOPHYSICAL ANOMALIES OF SOUTHWESTERN TANZANIA

by

ISAAC MAROBHE

with 32 figures, 15 tables and one appendix

This study deals with the interpretation of aeromagnetic data covering an approximate area of 50,000 km^2 lying between 8° S to 9°30′ S and 32° E to 35° E, Southwest Tanzania. The area includes different types of rocks and is also the junction of the two arms of the East African Rift System.

The magnetic anomaly maps presented as contour maps, greytone maps, and stacked profile maps show distinct zones which match the geological units of the basement rocks. Smooth anomalies characterize areas where basement rocks are covered by the Proterozoic and Neogene sediments. Areas covered with volcanics and metamorphics show rough texture. The study of magnetic lineaments has shown two prominent trends, one trending NW-SE and the second in the NE-SW. These lineaments have trends that coincide with those of structures in the rift system.

Several rock outcrops were sampled from which density, susceptibility and remanent magnetization measurements were made. The remanent magnetization was found to be high in mafic intrusives and ferruginous quartzites with Q ratios of above 10. The remanent magnetization was lower in volcanics, carbonatites, and granites with samples showing Q ratios less than 1.0. The susceptibility values were found to be low among granites, trachytes, gneisses, and carbonatites. Ultramafics, ferruginous quartzites, mafic rocks, and carbonatites rich in ore minerals were found to have high susceptibility values. The densities of rocks were also found to follow the same trend as susceptibility values.

Interpretation of digitized data using spectral analysis methods gave spectral depths ranging from 0.50 km to a maximum of 18 km. The shallow spectral depths were interpreted as the depths to the top of magnetic bodies. In some of the data windows where the basement rocks are overlain by sediments, the shallow depths were considered to correspond to the thickness of sediments. Deeper spectral depths were interpreted as due to lithological discontinuities within the crust. In the Rukwa basin the spectral depths obtained from analysis of gravity data correlated well with depths interpreted from gravity profiles across the L. Rukwa trough and also with spectral depths obtained from magnetic data.

The application of singular value decomposition method in the automatic optimization of magnetic anomalies using prism, dyke and slope models was studied. The method was then used in the interpretation of prominent anomalies observed in the study area. In addition some anomalies were interpreted using a combination of prism and two-dimensional polygonal models. The results of the quantitative interpretation of some of the anomalies, petrophysical studies and spectral analysis are discussed in relation to the geology of the area.

Key words: magnetic anomalies, gravity anomalies, lineaments, magnetic properties, density, airborne methods, tectonics, rift zones, Tanzania

Isaac Marobhe
Helsinki University of Technology
Department of Mining and Metallurgy
Laboratory of Engineering Geology and Geophysics
Vuorimiehentie 2A, Espoo 15, Finland

CONTENTS

INTRODUCTION

The use of airborne geophysical surveys in geology evolved from submarine detecting techniques using the Magnetic Anomaly Detector during the Second World War. After the war the detector was developed as a geophysical instrument by the Gulf Research & Development Company and was first used in aerosurveys in 1946 (Bates et al., 1982). Since then, the method has found wide applications both in the petroleum and mining industries as a fast way of mapping geologic structures favourable for the accumulation of ores and hydrocarbons. Airborne radiometric surveys were started in 1948 in Canada, whereas airborne electromagnetic surveys started to be used in the mineral industry in 1950 (Hood & Ward, 1969).

The use of aerogeophysical methods in Tanzania started in 1951 when the Hunting Aerosurveys Ltd., conducted aeromagnetic surveys over some parts of coastal Tanzania to study the basement structures and the extent of the sedimentary basins as part of the exploration programme for hydrocarbons in the country (Kent et al., 1971). Other geophysical surveys were conducted in 1959 and 1962 in Geita Goldfields southwest of Lake Victoria. The purpose of the survey was twofold. The first was to map the structures controlling the gold mineralization, and the second was to assess the effectiveness of airborne electromagnetic methods (AEM) in mapping subsurface structures and conductors in tropical conditions where hard rocks have undergone intensive weathering producing thick covers of conductive soils. According to Makowiecki et al. (1971), three systems, namely Afmag, Rotary field, and Rio Mullard were tested. Magnetic methods were also included in each of the surveys to supplement the AEM systems in mapping geologic structures.

The third aerogeophysical survey was conducted in Musoma Goldfields, east of Lake Victoria. The area was surveyed in 1965 with the purpose of mapping conductors and structures controlling the mineralization of gold. The survey conducted by Hunting Geology & Geophysics of United Kingdom and financed by the United Nations Development Programme, used magnetics and Rotary field system as surveying methods.

It was not until 1976, that the government of Tanzania made a contract with Geosurvey International to carry out regional aerogeophysical surveys covering the whole country. The survey started in 1976 and completed in 1980, included magnetics, radiometrics and EM-VLF. Batterham et al. (1983) have given a detailed account of the survey in which more than one million kilometers were flown at a spacing of 1.0 km and a flight altitude of 120 m above the ground. Detailed surveys were also conducted in some areas with a line spacing of 250 m and at an altitude of 90 m above the ground. The direction of survey lines was E-W.

According to data published by Hunting Geology & Geophysics (1983) only some parts of Tanzania are geologically mapped on the scale of 1:125,000 and 1:250,000. More human and financial resources are required to have the whole country geologically mapped and, where possible, to remap areas which were surveyed several decades ago.

Considering the costs of geological mapping, the regional geophysical survey has provided data from which the geological structures of the unmapped areas and areas covered with thick vege-
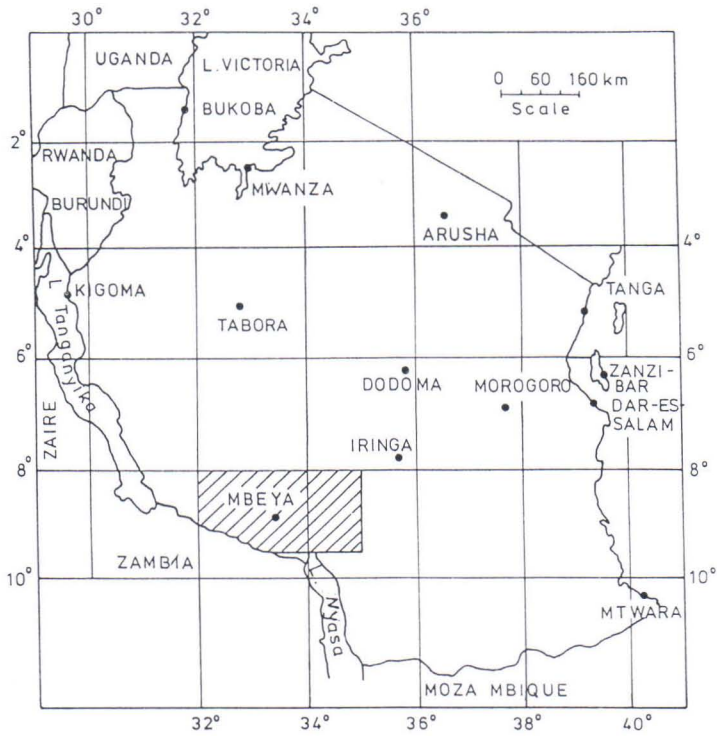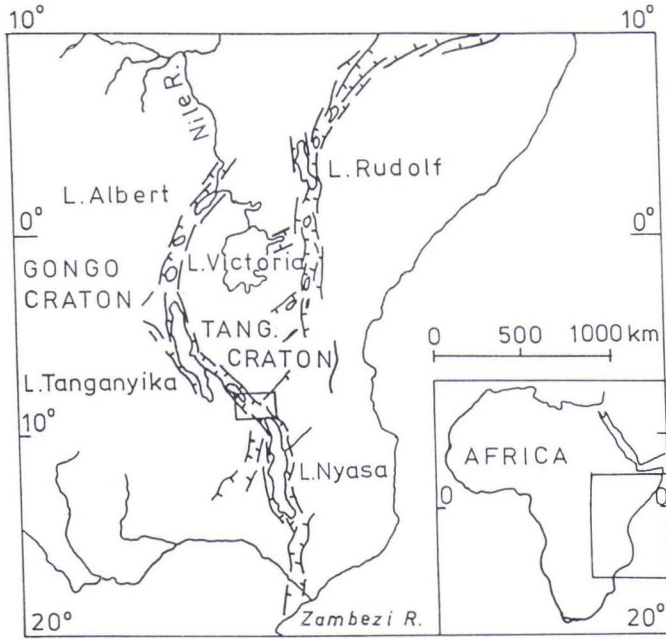
Fig. 1. Maps of East Africa and Tanzania showing the East African Rift System
and the location of the study area.

tation, permanent swamps, and basement structures overlain by sediments may be mapped at reduced costs.

The area under study has been geologically mapped and published in a series of maps on a scale of 1:125,000, each map covering an area of one quarter degree. Only one quarter degree of area lying between 8° S to 8°30′ S and 34° E to 34°30′ E has not been mapped.

Location and accessibility

The area under study lies between 32°E to 35°E and 8°S to 9°30′ S southwest of Tanzania and covers an approximate area of 50000 km². The location of the study area is given in Figure 1 where the East African Rift System is shown. The study area is centered around the administrative region of Mbeya and includes some parts of the contiguous region of Iringa. Most parts of the study area are accessible by road. However some areas in the Kipengere range (Figure A1) have rugged terrain and are unaccessible in the rainy season. The northern part of Buhoro trough is covered with permanent swamps which also limit accessibility. Other areas of limited accessibility due to dense vegetation are the volcanic mountains of Poroto and Rungwe. The whole area is generally of high altitude, with Mt. Rungwe reaching a height of 2960 m above sea level and the Kipengere Range a maximum height of 2900 m. The Buhoro trough has an average altitude of 1640 m, whereas Lake Rukwa is at an altitude of 1670 m above sea level.

Geophysical data

The regional airborne geophysical data surveyed by Geosurvey International between 1976 and 1980 is available at the Mineral Resources Division of the Ministry of Energy and Minerals. The data available is in the form of digital data stored on magnetic tapes, magnetic contour maps, total count contour maps, stacked profiles of K, U and Th counts, radiometric interpretation maps, and also stacked profiles of VLF-EM data. Although the digital data is available on tapes, efforts to acquire the data tapes failed and one tape made available by the Ministry of Energy and Minerals could not be read due to insufficient documentation. The documentation is required to facilitate retrieval of the data from the tapes. The data used in this study were kindly provided by the Commissioner for Geology of the Ministry of Energy and Minerals, in the form of maps and is part of the regional airborne geophysical data surveyed at a line spacing of 1 km and an altitude of 120 m above the ground.

The maps provided include the aeromagnetic contour maps, radiometric total intensity contour maps, stacked profile maps of Uranium, Thorium and Potassium counts, radiometric interpretation maps, and VLF-EM stacked profiles. The VLF-EM stacked profiles consist of the quadrature component and the total field.

Both aeromagnetic and radiometric maps were found to be of good quality but the VLF-EM data was found to be noisy in the sense that the stacked profiles appear as wiggles, with no relation to any geological structures. Due to this, the VLF-EM maps were not used in this study. The poor quality of VLF-EM data may be attributed to two reasons, one being the location of the transmitters used. Moscow and Cutler (Maine) are very far from the study area and therefore the signal reaching the receiver was weak. The second factor is the presence of thick conductive

soils which have the effect of attenuating the signal, making it much weaker and difficult to detect. The radiometric data was interpreted by the contractor using qualitative and statistical methods.

The aeromagnetic contour maps were digitized at the intersection of flight lines with contour lines and then interpolated at a square grid of 1 km by 1 km. The gridded data was then used to prepare greytone maps, stereographic projection maps, and also in spectral analysis to determine average depths to the top and bottom of magnetic bodies causing the anomalies. A study of major magnetic lineaments and provinces in re-

lation to geology of the area as well as the detailed interpretation of individual anomalies was carried out using the data. The use of singular value decomposition in optimization of magnetic anomalies was also investigated during the course of this study.

In addition gravity data covering the Lake Rukwa basin was provided by the Tanzania Petroleum Development Corporation. The details of the gravity survey with its interpretation has been covered by Peirce and Lipkov (1988). The gravity data was used in this study to constrain the depths obtained by spectral analysis of the aeromagnetic data.

Previous geophysical studies

Not much geophysical work has been carried out in the area. The geophysical studies so far reported in the area include the gravity surveys of the area around Mbeya (Aoki, 1969), the Rukwa trough (Peirce & Lipkov, 1988), and regional gravity survey over Rungwe volcanic provinces

(Ebinger et al., 1988). The gravity surveys show a negative Bouguer anomaly trending NW even in areas overlain by thick volcanics. The study of earthquake distribution for the Tanzanian region was presented by Båth (1975).

A Review of geology and tectonics

The area under study is of great geologic interest as it houses many rock types, including metamorphics exhibiting different grades of metamorphism, intrusives of various types, volcanics and sediments. Economically, the area has gold mineralization in the Chunya-Usangu block, the coalfields, carbonatites, and possibility of presence of hydrocarbons in the Rukwa trough. Preliminary studies on hot springs conducted by the Ministry of Water also suggest the presence of geothermal energy resources within the study area. The geology of the area is briefly described below.

The study area include parts of both the western and the eastern rifts of the East African Rift System. The Buhoro trough is part of the east-

ern rift, whereas the Rukwa-Songwe and Msangano troughs belong to the western branch. The crystalline basement in this area is partly covered by sediments of different ages ranging from Proterozoic to recent. The basement rocks are also overlain by Neogene volcanics whose eruption has been associated with the formation of the rift system in East Africa (Harkin, 1960).

The distribution of various rocks in the area is presented in a map given as Figure A1 compiled from published geological maps. The Precambrian basement rocks belong to four mobile belts namely Ubendian, Usagaran, Karagwe-Ankolean, and Bukoban. The last two are locally known as Ukingan and Buanji respectively. The young formations have been classified into

Table 1. Stratigraphy.

NEOGENE	young extrusives lacustrine deposits older extrusives
Creataceous	red sandstones, siltstones, grits
Karroo	green mudstone with magnesian limestones & calcareous sandstones red mudstones & siltstones with intercalated feldspathic sandstones coal measures basal conglomerates.
Buanji	quartzites, red shales, slates gabbro intrusives.
Ukingan	phyllites, schists granitic rocks
Usagaran	gneisses, marbles amphibolites
Ubendian	gneisses, schists high grade metamorphics meta-anorthosites granites mafic intrusives

Karroo, Cretaceous and Neogene. The general stratigraphy is given in Table 1 below.

The Ubendian mobile belt

The oldest rocks in this area belong to the Ubendian mobile belt dated 2200—1700 Ma. The Ubendian rocks occupy a large portion of the study area. For the purpose of description, the Ubendian may be subdivided into the following four blocks: the Ufipa block in the west, the Mbozi block in the south, the Chunya block in the northwest, and the Ubena in the east.

The Ufipa block

The Ufipa block in the west, consists of regionally metamorphosed rocks of which migmatitic biotite gneiss is the dominant rock type. Other rock types are charnockites, augen gneiss and ferruginous quartzites. The later occur as small outcrops along river channels due to the superficial cover of eluvial soils, which extend over wide areas obscuring the basement rocks and structures (Leonen et al., 1964, 1965). In the south the only outcrop is the NW-SE trending foliated granite. Within the block the rocks strike between NNW-SSE to WNW-ESE.

The Ufipa block is fault bounded against the Mbozi block, where the boundary is marked by a shear zone consisting of muscovite biotite schists. The schists separate the high grade metamorphic rocks of the Ufipa block from the medium grade metamorphics of the Mbozi block. In the north the two blocks are separated by the Msangano trough, which occurs as a graben.

The Mbozi block

The Mbozi block lies between the Msangano trough in the south and west, the Rukwa trough in the north, and the Songwe trough in the northeast and east. The geology of the area has been studied by Grantham et al. (1958), Kernerly et al. (1963), Brown (1962), McFarlane and Brock (1966), and Brock (1968). The block occurs as a horst, fault bounded against Msangano, Rukwa and Songwe troughs.

The Mbozi block consists of banded gneiss, granulites, quartzites and amphibolites, with the biotite, garnet and muscovite bearing banded gneiss being the predominant rock type. The granulites found in the southeastern part of the block are strongly foliated and amphibolites are found to have been developed within the granulites due to retrogressive metamorphism (McFarlane & Brock, 1966). Due to the ability of quartzites to resist forces of weathering, they occur as thick bands of outcropping ridges and hills. Three varieties of quarzites have been distinguished, namely ferruginous quartzites, muscovite quarzites, and garnet quarzites (McFarlane, 1963). The quartzites have been folded with the axis of folding trending in the NNE-SSW.

Unlike the Ufipa block, the Mbozi block is characterized by intrusives of mafic to alkaline compositions and includes carbonatites, syenites,

gabbros, pyroxenites, dolerite dykes and pegmatites. The Mbozi syenite-gabbro complex is the largest intrusive whose emplacement was controlled by NW-SE faults (Brown, 1962, Brock, 1968). The carbonatite intrusives southwest of Mbeya include the Panda Hill, Senjeri, Musensi and Mbalizi intrusives, which occur as plugs and dykes.

The Chunya-Usangu block

The Chunya-Usangu block is a horst between Rukwa and Buhoro troughs. The geology of the area was studied by Kernerly et al. (1962), McFarlane et al. (1963), and McFarlane and McDonald (1964). The predominant rock types are feldspathic granular gneisses and migmatitic granite gneisses. The migmatitic gneisses are highly metasomatized and granitized whereas the granular gneisses are slightly migmatized. Other rock types found in the area include metagabbros, metaperidotites, and ferruginous quartzites. The later form upstanding hills and ridges, possibly due to their resistance against weathering.

A large part of the area is covered by intrusive rocks which include granitoids, mafics and ultramafics. The granites which cover a large part of the area have been classified into synorogenic, late orogenic and postorogenic types (McFarlane & McDonald, 1964). The granodiorites and diorites are of late orogenic and intrude granitic gneisses.

The faults bounding the block are the major structures. However, within the block E-W shear zones have been observed of which the Mkondo Shear Zone is the most extensive and affects both the ultramafic and mafic rocks. Other structures are the NE-SW veins which have been found to control the gold mineralization.

The Ubena block

This block combines all Ubendian rocks found south of Buhoro trough and east of Nyasa escarpment. The Ubendian rocks in this block consist of meta-anorthosite complex, metasediments, and granitoids. The metasediments occur as schists, gneisses, quartzites, marbles, and migmatites, whereas the meta-anorthosite complex consist of metagabbros, meta-anorthositic gabbros, metanorites, metapyroxenite, and metadunites (Harpum & Brown, 1958, Harpum & Harris, 1958). The granitoids known as Ubena granites (Harpum & Brown, 1958) consist of adamellitic granites and granodiorites which are classified as synorogenic granites. The metasediments occur in the northeast extending south and eastwards, with a structural trend between east and east of northeast. The meta-anorthositic rocks occur in two areas separated by young metasediments and sediments. The western outcrops form the Upangwa Complex north of L. Nyasa, whereas the second occurs south of Buhoro trough in Ubena.

The Usagaran mobile belt

The rocks occurring in the east and southeastern part of the area belong to the Mozambique Belt, which is locally known as Usagaran in Tanzania. The Usagaran basement rocks include gneisses, quartzites, marbles and schists, all of which are of sedimentary origin. The rocks show a general strike in the NE-SW direction, but toward the north, E-W trends have been observed (Kursten, 1964). The gneisses in Njombe area are found in three belts striking N-S, NE-SW, and NW-SE. The contacts between these belts are obscured by soils (Fesefeldt, 1964). However, the contact between the N-S trending belt and the NE-SW trending belt is marked by sheared quartzites and dolerite dykes striking between 110° and 130°.

Other rocks are the granitic rocks of Ubena which include migmatitic granites and hybrid granites known as adamellites. The adamellites are intruded by young fine grained biotite microgranites. There is some confusion as to which belt the granitoids belong. Fesefeldt (1964) has assigned the rocks to Usagaran while Brinckman (1964) classified them as Ubendian. The

boundary between the Ubendian and Usagaran rocks has not been observed in the field. If it exists, it must either have been obscured by a superficial cover, or it is gradual.

Overlying the Usagaran in the northeast corner are the Ndembera volcanic series. The volcanics are mostly acidic and consist of andesites and rhyolites with a total thickness estimated as 2000 m (Kursten, 1964). The volcanics were formed in the E-W trending troughs created during folding and metamorphism of the Usagaran.

The Ukingan Series

The Ukingan is a group of low grade metamorphic rocks found northwest of Mbeya town and in the Kipengere area between Lake Nyasa and Buhoro trough. The Ukingan is part of the rocks belonging to the Karagwe-Ankolean Mobile Belt, of which a larger part is found in NW Tanzania extending into Burundi and Rwanda. These rocks lie unconformably on the Ubendian crystalline rocks. Harpum and Harris (1958) divided the Ukingan into three formations, namely the Matwaki Quartzites, the Ilolo Formation, and the Kipengere Formation. The Matwaki Formation consists of quartzite with intercalations of phyllitic schists, and it has been estimated to have a thickness of 220 m. Below the quartzites lie the Kipengere Formation, consisting of argillaceous assemblages with quartzite bands. The Ilolo Formation overlies the Matwaki and consists of rocks similar to those of Kipengere Formation. Due to intense folding and thrusting, the thickness of the Ilolo and Kipengere formations have not been estimated. The rocks of Mbeya Range consist of phyllites and schists. Both show northwesterly structural trend. In general the Ukingan has a structural trend parallel to that of the Ubendian. It has itself undergone intense movements which have resulted in thrusting and shearing, producing mylonites and cataclasites in some areas. These movements also affected the older rocks. The post-ukingan activities included the emplacement of granites in Chimala and in the Mt. Livingstone area, accompanied by intense metasomatic activities forming quartz and hematite, or quartz and specularite veins.

The Buanji series

The sedimentary rocks of Southwest Tanzania have been classified into three groups by Pentel'kov (1981), with respect to the formation of the rifts. The oldest group is the platform sediments deposited before the formation of rifts. The riftogenic platform sediments were deposited during the time of rifting, whereas the riftogenic sediments are those which were deposited within already formed rift structures.

The Buanji sedimentary series belong to a system of continental platform sediments and volcanics deposited during the late Precambrian in Tanzania, where they are known as the Bukoban sediments. In the study area these sediments outcrop at Kwimba in Chunya block and in Uwanji, where the name 'Buanji' has been given.

The Buanji series consist of quartzites, red shales, slates, sandstones, greywacke, and it overlies both the Ukingan and the Ubendian unconformably. Harpum and Brown (1958) have divided the Buanji into upper, middle, and lower divisions with estimated thicknesses of 370 m (1200 ft), 250 m (800 ft), and 460 m (1500 ft) respectively.

The Buanji rocks are intensely folded and thrusted parallel to the Ukingan tectonic movement. They have been intruded by gabbros and dolerite dykes which were emplaced in two phases (Harpum & Harris, 1958). The earlier phase of intrusives consists of leucogabbro, and the second phase of olivine gabbros and noritic differentiates. The emplacement of gabbros was also accompanied by small intrusives, mainly dolerite dykes. The Nkenza group of gabbros is also associated with magnetite seams found in the Mt Livingstone area.

Rift tectonics and young formations

Southwest Tanzania is characterized by fault zones which are associated with rifting. These rift

faults have been described by McConell (1972) to be genetically associated with Precambrian crustal lineaments developed in the mobile belts. The main faults bordering the troughs have been classified as right lateral faults (Tiercelin et al., 1987) which are found to affect rocks of Precambrian age to young deposits of Pleistocene. Most of the faults trend parallel to the NW-SE structural trend of the Ubendian rocks, but some are found to trend NE-SW. Recent chronological studies of Rungwe volcanics (Tiercelin et al., 1987, Ebinger et al., 1988) have helped to understand the age of movement along the main faults and specifically those which have displaced the volcanics. The movements on rift faults began in Pre-Karroo forming inland basins in which Karroo formations were deposited in the Rukwa, Songwe, and Nyasa troughs. These faults were reactivated again in the Mesozoic and Cenozoic times leading to the deposition of continental sediments. The Post-Karroo faulting which began in the Late Jurassic to Early Cretaceous led to the deposition of red sandstones found outcropping in the Songwe trough (Figure A1). The movements along Rukwa, Galula, Songwe and Nyasa faults have been described as dextral strike-slip faulting accompanied by normal movement (Tiercelin et al., 1987).

The Songwe trough southwest of Mbeya is marked by a series of step faults evidencing the movement which began in the Pre-Karroo and reactivated during the Late Jurassic-Early Cretaceous and also in the Pleistocene.

The Msangano trough south of Rukwa is filled with lake sediments which were deposited during Pleistocene. In the west the trough is bounded by the Ufipa fault which is characterized by a dextral strike-slip movement. The faulting along the Ufipa shear zone is estimated to have occurred in the Mid-Pleistocene (Peirce & Lipkov 1988). Therefore there is a clear difference in age between the Rukwa and Ufipa faults forming the borders of the Rukwa trough.

The Buhoro trough, trending NE-SW, is marked by N-S trending faults along the Usangu escarpment (Figure A1). Based on dating of volcanics found overlying the Precambrian rocks of the Usangu escarpment, the movement along these faults has been estimated to have developed in Early Pliocene (Ebinger, et al., 1988).

The rift faulting formed troughs in which continental sediments have been deposited. These young formations consist of continental sediments and volcanics which were deposited intermittently starting from Karroo to quite recent. The type of sediments is described below.

The Karroo Formations

The Karroo Formations form the platform riftogenic sediments which were deposited in continental subsidizing basins in most parts of South and East Africa. The major basins of the Karroo deposition are the NE-SW trending basins, while the NW-SE basins observed in the study area are side trends of the main basins. The Karroo rocks unconformably overly the Ubendian crystalline basement. They occur in downfaulted blocks along the northwesterly trending faults marking the southwestern boundaries of Rukwa and Nyasa troughs.

The sediments strike parallel to fault trends and dip towards northeast at angles of 20° to 35°. In the study area Karroo outcrops are found in three places shown on the geological map. According to McKinaly (1965), the rocks were deposited starting from Uppermost Carboniferous to Lower Jurassic, and consist of basal conglomerates, sandstones, sandy mudstone, shales, coal beds, and varved siltstones.

Harkin (1955) has given a detailed account of the Karroo Formations including estimates of formation thicknesses. In Songwe-Kiwira near L. Nyasa the thickness is about 800 m while in the Galula coalfield overlooking the Rukwa trough, the thickness is estimated at 1600 m. Some of the rift faults in the area cuts the Karroo sediments whereas some formations are found overlying the unaffected basement.

Cretaceous sediments

The Cretaceous sediments consist of current bedded red sandstones with clayey and silty shale intercalations overlying both the Karroo and basement unconformably and dipping towards northeast at small angles (Spence, 1954, Harkin, 1955). The Cretaceous sediments are found south of Tukuyu, along the Kiwira and Songwe river valleys and near the Galula Coalfield where the sediments reach a thickness of 370 m (1200 ft).

Neogene volcanics

The volcanics in the area of study cover an area of about 307 km^2 and were erupted at the junction of the Nyasa-Rukwa trough and the Buhoro trough. Harkin (1960) has divided the volcanics into older extrusives erupted during the Pleistocene and having been subjected to erosion, and the young extrusives appearing uneroded. The last eruption occurred in the 19th century (Harkin, 1960). The rock types include basalts, trachytes, phonolites and their intermediaries. The older volcanics consist of basalts, tuffs and trachytes whereas the young extrusives consist of a series of basalts with phonolites. The phonolites are found mainly in the north, extending into the Buhoro trough. The volcanics overlie both the basement and sedimentary formations discussed above. The young volcanics overlie the lacustrine sediments. The thickness of the volcanics has not been estimated. The eruption of volcanics is believed to have been controlled by the structures within the basement which are presently masked by the volcanic cover.

Lake sediments

The lacustrine sediments known here as lake beds are well developed in the Rukwa, Msangano and Nyasa troughs whereas, in the Buhoro trough scattered outcrops of lake beds have been mapped. Most of them are covered by colluvial soils. These sediments reveal the extent of ancient lakes which once occupied the rift basins. In the Songwe trough the lake beds consist of finely laminated quartzites, feldspar sands, and white loamy material. The sediments in the Buhoro trough consist of conglomerates derived from the volcanics and sandstones. In the Nyasa trough southeast of Tukuyu the sediments are overlain by the volcanics. The thickness of the sediments has not been estimated. The gravity study of the Rukwa trough gives a maximum depth of 7 km (Peirce & Lipkov, 1988), but this includes also the older sediments.

Other sediments covering the hard rocks are the residual soils, alluvial, and river valley clays which cover large parts of the area, thus obscuring the basement rocks.

MAGNETIC PROVINCES AND LINEAMENTS

Magnetic provinces

The geological map of the study area presented in Figure A1 shows that most of the basement rocks are overlain by sediments, residual soils, and swamps. In some places, particularly in the west and northeast, the outcrops of the basement rocks are found only along river channels. These superficial covers together with swamps obscure the geological structures of the basement and therefore can not be mapped by conventional surface methods.

The total field aeromagnetic map of the study area presented as Figure A2, reflects the region-

al structures which show two trends, one trending NW-SE and the second in the NE-SW. The NE-SW trend is more pronounced in the north and northeastern part.

The magnetic greytone image maps presented in Figure 2 and 3, and the stacked profile map of Figure 4, were prepared from data digitized from original contour maps and gridded using a square grid of 1 km. The greytone map shown in Figure 2 was prepared using all the data points whereas that given in Figure 3 was prepared by removing the average magnetic field. Attempts to enlarge the greytone image maps resulted in distortion as the pixels became large as seen in Figure A3. The greytone and the stacked profile maps helped to distinguish zones or provinces characterized by high intensity anomalies from low intensity anomalies. The lightest tone on the

Fig. 2. The greytone magnetic map prepared from digitized data. The light tone indicates low intensity magnetic anomalies and the dark tone corresponds to high intensity magnetic field.

Fig. 3. The greytone image map prepared from aeromagnetic data by removing data points with mean value of the total field. The points removed appear as black dots.
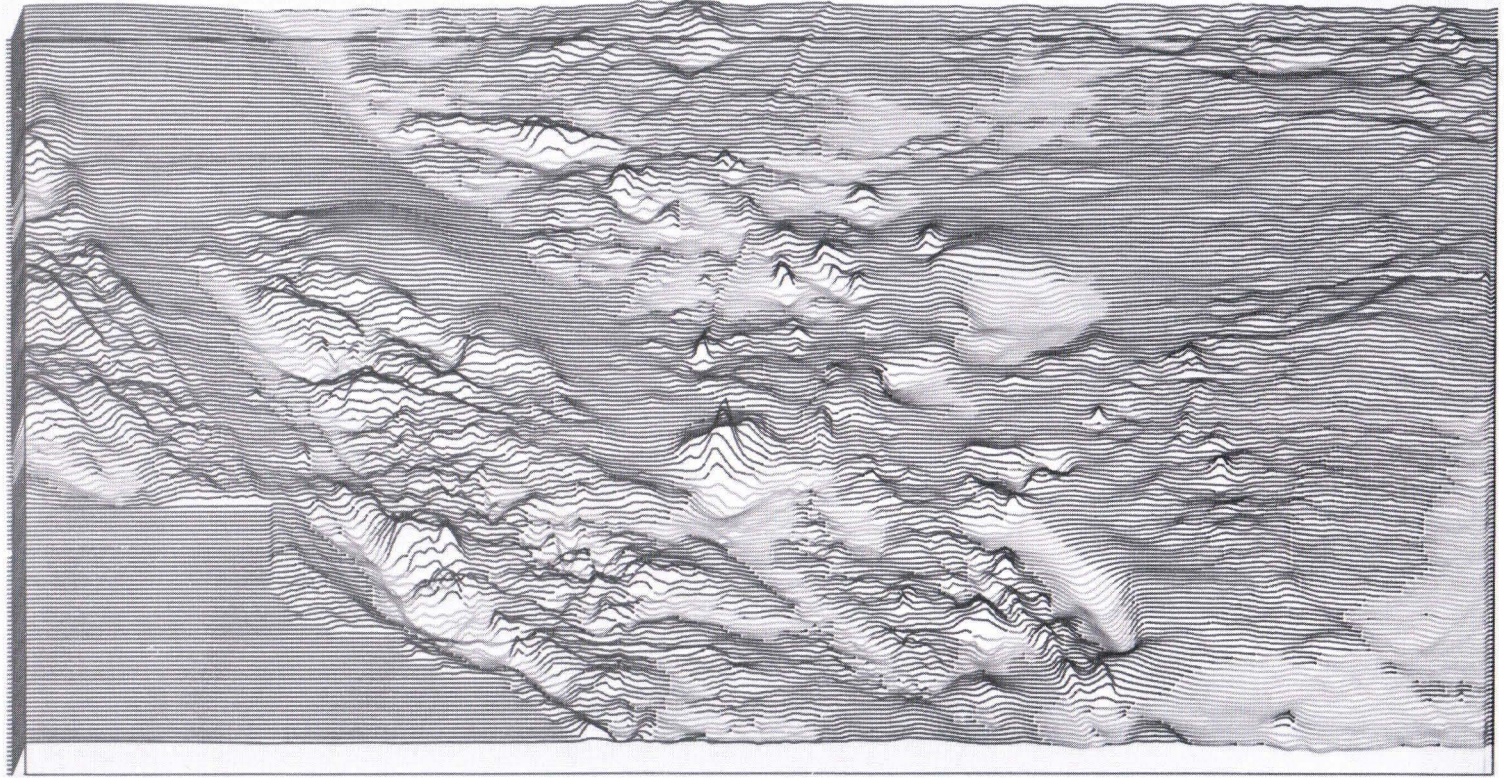
Fig. 4. The aeromagnetic map presented in form of stacked profiles. The smooth profiles depict areas with granitic rocks or where basement rocks are covered with sediments.
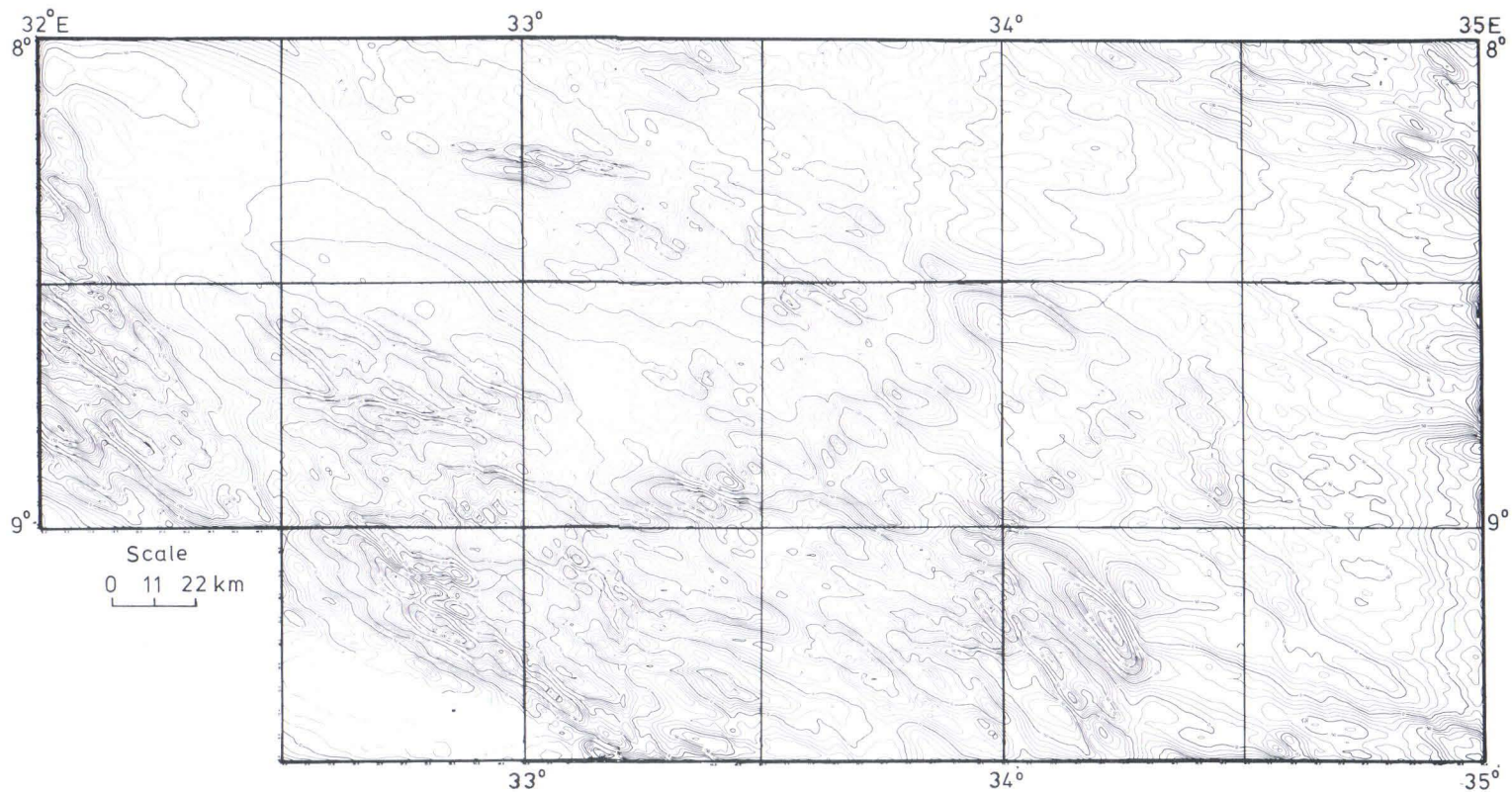
Fig. 5. Map of upward continued aeromagnetic data. The height of continuation is 2.5 km above the plane of observation. The NW-SE lineaments are enhanced whereas most of the NE-SW lineaments have been filtered out. The contour interval is 10 nT with the zero contour corresponding to 33,800 nT.

image map represents areas with low intensity anomalies. Such anomalies are found mainly in the southeast, extending into the central part of the Buhoro trough and, in the northwest extend into the Chunya-Usangu block. The intermediate tone was observed over the Rukwa-Msangano troughs, the northern part of Buhoro trough, the Ubena granitoids, and areas covered with volcanics. The dark tone represents areas with high relief positive anomalies which are found in the Ufipa and Mbozi blocks in the southwest and in some parts of the Usangu escarpment. The Rungwe volcanics southeast of the Rukwa trough are characterized by low to high relief magnetic anomalies. The stacked profile map of Figure 4 shows high amplitude anomalies in the Ufipa and Mbozi blocks whereas in areas with sedimentary cover the profiles appear as straight lines without any anomaly. Individual anomalies of high amplitudes are clearly seen on the stacked profile map of Figure 4.

The greytone image map and stacked profile maps described above contain both high and low frequency anomalies. The high frequency anomalies are caused by shallow bodies of limited lateral extent whereas the deep seated bodies of large lateral extent are the sources of the low frequency magnetic anomalies. The separation of the high frequency component helps to enhance the low frequency anomalies due to deeper sources masked by the high frequency anomalies.

The low frequency magnetic anomalies were enhanced by upward continuation through Fourier transform. The Fourier transform was calculated using subroutine FFT3D of IMSL (1984). The Fourier coefficients obtained were multiplied by a transfer function (Nagy, 1988) for the upward continuation given by

$$T (u, v) = \exp (-h\sqrt{(u^2 + v^2)}) \quad (1)$$

where u and v are angular frequencies in the N-S and E-W directions, and h is the height of continuation given as a fraction of the data grid.

The product of the Fourier coefficients and the transfer function was then inversely transformed

to obtain the upward continued data at height h. The height of 2.5 km above the observation plane was used in arriving at the regional magnetic map presented in Figure 5. The NW-SE and easterly trending anomalies, especially the lineaments, are further enhanced while the NE-SW lineaments especially in the southeast were found to be attenuated. However, in the Buhoro trough some circular anomalies were found to define a few NE-SW trending lineaments.

The removal of high frequency anomalies in the Rungwe volcanic area has revealed the NW-SE lineaments which are interpreted as a continuation of faults connecting the Nyasa trough in the southeast of the study area to Rukwa and Songwe troughs in the northwest.

The greytone magnetic image map, the original contour maps, and the stacked profile map were used to subdivide the magnetic anomaly map into provinces depending on the magnetic pattern, relief, and anomaly shapes. For simplicity, the aeromagnetic anomaly map was divided into eight provinces (Figure 6) as listed below :

1. The Ufipa province
2. The Rukwa-Msangano province
3. The Mbozi province
4. The Buhoro province
5. The Chunya-Usangu province
6. The Ubena province
7. The Kipengere province
8. The Rungwe province

The Ufipa province

The Ufipa magnetic province in the west is characterized by high relief magnetic anomalies with NW-SE magnetic texture. This pattern of the magnetic anomalies continues further north into the Rukwa trough, and in the east it terminates against the magnetic lineament of the Ufipa fault. The negative anomaly in the south is caused by the sheared granitic intrusion of Miamba Hills. The high positive amplitude magnetic anomalies with amplitudes in the order of 950 nT are found in areas where isolated outcrops of fer-
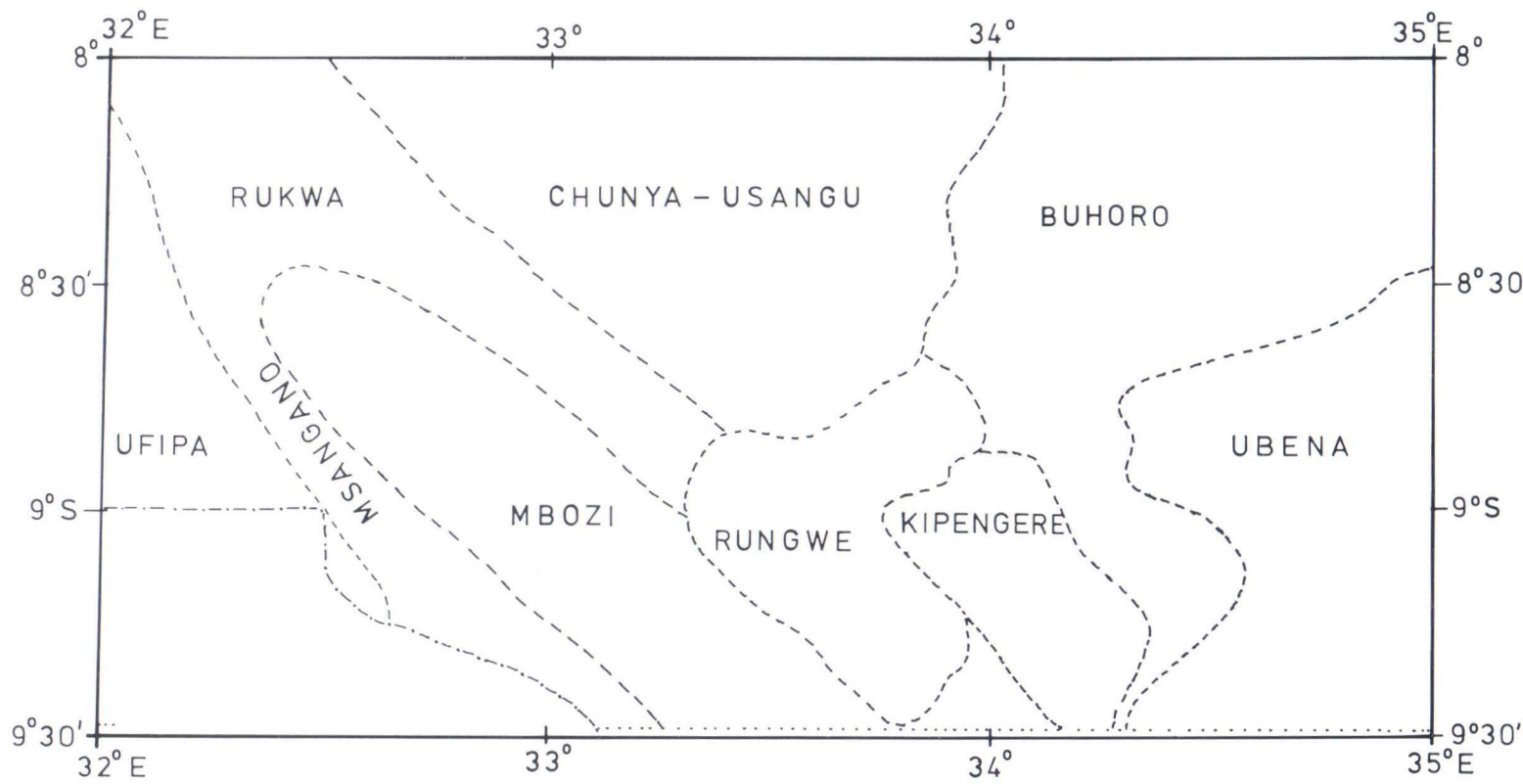
Fig. 6. Map showing distribution of magnetic provinces.

ruginous quartzites interbanded with migmatitic gneisses have been mapped. Judging from the continuity of the magnetic anomalies the quartzites seem to extend over a large area. The magnetic relief also decreases towards the south due to the changing of rocks from gneisses into schists of the Ufipa shear zone and sheared granites of Miamba Hills.

The Rukwa-Msangano province

This province occurring within the troughs of the western limb of the East African Rift System is characterized by magnetic anomalies of an intermediate relief and smooth anomalies suggesting deep seated sources. The relief of the anomalies of the Rukwa trough is generally higher than the adjacent province of Chunya, suggesting that the basement rocks underlying the lake sediments consist of the high grade metamorphic rocks of the Ufipa and Mbozi blocks. The Rukwa province continues southwards and grades into a low relief magnetic zone in the northeast of Mbeya. This low relief magnetic zone is caused by the schists of the Mbeya range.

The Msangano, which is a graben structure between the Ufipa fault in the west and Kalungu faults in the east, is characterized by linear magnetic anomalies parallel to both the Ufipa and Kalungu faults. Within the Msangano trough, circular magnetic anomalies together with the high amplitude anomaly corresponding to the Mbozi gabbro syenite complex, form a belt of anomalies trending in NW-SE. Some of these anomalies are caused by outcropping intrusive bodies but further north in the Msangano trough, the circular anomalies are due to intrusive rocks overlain by lake sediments. The anomalies reveal the areal extent of the magmatic activities which led to the formation of the Mbozi gabbro syenite complex and other bodies outcropping in the south.

The prominent anomaly in the Msangano province is that due to the Mbozi gabbro syenite complex with amplitudes ranging from 500 nT to 1960 nT. The body trends in the NW-SE and lies within the graben structure bounded by the Kalungu fault in the east and Ufipa fault zone in the west. The individual magnetic anomalies within the trough trend in different directions, but the most prominent is the E-W trend.

The Mbozi province

The Mbozi magnetic province lies between the Msangano in the west and Songwe trough in the east while in the north it is marked by the Galula lineament, which separates it from the Rukwa trough. The province shows a variety of anomaly trends including the NW-SE trend in the northern part and the NE-SW trend in the south. Some anomalies trend in E-W while a few trend N-S. The magnetic relief is higher in the north where dolerite dyke swarms have been mapped. The circular positive anomalies southwest of Songwe trough are related to the carbonatite intrusives of Musensi and Panda Hill. The positive circular anomaly west of Musensi may also be caused by a carbonatite intrusion as it lies in the zone of carbonatization. The strong negative anomalies in the south located at 9°08′ S and 33°10′ E and crossed by NE-SW lineaments occur in an area covered with eluvial and alluvial soils and as such no surface geological structure is found to match the anomalies. The north trending linear anomaly marked id in the south is due to pigeonite dolerite dyke mapped south of Itumba whereas the E-W striking anomaly has no correlation with any mapped geologic structure in the area. The anomalies strike in the direction of the flight lines and cover several flight lines which makes them to be true anomalies caused by geologic structures.

The Rungwe province

The Rungwe province covers an area south of the Buhoro trough and extends southeastwards to northeast of Lake Nyasa. The province is characterized by high frequency magnetic anoma-

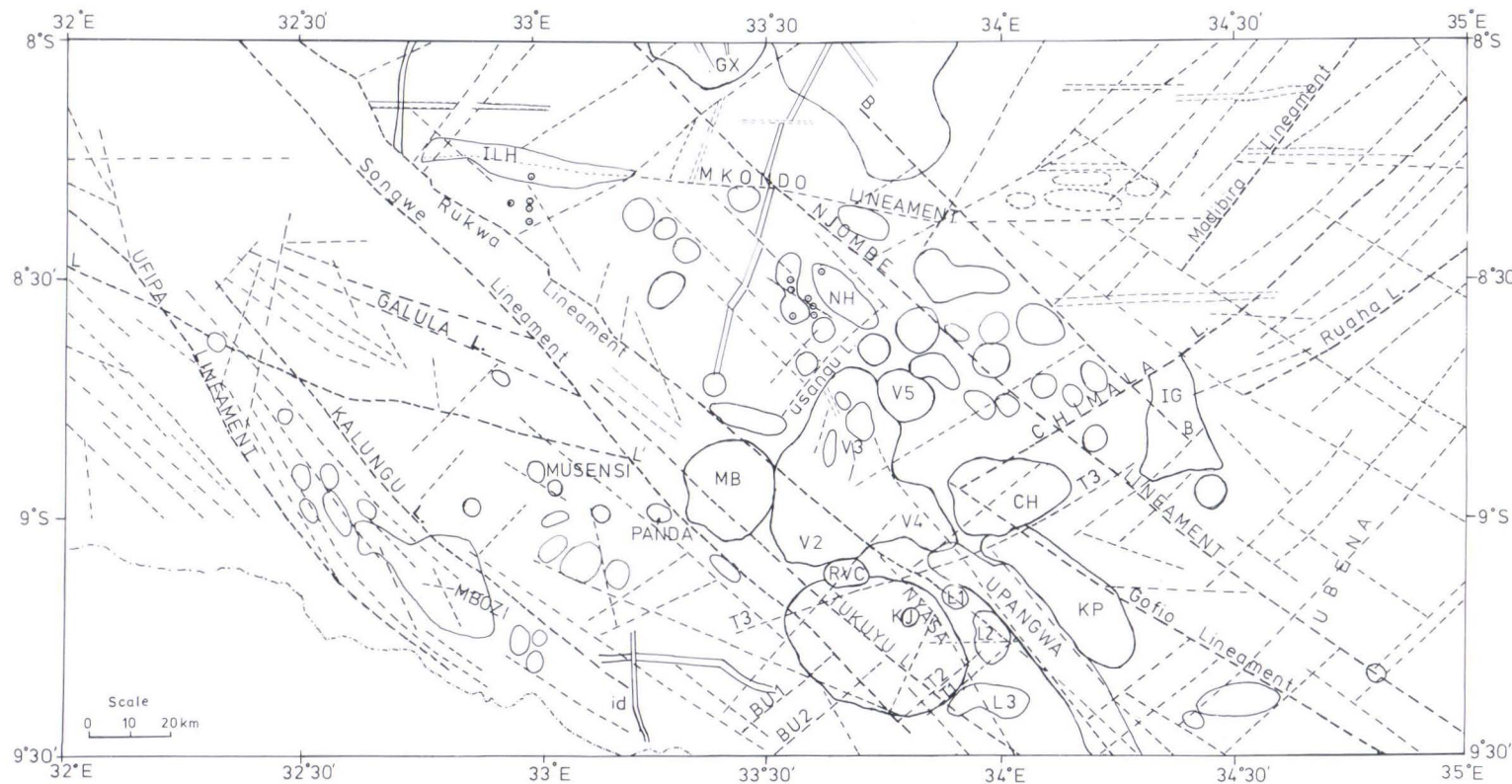Fig. 7. Interpretation map showing magnetic lineaments, provinces, and prominent anomalies due to intrusive rocks. The lineaments were interpreted from original contour maps, the stereographic projection map, and stacked profiles. KP = Kipengere Anomaly, MB = Mbeya Anomaly, IG = Igawa Anomaly, CH = Chimala Anomaly, NH = Nsamya Hills Anomaly, ILH = Ilunga Hills Anomaly, V1 to V5 = Rungwe Anomalies

lies thought to be due to volcanics in the area. The province may be subdivided into zones marked V1 to V5, Figure 7, showing different anomaly patterns. The zones marked V1 and V2 are characterized by low amplitude anomalies with a few isolated high amplitude anomalies associated with volcanic centers, of which Kiejo and Rungwe marked KJ and RVC respectively on the map of Figure 7, are the largest. The zone is also characterized by small dipole-like anomalies. Zones V2 and V4 contain anomalies of circular shape which mark the extent of volcanic rocks north of Rungwe volcanic center.

The anomalies marked V3 and V4 occur in areas with outcropping basaltic lavas with V3 showing a N-S trend and positive amplitude of moderate relief. Zone V4 has similar characteristics with V1 and V2 in the south. The anomaly patterns marked V5 occur in areas with phonolitic volcanics in the southern end of the Buhoro trough. These negative amplitude anomalies extend further north in the Buhoro trough where the exposed rocks are the lake beds and colluvial sediments suggesting the presence of volcanics overlain by the lake sediments. However, the alignment of the Kipengere, Chimala and Nsamya Hills anomalies with this negative anomaly, may suggest that the source of the anomaly is within the basement rocks and may be mafic rocks which intruded during the Buanji or metamorphosed ultramafics similar to that of Nsamya Hills in the Usangu escarpment.

The large anomaly marked MB (Figure A2) and referred to here as Mbeya Anomaly is a high amplitude anomaly occurring in an area covered with basalts and centered over the town of Mbeya. The anomaly has an amplitude of about 3360 nT, the largest amplitude in the study area, and is possibly due to a deep seated volcanic plug along which the Mbeya basalts were extruded or is due to intrusives related to carbonatite activities and enriched in magnetic minerals. The quantitative interpretation of this anomaly is discussed later. The anomaly itself trends NE-SW but is found to be superimposed on NW-SE trending

lineament which is clearly evident in the upward continued map (Figure 5).

The Buhoro province

The Buhoro magnetic province lies in the central part of the study area and is characterized by two sets of anomaly patterns which include circular anomalies in the south and NE-SW and E-W trending anomalies in the north. The southern part is also crosscut by NW-SE trending lineaments which continue into both sides of the crystalline basement. The high amplitude circular anomalies observed in the southern part of the Buhoro trough may be caused by volcanics or mafic intrusive rocks similar to those observed in the Usangu escarpment.

The E-W trending magnetic anomalies are related to the Proterozoic volcanics of Ndembera series which were deposited in E-W striking basins (Kurstein, 1964).

The NE-SW trending anomalies occur in areas where the basement is predominantly granitic and the anomalies are generally of low amplitudes. It can be concluded that the difference in magnetic anomaly patterns in the Buhoro trough is due to the change in the nature of basement rocks as marked by the NW-SE trending lineament labelled BB on the map of magnetic lineaments (Figure 7).

The Chunya-Usangu province

The Chunya-Usangu magnetic province lies between the Buhoro trough in the east and Rukwa trough in the west. The province may be subdivided into two zones demarcated by an E-W magnetic lineament. The southern part is characterized by isolated circular and elongated anomalies of high magnetic relief. The northern zone on the other hand consists of low amplitude anomalies with NNE-SSW magnetic texture in the west while the eastern part is characterized by relatively smooth magnetic anomalies which

correlate with outcrops of muscovite biotite granites. The high amplitude magnetic anomalies in the southern zones are due to ultramafic and mafic intrusives which include the metaperidotites and metagabbros of Nsamya Hills in the Usangu escarpment. The anomaly over Nsamya Hills has an amplitude of 1600 nT whereas the E-W elongated anomaly caused by ultramafic and mafic rocks has an amplitude of 1200 nT. The magnetic data show that the metagabbroic bodies cover a larger area than mapped on the surface, with some bodies extending into the Buhoro trough where they are overlain by sediments. The norite intrusives of Mkutano Hills give rise to a group of anomalies suggestive of a common origin at depth. The isolated anomalies of intermediate relief are related to ferruginous quartzites of Itewe Hills, Holi Hills and others.

The southern part of the Chunya-Usangu magnetic province is also cut by NW-SE lineaments along which small circular anomalies of intermediate relief occur. These are thought to be associated with diorite, granodiorites and postorogenic granites. The northern zone is characterized by NE-SW trending magnetic grain, generally of low amplitudes and related to granitic intrusions and gneisses. The zone marked Q is a magnetic quiet zone observed over the muscovite biotite granite of Kinguamuma whereas the anomaly marked GX is a high amplitude anomaly observed over a granite body intruded by N-S striking iron reefs. The NW-SE magnetic lineaments parallel to Rukwa lineament also extend to this zone.

Other prominent features of the province are the N-S linear anomalies most probably caused by dolerite dykes which do not outcrop on the surface. The linear anomalies are part of long linear anomalies observed north of Rukwa trough and extending northwards as far as south of L. Victoria (Batterham et al., 1983). The magnetic texture of this province differs very much from that observed in the Ufipa and Mbozi block.

The Ubena province

The eastern part of the study area, south of Ruaha magnetic lineament is characterized by low relief anomalies trending NE-SW and terminating in the south against smooth anomalies of the Kipengere Range. The Ubena province also consists of a few isolated dipole like anomalies of high amplitude. The zone marked IG is due to crystalline rocks of Igawa which include lenses of ferruginous quartzites, and meta-anorthositic rocks which belong to the Ubendian crystalline basement. The high amplitude long wavelength anomaly south of Ruaha lineament matches with a young granitic intrusive partially covered with residual soils. The magnetic relief in the province decreases towards the south where the basement rocks are overlain by both Ukingan metasediments and Buanji sediments. This province is characterized by NE-SW magnetic texture.

The Kipengere province

This zone occurs north of Lake Nyasa and is characterized by high amplitude anomalies trending in the NW-SE and crosscut by NE-SW trending linear anomalies. The smooth anomalies in the northeast and south characterize areas covered with intensely folded metasediments of Ukingan and sediments of Buanji, whereas in the west the smooth anomalies are related to the mylonites in the Nyasa escarpment.

The high amplitude negative anomaly trending NW-SE and named here as Kipengere Anomaly, may be due to a deep seated magnetic intrusive beneath the Buanji sediments. In the west the province is characterized by high relief magnetic anomalies which coincide with the strongly sheared rocks of the Upangwa area. However, the cause of the high amplitude anomalies are intrusive rocks which have invaded the shear zones and include meta-anorthosites, gabbros, and norites assigned to the Upangwa meta-anorthosite and Nkenza gabbro extrusives.

The Kipengere magnetic province is separated

from the Buhoro in the northwest by a circularly shaped anomaly marked CH in Figure 7. This anomaly is found in an area where granites and gabbros have intruded the Buanji continental sediments. The granite body is older than the gabbros (Teale et al., 1962) and both have been in-truded by dolerite dykes. The size of the anomaly and occurrence of dolerite dykes in the area suggest that the source of the anomaly is an intrusive rock of mafic to ultramafic composition of larger areal extent than the mapped gabbro.

Magnetic lineaments and tectonics

Magnetic lineaments have been defined by Gay (1972) as a disruption in the contour pattern of magnetic anomalies, caused by juxtaposition of blocks of rocks with different magnetic susceptibilities. Therefore, magnetic lineaments reflect zones of weaknesses within the basement rocks along which some movement has taken place. These zones may include faults, shear zones, and contacts due to intrusive and extrusive rocks.

In this study, the magnetic lineaments were determined from aeromagnetic total field contour maps, stereographic projection map prepared from digitized data and stacked profile maps including maps upward continued to a height of 580 m above the ground and downward continued to a depth of 1 km. The lineaments from the stereographic projection map and contour maps were recognized using diagnostic features outlined by Gay (1972). The criteria used are:

1. Termination of magnetic lows and highs which tend to terminate against lineaments.
2. Steepening and flattening of gradients which is easily recognized even on conventional contour maps.
3. Straight pattern of magnetic contours.
4. A combination of two or more of the above mentioned diagnostic features.

The stereographic projection map was prepared from aeromagnetic data gridded at 1.0 km by 1.0 km and hence small lineaments were filtered out during the process of digitization. The original conventional contour maps on the scale of 1:100,000 and photographically reduced maps to a scale of 1:625,000 were also used in this study

to outline magnetic lineaments. The later was used as a base map on which all lineaments were plotted. Some of the lineaments are shown in Figure 7, where the major lineaments are given names and some minor lineaments are not shown. The strike of each lineament was then measured on a scale of between 0° and 180°. The measurements were statistically grouped in classes of 5° in size and plotted using histograms. Figure 8 shows a plot of frequency distribution of the direction of lineaments from which two prominent trends emerge, one with a peak between 35° and 50° and the other with a peak be-
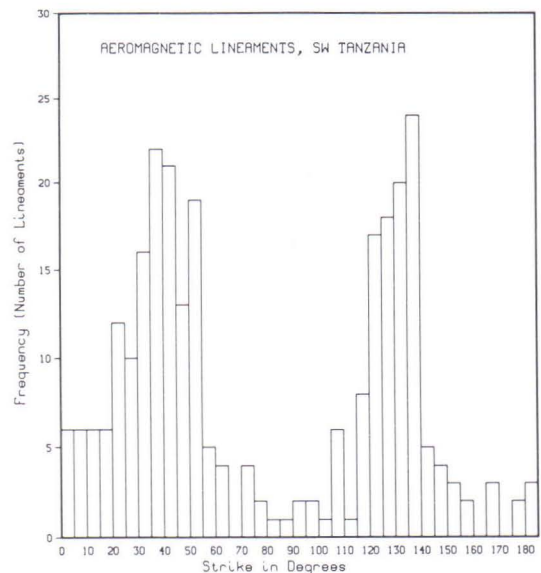

Fig. 8. The plot of frequency of lineaments against their strike direction. The two peaks correspond to major structures, trending NW-SE and NE-SW observed in the study area.

tween 120° and 140°. In general these two trends reflect the east and west rift fault trends as indicated in the geological map of the study area (Figure A1). Another significant trend of lineaments is the easterly trend observed mainly in the northeastern corner, the Chunya-Usangu block, and also in the southern part of the Mbozi block. A few lineaments were found to trend in the N-S direction.

Apart from these general comments, some individual lineaments have been found to have direct correlation with geologically mapped shear zones or faults. However, several lineaments identified from the aeromagnetic maps were found to have no relation with any known geological structures. Such lineaments have been interpreted as being due to old basement structures overlain by a superficial cover of sediments, soils or volcanics. It is also possible that the lineaments are due to deep seated crustal structures with no surface manifestation.

The main magnetic lineaments and their correlation with known faults, shear zones or rock contacts are now described. Some of the lineaments which do not correlate with known geological structures are also discussed.

The Rukwa lineament

The Rukwa fault marks the northern boundary of the Rukwa trough. The fault is well defined in the northwest, where interpretation of gravity data has indicated a listric fault with a maximum throw of 7 km (Peirce & Lipkov, 1988). Towards the southeast the fault disappears into the metasediments of the Mbeya range. However, the aeromagnetic data indicates a continuous lineament which correlates well with the Rukwa fault and can be traced through the metasediments and Rungwe volcanics. The lineament also continues into the Mt. Livingstone area where it is found to correlate with a shear zone along which gabbroic intrusives have been emplaced. The zone of shearing characterized by cataclastic rocks (Harpum & Harris, 1958) con-

tinues further south beyond the study area.

The continuity of the Rukwa lineament across the volcanics into Nyasa trough and the presence of a shear zone along the lineament suggest that, the Rukwa Fault in the northwest occurred along a pre-existing zone of weakness. The fault here appears zigzag as a result of change of direction where it intersects the NE-SW trending lineaments.

The Songwe lineament

The Songwe lineament is a name given here to the lineament trending NNW-SSE and marking the southern limit of Songwe trough. The lineament is subparallel to the Rukwa lineament and together they form a graben structure occupied by the present L. Rukwa. In the south it extends into Rungwe volcanics south of Tukuyu, where it is masked by low amplitude anomalies. There is another subparallel magnetic lineament south of the Songwe lineament. The anomalies associated with carbonatite intrusive of Panda Hill and other anomalies are observed between the two lineaments.

There are no geologically mapped faults which correlate with the lineaments, but this may be due to the surface cover of sediments and volcanics. However, there are several indirect indicators such as, hot springs southwest of Mbeya which lie in the vicinity of the Songwe lineament, and the coincidence of the lineament with a course of a river in the south. The high relief magnetic anomalies of the Mbozi block terminate against the lineament suggesting the presence of a contact between the metamorphics of Bundali Hills and sediments or volcanics in the east. The existence of a fault or contact is also revealed by an abrupt change of Bouguer anomaly values between Bundali Hills and Tukuyu (Aoki, 1969).

The Galula lineaments

The Galula lineaments is the name given to the group of lineaments marking the southern

boundary of Rukwa trough and trending N130°E. One of the lineaments correlates with the Galula fault along which some rocks belonging to the Karroo Formation which include coal measures of Galula and Muassa coalfields. The Galula fault is a normal fault with a throw towards the northeast. The second lineament lying north of Galula fault forms a narrow graben with the latter. This narrow graben is separated from the Rukwa graben by the Ivuna uplift which is also evident in the gravity data (Peirce & Lipkov, 1988). Both lineaments terminate against the NE-SW trending lineaments in the Msangano trough and in the southeast they terminate against the Songwe lineament. These lineaments may have been formed as a result of strike slip movement along Kalungu and Songwe faults.

The lineament marked LL' (Figure 7), south of the Galula lineament, crosses the Msangano trough and continues into the Ufipa block in the west. The lineament occurs as a linear negative anomaly, whose amplitude diminishes towards the east near the Songwe lineament. There is no mapped geological structure associated with the lineament, except one brecciated quartzite north of Itaka, which coincides with this linear anomaly. The lineament may be a reflection of the strike slip faulting along the Songwe and Kalungu faults. The circular anomaly in Msangano trough lies along the lineament.

The Ufipa-Mbozi lineaments

The lineaments across the Ufipa and Mbozi blocks as well as the Msangano trough show two major trends. The major lineaments strike between 120° to 150°. The other set of lineaments strike between 30 to 60° and few lineaments trend more or less N-S. The lineaments marking the Msangano trough correlate well with the Ufipa and Kalungu fault zones, which border the Msangano graben. The Ufipa lineament extends into the Rukwa trough in the north where it terminates against an E-W trending lineament. In the south the lineament continues beyond the

study area into Zambia. The lineament is well defined along its entire length as it marks the contact between the high relief magnetic anomalies of the Ufipa block and smooth anomalies of the Msangano trough.

The Kalungu lineament in the east correlates with the Kalungu fault and partly with the Nyimbili fault in the south. Both faults are normal faults with a throw towards the southwest. The southern part of Msangano trough is characterized by several NW-SE trending lineaments, some of which terminate against the N-S lineament observed within the trough which extends northwards into the northwestern corner of the Mbozi block. Along the lineaments lie circular to ellipsoidal shaped anomalies most of which are due to mafic-alkaline intrusives. Some of them are due to outcropping intrusives but a few are due to intrusives overlain by lake sediments.

The NE-SW lineaments observed in the Mbozi block correlate with fold axes of the Itumba quartzites in the Umalila Mountains, south of Panda Hill. In the northwest towards the Rukwa trough, the NE-SW lineaments continue into the trough and correlate partly with dyke intrusives. The Mbozi gabbro syenite complex terminates the NE-SW lineaments while the N-S trending anomaly is due to a dolerite dyke which has been mapped south of Itumba.

The lineaments within the Ufipa block are parallel to the Ufipa lineament and some are related to the contact zones between various metamorphic rock types or fault zones. The Kanda fault trending NNW-SSE correlates with one of these lineaments. Within the block there are magnetic lineaments trending in the NE-SW with some lineaments crossing the Msangano trough into the Mbozi block.

The Buhoro lineaments

The Buhoro trough, trending NE-SW, is characterized by linear magnetic anomalies showing three major trends. The majority of the lineaments trend between NNE and NE parallel to the

major trend of the trough. Several other lineaments trend east-west and few show northwesterly trend.

Some of the lineaments show correlation with known faults or shear zones. The lineament called Ruaha correlates with the Ruaha fault, north of Malangali, and also quartz reefs are found along some portions of the lineament. The magnetic data indicate a continuous lineament extending into Buhoro flats, with amplitude diminishing towards the west. Another lineament marked Madibira (Figure 7) correlates with a relatively young fault located at 8°14'S and 34°32'E, which has displaced Neogene lake beds (Fig. A1).

Further west the NE-SW lineaments define the boundary between the trough and Usangu escarpment. The lineaments do not correlate directly with the Usangu fault. This may be due to the fact that the fault was inferred from topographical features (Teale et al., 1962).

The E-W trending magnetic lineaments are found mainly in the northeast within the basement and in the Buhoro trough. The quartz reefs mentioned under the section of the Usagaran Mobile Belt above, and which indicate a zone of weakness within the crust, correlate with some of the E-W lineaments. Geological studies of Ndembera volcanics found in the NE suggest that the volcanics were deposited in E-W trending basins (Kursten, 1964). The lineaments may therefore be interpreted as being due to basement structures which developed prior to the emplacement of the volcanics.

Within the trough and adjacent areas, there are several lineaments trending NW-SE parallel to the Njombe lineament (Figure 7). The most prominent of this is the lineament marked BB which separates high amplitude circular anomalies in the south from low amplitude linear anomalies in the northeastern part of Buhoro trough. Due to sedimentary cover this lineament has no correlation with any known fault. This lineament is interpreted here as an indication of a contact zone between the southern crystalline basement consisting of high grade metamorphics and mafic intrusives, and the northern granitic basement.

The Mkondo lineament

The E-W magnetic lineament within the Chunya block correlates with the Mkondo shear zone and is here called the Mkondo lineament. The magnetic data shows a continuous lineament terminating against the Rukwa trough in the west and extending further east in the Buhoro trough. The lineament separates two blocks with different magnetic characteristics and appears to mark the northern limit of the ultramafic and mafic intrusives of the Ilunga Hills (Figure A1).

Other E-W trending lineaments are found north of the Mkondo shear zone and the northeastern corner of the study area. The lineament located around 8°15' S in the Rukwa trough is due to deep seated faults within the basement, whereas the positive linear anomaly at 8°10' S and 32°48' E appears to be caused by a dyke-like body.

Another lineament located at 8°07' S and 33°33' E displaces the N-S trending linear anomaly caused by a dyke-like body and the displacement suggest dextral strike-slip movement.

The Tukuyu-Nyasa lineaments

These are sets of lineaments observed in the volcanic area of Tukuyu and the sheared zone of Nyasa escarpment. The lineaments trend in the NW-SE and NE-SW, the former being the prominent trend. The Tukuyu lineament, which correlates well with a fault mapped in areas where basement rocks are exposed, extends further northwestward into Songwe trough and southeastward into Nyasa trough, where the basement is overlain by lake sediments.

The Nyasa lineament marks the Nyasa escarpment and correlates with the Nyasa fault. This lineament extends further northwestward into the Poroto Mountains and is slightly oblique to the

Rukwa lineament. Recent geological studies have established that apart from the vertical displacement of the Nyasa fault, there has been dextral strike slip displacement (Tiercelin et al., 1988). The extension of the Songwe lineament and others mark the southern boundary of the crystalline basement and correlates with some of the faults affecting Karroo and Cretaceous sediments.

The NE trending lineaments (T1 to T3, BU1 and BU2) in Figure 7 have not been mapped as most of them are found in areas where the basement is overlain by sediments or volcanics. However, the lineaments trend subparallel to the faults observed in the Nyasa escarpment. One of the lineaments crosses the Rungwe volcanic center northwards into Buhoro trough. The lineament marked T1 lies near the boundary between the volcanics and lake sediments in the Nyasa trough and it is partly marked by a change of magnetic pattern from a complex pattern caused by high frequency anomalies to a smooth pattern of anomalies. The lineament T3 correlates well with the fault affecting the Buanji sediments south of the Chimala magnetic anomaly. The lineaments marked BU1 and BU2 occur in the Bundali Hills and extend north into the region of the Rungwe volcanics.

The Njombe lineament

The Njombe lineament is a long lineament trending NW-SE and crossing Njombe area. The lineament which is subparallel to the Rukwa lineament runs through the Buhoro trough into the Chunya block and extends on both sides beyond the study area. In the south around Njombe, the lineament correlates with sheared quartzites and dolerite dykes striking in the same direction. These features are surface indications of the presence of a zone of weakness within the basement rocks along which dolerite dykes have

intruded. The shearing of the quartzite dykes suggest tectonic movement along the lineament.

The tectonic movement along the lineament is evident in the Chunya block where it displaces the N-S striking linear anomaly (Figure 7) suggesting a sinistral strike-slip movement, which is in agreement with the dextral strike-slip displacement along the Rukwa lineament observed by Tiercelin, et al. (1988). Some of the NE-SW lineaments observed in the Ubena granitoids terminate against this lineament.

The Kipengere lineaments

The geology of the Kipengere area, south of Buhoro trough consists of intensely folded metasediments and sediments. The intense folding led to thrusts and overthrusts of surface rocks. The magnetic lineaments observed in this area do not correlate with known thrusts but the lineaments trend more or less in the same direction as the thrusts. The magnetic lineaments observed are considered to be due to a deep seated shearing within the basement underlying the folded sediments. The thrusts of sediments must have been formed by shearing in the basement along Gofio lineament. The lineament defined by the alignment of positive anomalies in Upangwa is slightly oblique to the continuation of the Rukwa lineament in the area. The striking feature is the alignment of the Kipengere anomaly, the circular anomalies east of Usangu lineament, and anomalies in Chunya block related to gabbroic intrusives. The alignment suggest an old basement structure trending NW-SE and which controlled the emplacement of the intrusive rocks. South of the Kipengere anomaly lies NE-SW lineaments which are correlated with faults affecting the sheared basement and the Ukingan metasediments. These lineaments extend eastward into the Ubena granitoids.

DENSITY AND MAGNETIC PROPERTIES OF ROCKS

Several rock outcrops from the study area were sampled for petrophysical studies. Most of the rocks sampled were intrusives and volcanics, among them being the Rungwe volcanics, Panda Hill Carbonatite, and the Mbozi Gabbro-Syenite Complex. Others include the Chunya granitoids and Itewe Hills ferruginous quartzites. The location of outcrops sampled are shown in Figure 9. Some susceptibility measurements were done on rock outcrops using the susceptibility meter model TH-15 manufactured by Geoinstruments Oy of Finland.

The samples were prepared by drilling cores of 32 mm in diameter from hand specimens. The cores were then cut into cylinders of heights ranging from 26 mm to 29 mm. This height gives the ratio of height to diameter of 0.8 to 0.9 suitable for remanent magnetization studies as the field due to such a cylinder approximates the field of a dipole placed at the center of the cylinder(Collinson, 1983). A total of 147 samples were prepared from which susceptibility, remanent magnetization, and density were measured.

The density measurements were determined by weighing a sample in air and repeating the measurement with the sample completely immersed in water. The remanent magnetization measurements were done using the remanent magnetometer model JH-9 whereas the susceptibility measurements were done using the susceptibility meter model TH-1, both manufactured by Geoinstruments Oy of Finland. The measurements were computer controlled and the average of ten measurements was recorded as the final value in each of the properties measured.

The susceptibility measurements were used to calculate the induced magnetization using the local ambient field of 33,500 nT. Both, induced and remanent magnetization are given in Am^{-1}. The remanent and induced magnetization were used to calculate the Koenigsberger ratio which is the ratio of remanent magnetization to induced magnetization. The direction of the remanent magnetization was not determined as the samples were not oriented. The results of the measurements are briefly described below.

The Panda Hill carbonatite

The Panda Hill carbonatite is located at latitude 8° 59.5′ S and longitude 33° 14′ E and it is about 20 km southwest of Mbeya town (Figure A1). The carbonatite is an intrusive rock which is dominantly calcitic and partly dolomitic (Fawley & James, 1955, Suwa, et al., 1969). The main accessory minerals are siderite, ankerite, biotite, magnetite, pyrochlore, and apatite. The intrusion has been geologically studied but no petrophysical studies have been done.

A total of seventeen samples were collected from the carbonatite body including the magnetite veins. The density, remanent magnetization, and susceptibility measurements are presented in Table 2 below from which it is found that the density ranges from 2520 kgm^{-3} to 3770 kgm^{-3}, with sample 24431 having the highest density.

The average density for carbonatite rocks excluding samples rich in ore minerals was found to be 2770 kgm^{-3} whereas the average density of carbonatite samples rich in ore minerals was found to be 3326 kgm^{-3}.

The susceptibility of the carbonatite samples was found to be generally low except for samples rich in iron oxide minerals. The Koenigsberger ratio ranges from nil to 57.40. The samples with a density above 3120 kgm^{-3} were found to have high susceptibility and remanent magnetization due to the presence of iron oxide minerals as accessories. However, few samples (24438, 24439) with low density were found to have high remanent magnetization.

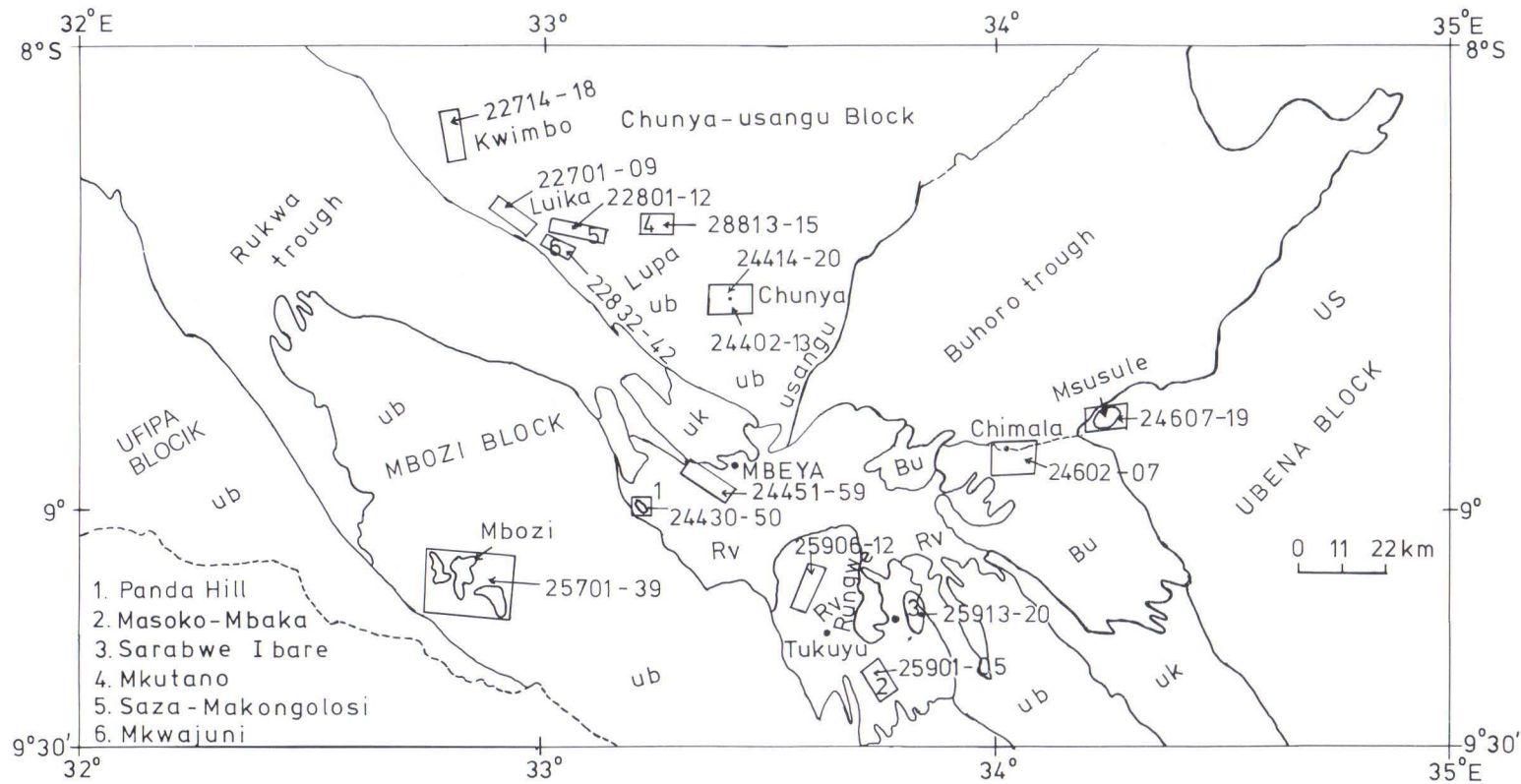Previous petrographical studies (Fawley & James, 1955, Fick & Van Der Heyde, 1959,

Fig. 9. Map showing location of outcrops sampled for petrophysical studies.

Table 2. Petrophysical data of the Panda Hill carbonatite.

Sample	Density kgm^{-3}	K x10^{-6}	J$_R$ Am^{-1}	J$_r$ Am^{-1}	Q ratio	Rocktype
24430	3120	681	0.80	2.28	0.35	carbonatite
24431	3770	5720	100.00	19.20	57.41	carbonatite
24432	2890	538	nil	1.80	nil	carbonatite
24433	3430	2380	176.00	7.97	22.07	carbonatite
24434	2880	2380	6.10	7.97	0.77	carbonatite
24435	3140	4780	665.0	16.00	41.53	carbonatite
24437	2690	485	0.61	1.62	0.38	carbonatite
24436	2890	281	0.04	0.94	0.05	carbonatite
24438	2800	2730	10.30	9.15	1.13	carbonatite
24439	2930	10700	102.00	35.80	2.85	carbonatite
24440	2760	1520	1.32	5.09	0.26	carbonatite
24441	2810	607	0.31	2.03	0.15	carbonatite
24442	2770	8150	0.38	27.30	0.01	carbonatite
24444	2690	3410	100.00	11.40	8.75	carbonatite
24443	3740	84500	1050.00	283.00	3.71	carbonatite
24445	3150	44500	1300.00	149.00	8.72	carbonatite
24450	2520	955	0.26	3.20	0.08	carbonatite

Suwa, et al., 1969) have shown that the oxide minerals present in the carbonatite body include magnetite, hematite, ilmenite, and goethite. In this work petrographical studies were done on several samples collected from the carbonatite. The samples with high and low remanent magnetization were studied to determine the type of ore minerals.

In most of the samples studied, magnetite, haematite, ilmenite, and goethite were found to be the major oxide minerals. In some samples magnetite was found to be replaced by hematite, in a process known as martitization. The sample 24431 with the highest Q-value was found to consist entirely of ore minerals of which haematite was the major mineral. The haematite was found to replace magnetite to the extent that the latter is found occurring as small remnant grains. The haematite is also found altered to limonite along cleavages and ilmenite was observed within the haematite. The high Q-value may be explained by the presence of remnants of magnetite and ilmenite which may have retained the remanent magnetization.

The samples (24433, 24435, 24439, and 24445) with high remanent magnetization were found to consist of mainly carbonatite minerals with magnetite, haematite, and ilmenite as accessory oxide minerals. The predominant minerals in samples 24433 and 24435 were found to be haematite and goethite occurring as secondary minerals formed by an alteration of magnetite. The magnetite itself was found in small amounts as remnants. The samples 24439 and 24445 were found to consist of magnetite as the major ore mineral occurring as large crystals. Haematite occurring as needles was observed within the magnetite and in addition pyrochlore was observed in sample 24439. In another sample 24442, the amount of ore minerals was found to be small with magnetite being the main ore mineral and haematite was found as exsolution within magnetite crystals.

The samples 24430 and 24441 characterized by low remanent magnetization and susceptibility values, were found to consist of carbonate minerals, with haematite, pyrochlore, ilmenite and apatite as accessory minerals. Haematite with exsolution of ilmenite lamels was found to be the main ore mineral in sample 24430. Euhedral crystals of pyrochlore with inclusions of ilmenite, apatite and carbonate minerals were also found but in less quantities compared to haematite. In sample 24441, pyrochlore was found to be the

major accessory mineral. Apatite was present as inclusions within the pyrochlore crystals, and haematite with lamels of ilmenite and inclusions of carbonate minerals was also observed.

It is therefore apparent that high remanent magnetization is related to the presence of magnetite and ilmenite. The samples with high density were found to be relatively rich in haematite and other oxide minerals of iron.

The Rungwe volcanics

The Rungwe volcanics have been briefly described above under the section of young formations. In this study the basalts and trachytes of Mbeya and Tukuyu were sampled. A total of twenty seven samples of which five are trachytes, two scoria, and the rest basalts, were collected. Samples numbered 24451 to 24459 were collected from basalts south and southwest of Mbeya town whereas samples numbered 25901 to 25920 were collected from volcanic outcrops in Tukuyu

(Figure 9.). The results of petrophysical measurements for these samples are tabulated in Table 3 from which the density of the volcanics range from 2360 kgm^{-3} to 3070 kgm^{-3}. The average density for trachytes is 2560 kgm^{-3} and basalts have an average density of 2800 kgm^{-3} which is of the same order as the density of the Panda Hill carbonatite intrusive (Table 2).

The volcanics show a wide range of susceptibility values, with basalts ranging from 2160 ×

Table 3. Petrophysical data of the Rungwe volcanics.

Sample	Density kgm^{-3}	K x10^{-6} SI	J_R Am^{-1}	J_r Am^{-1}	Q ratio	Rocktype
25901	3070	68100	101.00	228.00	0.44	basalt
25903	2900	14900	631.00	49.90	12.64	basalt
25904	3020	42500	83.90	142.00	0.59	basalt
25905	2970	46600	47.70	156.00	0.31	basalt
25906	2360	9360	27.40	31.40	0.87	trachyte
25907	2870	16100	12.00	53.90	0.22	basalt
25908	2870	15200	31.00	50.90	0.61	basalt
25909	2880	68100	21.60	228.00	0.09	basalt
25910	2600	9410	0.54	31.50	0.02	trachyte
25911A	2750	67300	32.20	225.00	0.14	Trachyte
25911	2630	17600	3.44	59.00	0.06	Trachyte
25912	2870	58700	7.85	197.00	0.04	basalt
25913	2950	10200	16.90	342.00	0.05	basalt
25914	2440	28700	5.03	96.10	0.05	trachyte
25915	2420	22500	245.00	75.40	3.25	trachyte
25916	2610	87700	63.70	294.00	0.22	basalt
25917	2770	4550	65.00	15.20	4.26	basalt
25918	2800	9370	27.30	31.40	0.87	basalt
25919	2630	5760	20.40	19.30	1.06	scoria
25920	2720	5060	5.03	17.00	0.30	scoria
24451	2810	10200	20.40	342.00	0.06	basalt
24452	2640	46600	83.90	156.00	0.54	basalt
24453	2790	73000	160.00	245.00	0.65	basalt
24456	2630	3260	14.10	10.90	1.29	basalt
24457	2600	2160	3.07	7.24	0.42	basalt
24458	2640	23600	42.20	79.10	0.53	basalt
24459	2690	22100	172.00	74.00	2.32	basalt

10^{-6} to 87700×10^{-6} SI and the susceptibility of trachytes range from 9360×10^{-6} to 67300×10^{-6} SI. The Q-ratios are low in general, only six samples out of twenty seven have a Q-ratio greater than 1.0, with 12.6 being the highest ratio observed. This data suggests that the remanent magnetization is not significant in the volcanics.

The Mbozi gabbro syenite complex

The Mbozi gabbro-syenite complex is a ring structure consisting of a variety of rock types including nepheline syenite, gabbro, pyroxenites and dolerite dykes (McFarlane & Brock, 1966). Brock (1968) described the petrology and formation of the rocks of the ring structures. The struc-
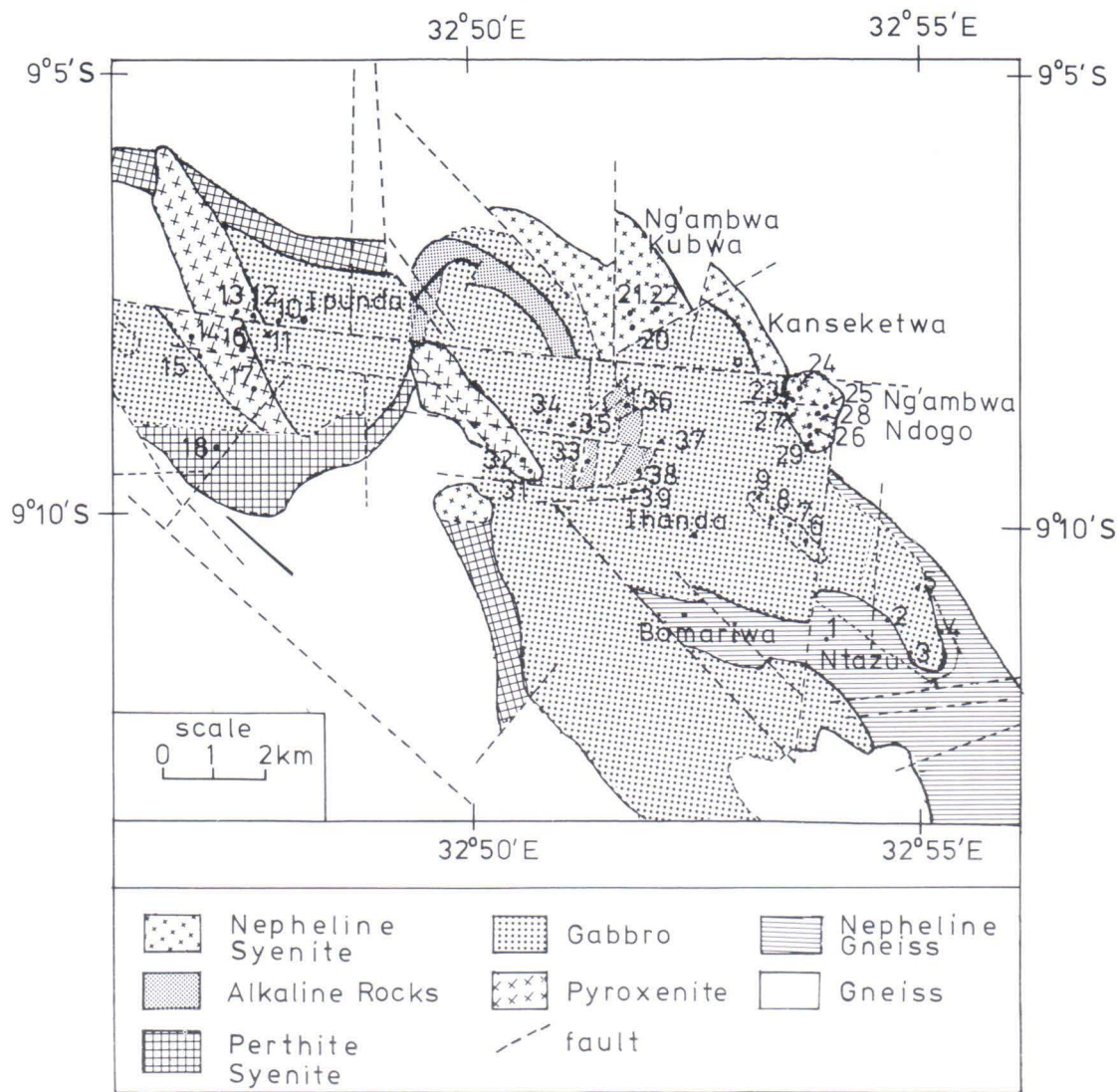

Fig. 10. Map of Mbozi gabbro-syenite complex showing the location of samples collected.

ture is located within the Msangano Rift and show a northwesterly trend.

Thirty six samples were collected from rock outcrops, which included syenites, dolerite dykes, pyroxenites, gabbros, and other rock types of the ring complex. The distribution of samples is shown in Figure 10. The samples were analyzed for density, susceptibility, and remanent magnetization and the results are tabulated in Table 4.

The density of rocks range from 2590 to 3480 kgm^{-3} of which nepheline bearing syenites were found to have the lowest densities with an aver-

age of 2660 kgm^{-3}. Higher densities were observed among the pyroxenite rock samples which show densities with values above 3200 kgm^{-3} with an average of 3290 kgm^{-3}. The gabbros, dolerites and breccia were found to have intermediate densities with an average of 2980 kgm^{-3}.

The rocks of the gabbro-syenite complex are characterized by high remanent magnetization and susceptibility. The susceptibility ranges from 630×10^{-6} SI to 84500×10^{-6} SI. The lowest susceptibility values are found among nepheline bearing syenite, whereas high values were ob-

Table 4. Petrophysical data of the Mbozi gabbro syenite complex.

Sample	Density kgm^{-3}	K x10^{-6} SI	J_R Am^{-1}	J_r Am^{-1}	Q ratio	Rocktype
25701	2920	657	121.00	2.20	54.98	gabbro
25702	2770	2600	40.80	8.71	4.68	gneiss
25703	3040	32100	231.0	108.00	2.15	dolerite
25704	2690	4030	65.30	13.50	4.84	gneiss
25705	2720	7590	82.80	25.40	3.26	dolerite
25706	3120	7070	267.00	23.70	11.27	breccia
25707	2750	42800	68.60	143.00	0.48	breccia
25708	3110	9950	220.00	33.30	6.60	breccia
25709	2910	7360	422.00	24.70	17.12	dolerite
25710	3190	11700	2230.00	39.20	56.90	gabbro
25711	3260	34000	801.00	114.00	7.03	pyroxenite
25712	3290	26600	156.00	89.10	1.75	pyroxenite
25713	3160	5830	5510.00	19.50	282.07	dolerite
25714	3300	84500	1170.00	283.00	4.13	pyroxenite
25715	3370	13200	4000.00	44.20	90.46	pyroxenite
25716	3480	19700	7410.00	878.00	84.43	pyroxenite
25717	2940	50000	65.00	167.00	0.39	gabbro
25718	3140	1950	388.00	6.53	59.40	gabbro
25720	2610	3060	74.50	10.30	7.27	syenite
25721	2650	54400	242.00	182.00	1.33	syenite
25722	2640	52600	2000.00	176.00	11.35	syenite
25723	2620	41400	82.50	139.00	0.59	syenite
25724	2690	46700	1010.00	156.00	6.46	syenite
25725	3010	70300	7770.00	236.00	32.99	dolerite
25726	2790	79300	645.00	266.00	2.43	gabbro
25728	2910	5830	254.00	19.50	13.01	gabbro
25729	3300	26400	3020.00	88.40	34.15	gabbro
25731	3210	34100	5660.00	114.00	49.55	gabbro
25732	3300	22800	6740.00	76.40	88.24	gabbro
25733	2590	5950	95.30	19.90	4.78	syenite
25734	3220	16100	786.00	53.90	14.57	gabbro
25735	3100	20200	2620.00	67.70	38.72	gabbro
25736	3210	16900	624.00	56.60	11.02	gabbro
25737	2770	1580	3.60	5.29	0.68	syenite
25738	2740	627	127.00	2.10	60.46	syenite
25739	3120	4890	854.00	16.40	52.13	dolerite

2

served among the pyroxenite samples.

The samples show high remanent magnetization with most samples having Q-values between 10 and 90. The results suggest that remanent magnetization is dominant and therefore magnetic anomalies observed over the complex have large component due to remanent magnetization.

Brock (1968) has reported the petrographical studies of the ring structure in which three major rock types were distinguished. The oldest rocks are gabbros and pyroxenites which were deformed and faulted before the emplacement of alkali rocks. The emplacement of alkali rocks was also accompanied by metasomatism which altered the old rocks.

In this study qualitative petrographical studies of some selected samples were done to determine the ore minerals which are thought to influence the petrophysical properties of rocks. The samples were selected from the major rock types.

The gabbro rock sample 25701 was found to be an altered gabbro with a low content of ore minerals of which pyrrhotite was found to be the predominant. The gabbro samples 25706, 25710, and 25732 were found to represent the altered gabbros and magnetite was found to be the major ore mineral in which ilmenite occurred as exsolution. Other ore minerals found were pyrrhotite, chalcopyrite and pyrite.

The ultramafic rocks which occur as pyroxenite were described by Brock (1968) to be rich in iron ores with magnetite found in association with spinel being the predominant mineral. One of the samples studied (25713) was found to be altered in which pyroxenes and olivines were altered into hornblende. The ore minerals present were found to be associated with the alteration, and magnetite with ilmenite exsolutions was found to be the major ore mineral. Chromite was also observed occurring as grains surrounded by rims of magnetite. The sulphide minerals present were pyrrhotite within which grains of pyrite, chalcopyrite and spharelite were found. In sample 25716, the ore minerals found were predominantly oxides which were found to occur in association with green spinel. The main ore mineral was magnetite with exsolution of haematite and in addition ilmenite and rutile were observed within magnetite grains.

The syenite rocks which are the youngest rocks of the complex were found to be poor in ore minerals. In sample 25721, magnetite was found to be the main mineral in which ilmenite was found as exsolution. The sample 25738 with alkalic composition was found to consist of pyrite as the major opaque mineral with its grains surrounded by magnetite. Chalcopyrite was also found to be present.

The petrographical studies suggest that density, susceptibility and remanent magnetization are related to the ore mineral composition of the rocks. The syenites with low content of ore minerals were found to have low densities, susceptibilities and low remanent magnetization.

The Chunya granitoids and Itewe Hills quartzites

The granites and diorites of the area around Chunya town and ferruginous quartzites of Itewe Hills located at 8° 34′ S and 33° 24.5 ′E (Figure A1) were sampled. The samples of ferruginous quartzites and granitic gneisses (24402 to 24413) were collected from trenches across Itewe Hills whereas samples numbered 24414 to 24420 were collected from granitic and dioritic rocks northwest of Chunya town (Figure 9).

The results of the measurements are summarized in Table 5 from which it can be seen that the ferruginous quartzites have densities ranging from 3150 to 3420 kgm^{-3} with an average density of 3310 kgm^{-3} whereas the granitic gneisses in contact with the quartzites have an average density of 2610 kgm^{-3}. The high density of the quartzites is due to high content of magnetite in the samples. The diorites and granites of Chunya

have densities ranging from 2590 kgm^{-3} to 3100 kgm^{-3} with an average of 2980 kgm^{-3}.

The susceptibility is high for ferruginous quartzites ranging from 7430 $\times$ 10^{-6} to 98600 $\times$ 10^{-6} SI with an average of 34700 $\times$ 10^{-6} SI and also which have high remanent magnetization exceeding the induced magnetization as reflected in the high Q ratios of 46 to 402. The gneisses surrounding the quartzites have an average susceptibility of 984 $\times$ 10^{-6} SI and show low Q ratios less than 1.0 with an exception of one sample which has higher susceptibility and remanent

magnetization. The diorite rocks of Chunya have average susceptibility of 980 $\times$ 10^{-6} SI which is in the same order as the average susceptibility of the granitic gneisses discussed above.

The aeromagnetic map does not show any appreciable anomaly in the area of Itewe Iron Hills despite the large susceptibility contrast between the gneisses and quartzites, high remanent magnetization and the fact that the Itewe Hills strike over a distance of 3.75 km in NNE-SSW, oblique to the flightline direction.

Table 5. Petrophysical data of the Chunya granitoids and quartzites.

Sample	Density kgm^{-3}	K x10^{-6} SI	J_R Am^{-1}	J_r Am^{-1}	Q ratio	Rocktype
24402	3300	98600	15300.00	330.00	46.32	quartzite
24403	3360	14600	3500.00	49.00	71.56	quartzite
24404	3420	11000	14800.00	37.00	401.63	quartzite
24405	3360	45500	8960.00	152.00	58.78	quartzite
24406	3320	7430	2270.00	24.90	91.20	quartzite
24407	2600	922	0.41	3.09	0.13	gneiss
24408	2590	872	0.12	2.92	0.04	gneiss
24410	3360	20600	7740.00	69.00	112.16	quartzite
24411	3150	12200	15000.00	40.90	367.02	quartzite
24412	3220	68000	27600.00	228.00	121.16	quartzite
24413	2630	1160	44.00	3.89	11.32	gneiss
24414	3050	549	0.44	1.84	0.24	diorite
24415	2690	553	43.70	1.85	23.59	gneiss
24416	3100	948	1.59	3.18	0.50	diorite
24417	3050	2270	602.0	7.60	79.16	diorite
24418	2590	448	2.49	1.50	1.66	granite
24419	3070	1260	2.39	4.22	0.57	diorite
24420	3020	804	1.20	2.69	0.45	diorite

The Lupa granitoids

The Lupa intrusives include diorites, granodiorites and granites found east of L. Rukwa and south of Ilunga Hills (Figure 9) from which samples were collected. The results of petrophysical measurements are summarized in Table 6 from which it can be seen that the densities of the rocks range from 2570 kgm^{-3} to 3080 kgm^{-3}. The density of the granitic rocks ranges from 2570 to 2760 kgm^{-3} with an average density of 2690 kgm^{-3}. The Mkutano norite has an average

density of 2970 kgm^{-3} whereas the diorites and granodiorites combined have an average density of 2860 kgm^{-3}.

The lower susceptibility values are shown by granites but within the group the sheared and hornblende bearing granites have higher susceptibilities compared to other types of granites. The lowest value of 170 $\times$ 10^{-6} SI is due to a sandstone collected from the sediments of Kwimba Hill and which belongs to the Bukoban continen-

tal sediments. The samples 22810 to 22812 were found to be sheared mafic rock in which magnetite was found to fill the fractures.

The remanent magnetization is higher for diorites, norites and contaminated hornblende

granites most of which have Q ratios greater than 1.0. The gneisses and granites have very low Q ratios with exception of gneisses surrounding the ferruginous quartzites, and the magnetization of these rocks may be predominantly induced.

Table 6. Petrophysical data of the Lupa granitoids.

Sample	Density kgm⁻³	K x10⁻⁶ SI	J_R Am⁻¹	J_r Am⁻¹	Q ratio	Rocktype
22801	2730	2060	33.00	6.90	4.78	granite
22802	2660	816	0.42	2.73	0.15	granite
22803	2760	3290	261.00	11.00	23.68	c.granite
22804	2710	1950	10.40	6.53	1.59	c.granite
22805	2880	1010	0.89	3.38	0.26	dolerite
22806	2720	2060	16.80	6.90	2.43	c.granite
22807	2670	3180	14.10	10.70	1.32	s.granite
22808	3080	2730	4.59	9.15	0.50	aplite
22809	2850	1970	2.31	6.60	0.35	diorite
22810	2780	20300	2340.00	68.00	34.41	mafic
22811	2780	15200	2300.00	50.90	45.17	mafic
22812	2800	16500	2770.00	55.30	50.11	mafic
22813	2950	1160	18.60	3.89	4.79	norite
22814	2970	1200	73.80	4.02	18.36	norite
22815	2980	4920	267.00	16.50	16.20	norite
22832	2720	1300	33.60	4.35	7.72	diorite
22833	2970	8920	2890.00	29.90	96.71	dolerite
22834	2640	970	9.89	3.25	3.04	granite
22835	2870	923	0.59	3.09	0.19	aplite
22838	2650	4860	36.30	16.30	2.23	diorite
22839	2720	9040	3.61	30.30	0.12	granite
22836	3030	1030	0.72	3.45	0.21	gr.diorite
22840	2870	913	0.09	3.06	0.03	gneiss
22701	2610	169	0.01	0.57	0.03	granite
22702	2590	282	0.01	0.95	0.01	granite
22703	2640	419	0.04	1.40	0.03	gneiss
22704	2640	402	0.01	1.35	0.01	gneiss
22706	2660	418	0.04	1.40	0.03	s.gneiss
22708	2660	279	0.03	0.94	0.04	granite
22709	2900	326	0.02	1.09	0.02	diorite
22714	2710	334	0.07	1.12	0.06	b.quartzite
22715	2630	464	0.03	1.55	0.20	B.granite
22716	2570	265	0.05	0.89	0.06	p.granite
22717	2600	173	0.01	0.58	0.01	sandstone
22718	2590	414	0.01	1.39	0.01	B.granite

note: p. = porphyry B. = Biotite, b. = banded, gr. = granitic/grano, c. = contaminated, s. = sheared

The Chimala rocks and Msusule granodiorite

These rock samples were collected from the Msusule granodiorite and other rocks around Chimala south of Buhoro trough (Figure 9.). The

rock types sampled in Chimala includes gabbros, dolerites, and granite. The results of measurements are tabulated in Table 7 below.

The density of rocks range from 2550 to 2900 kgm^{-3} with granodiorites having an average of 2730 kgm^{-3} and the average density of dolerites is 2840 kgm^{-3}. The density of granite observed is rather low compared to other granites. The low density may be explained by the presence of fractures in the rock samples. The susceptibility is found to range from 521 $\times$ 10^{-6} to 7410 $\times$ 10^{-6} with quartzite and granites showing low susceptibility values, whereas gabbros, granodiorites, and dolerite dykes show high susceptibilities.

All samples have high remanent magnetization, which is revealed in the high Q ratios that are generally above 1.0. The granodiorites exhibit a wide variation of remanent magnetization which may be attributed to variations in the mineralogical composition of accessory minerals.

Table 7. Petrophysical data of Chimala rocks and Msusule granodiorites.

Sample	Density kgm^{-3}	K x10^{-6} SI	J_R Am^{-1}	J_r Am^{-1}	Q ratio	Rocktype
24602	2750	7410	1080.00	24.80	43.51	gabbro
24603	2850	5060	171.00	17.00	10.09	dolerite
24604	2580	2770	23.50	9.28	2.53	gabbro
24605	2830	1680	34.10	5.63	6.06	dolerite
24607	2550	707	7.45	2.37	3.15	granite
24608	2550	521	5.90	1.75	3.38	quartzite
24611	2800	3990	9.80	13.40	7.33	granodiorite
24612	2630	4100	13.90	13.70	1.01	granodiorite
24614	2740	3240	976.00	10.90	89.92	granodiorite
24615	2690	1130	1910.00	3.79	504.56	granodiorite
24616	2900	4960	1350.00	16.60	81.25	dolerite
24617	2790	1560	485.00	5.23	92.81	dolerite
24618	2760	1830	518.00	6.13	84.50	granodiorite
24619	2750	1520	35.80	5.09	7.03	granodiorite

Summary of petrophysical studies

The results of the petrophysical measurements are summarized in Table 8, where the samples are grouped according to rock types. The lowest densities and Q-values are found among granites, gneisses and carbonatites. The high Q ratios among gneisses are due to samples collected around the ferruginous quartzites of Itewe. There is a remarkable difference in density between the ordinary carbonatite and the ore bearing carbonatite as shown in Table 8. The average density of carbonatite samples was found to be very close to the average density of basalts. The abnormally low density values shown by some granite and gabbro samples are caused by fracturing of the rock outcrops sampled.

To study the relationship between the properties measured, four correlation diagrams were plotted. The plots of density against susceptibility, Q-values against susceptibility, density against remanent magnetization, and induced against remanent magnetization, are given in Figures 11 and 12.

There is some linear correlation between induced and remanent magnetization as is shown in Figure 11 top for most of the rock types with exception of volcanic rocks and granites having both low susceptibility and remanent magnetization. There is no clear correlation between density and susceptibility as shown in Figure 11 bottom, whereas the plot of density against rema-
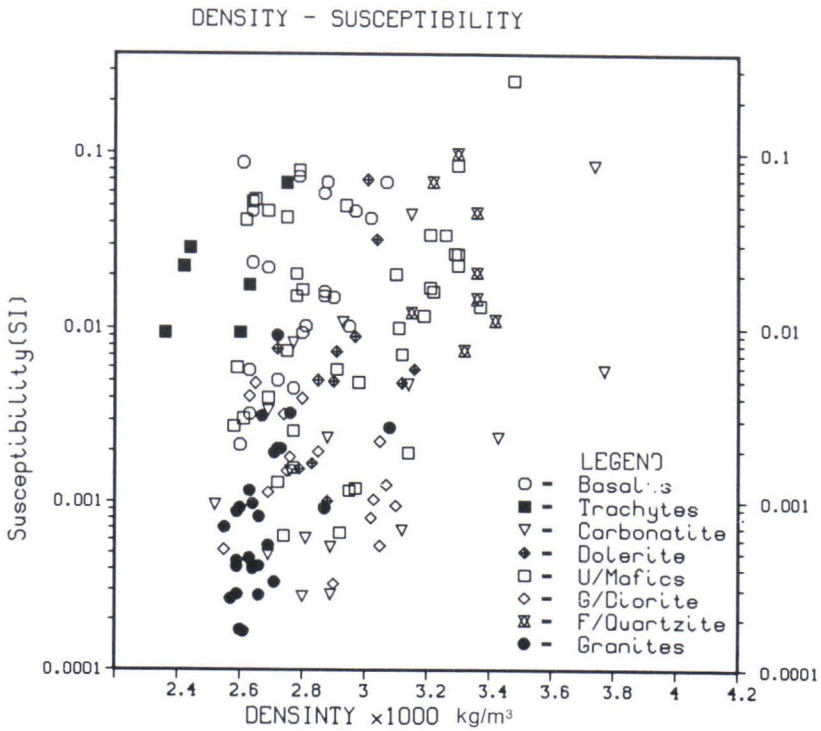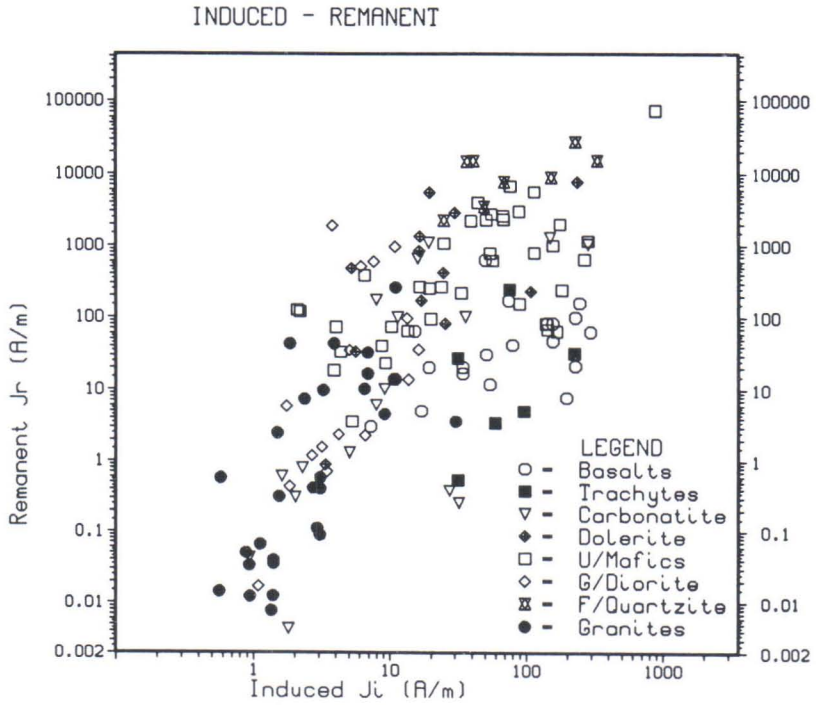
Fig. 11. Correlation diagram between induced and remanent magnetization (top) and correlation diagram between density and susceptibility (bottom).
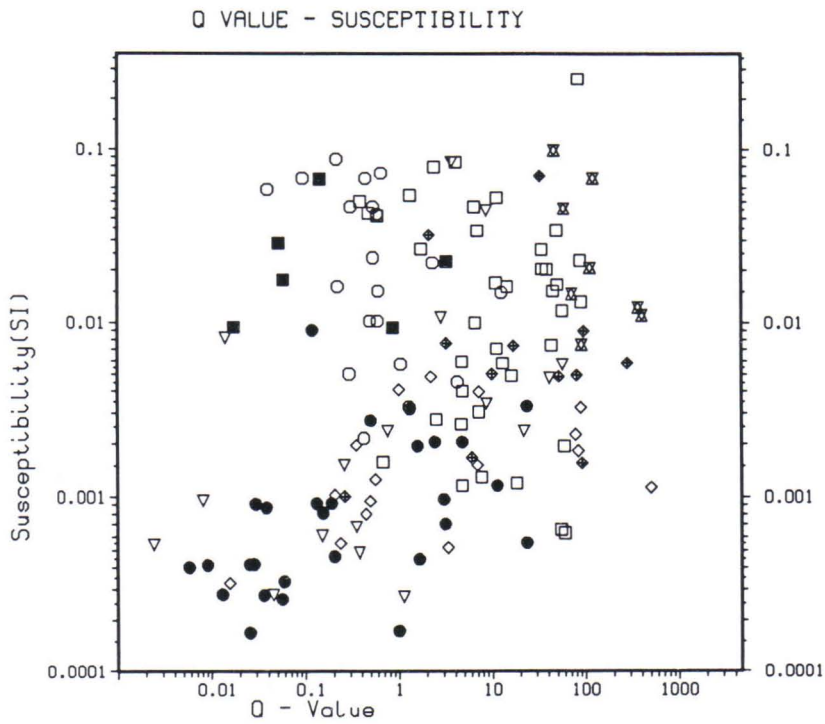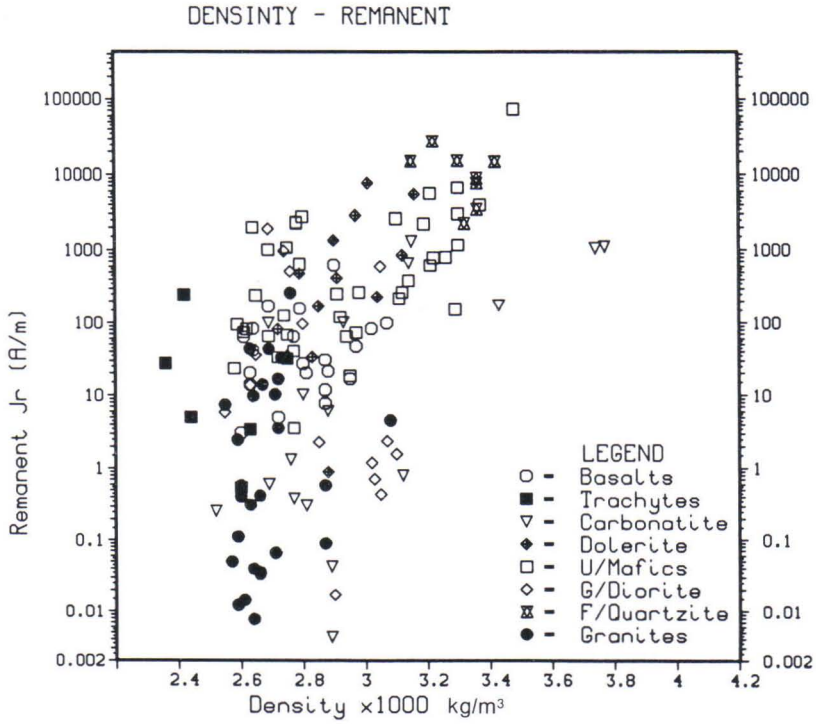
Fig. 12. Correlation diagram between density and remanent magnetization (top), cor-
relation diagram between Q value and susceptibility (bottom).

nent magnetization, Figure 12 bottom show some linear correlation for mafics, ultramafics, and dolerites. The correlation observed between the induced and remanent magnetization may indicate that the same minerals are responsible for the susceptibility and remanent magnetization.

The correlation between the density and remanent magnetization may be attributed to presence of iron oxide minerals which have the effect of increasing both density and remanent magnetization.

Table 8. Summary of Petrophysical Data.

Rock Type	Number of samples	Mean density (kgm⁻³)	K(x10⁻⁶ SI) Range	Q ratio Range
granites	16	2650	169— 3290	0.01— 23.7
gneisses	10	2678	402— 2600	0.01— 23.6
grano/diorite	16	2863	521—20300	0.21—504.0
syenites	8	2663	627—54400	0.59— 60.5
dolerites	10	2917	1560—79300	2.15— 96.7
mafics	23	2925	657—79500	0.39— 88.2
ultramafics	5	3305	5830—84500	1.75—282.0
carbonatites	10	2770	281— 8150	nil— 8.8
carbonatite(ore)	7	3326	681—84500	0.35— 57.4
quartzites(fe)	8	3311	7430—98600	46.32—401.0
basalts	21	2796	2160—87700	0.04— 12.6
trachytes	6	2553	9360—67300	0.02— 3.3
aplite	2	2975	923— 2730	0.19— 0.5
others	3		173— 521	0.01— 3.4

K is susceptibility

SPECTRAL ANALYSIS OF AEROMAGNETIC AND GRAVITY DATA

The spectral analysis has often been used in the interpretation of magnetic data with purpose of determining depths at which magnetic anomalies originate. If the area covered by the magnetic data is large enough the maximum depths obtained from such data will reflect the depth at which the magnetic minerals loose the ability to retain magnetization. This is caused either by high temperatures above the Curie points of the magnetic minerals or by a change in phase from solid to subliquid. In areas with high heat flow, such depths are abnormally shallow. This criteri-

on has been used to delineate areas with high geothermal gradients from aeromagnetic data (Bhattacharrya & Leu, 1975, Connard et al., 1983, Okubo et al., 1985). In the cratons, where geothermal gradients are normal, the maximum depths obtained from spectral analysis correspond to the thickness of the crust.

In the present study spectral analysis of both the magnetic and gravity data have been carried out in effort to determine depths to tops and bottoms of bodies causing magnetic and gravity anomalies.

The Methodology of determining depths from amplitude spectrum

The principles underlying the use of power spectrum in determining average depths to tops and bottoms of magnetic layers have been outlined by several authors Naidu (1969), Spector and Grant (1970), Hahn et al. (1976). The latter utilized the downward continuation of potential data to determine the depth to magnetic sources. Spector and Grant (1970) suggested the method which uses an ensemble of prismatic bodies as a model for calculating the power spectrum of the total field intensity magnetic anomalies. The power spectrum of anomalies due to individual prismatic bodies making an ensemble depends on the depths to top and bottom of the prism, the mean size of the upper faces of the prisms, the inclination and declination of the earth's magnetic field, and finally on the magnetic moment per unit depth.

The spectrum of magnetic or gravity anomaly data is obtained by the Fourier transformation of the data in two dimensions. The discrete Fourier transform of magnetic and gravity anomaly due to a number of prisms given by Bhattacharrya and Navolio (1976) was modified by Ruotoistenmäki (1987) in the form of

$$F(u, v) = C.\exp(-sh_1) - \exp(-sh_2).E \qquad (2)$$

where

$$C = -1/(uvs) \text{ for gravity data,}$$
$$= -1/(uv) \text{ for magnetic data}$$

$$E = \Sigma [(\exp(-iu_1) - \exp(-iu\alpha_2)).$$
$$(\exp(-iv\beta_1) - \exp(-iv\beta_2).P] \qquad (3)$$

The factors h_1 and h_2 are the average depths to the top and bottom of the magnetic layer respectively, u and v are the angular frequencies along the two orthogonal axes along which the data grid is aligned, and s is the radial frequency given by

$$s = \sqrt{(v^2 + u^2)} \qquad (4)$$

The factors α_1, α_2, β_1 and β_2 are the coordinates of the corners of the prism and the summation is for n prisms. The physical factor P is given by

$$p = 2\pi M_o s^{-2} [-lLu^2 - mMv^2 + Nns^2 - a_{12}uv$$
$$+ ia_{13}us + ia_{23}vs] \text{ (for magnetics)}$$
$$= 2\pi G\delta \text{ \{for gravity\}} \qquad (5)$$

where $a_{13} = Ln + Nl$, $a_{23} = Mn + Nm$, $a_{12} = Lm + Ml$, and whereas L, M, and N are the directional cosines of the magnetization vector associated with the sources. The factors l, m, and n are directional cosines of the earth's magnetic field and Mo is the intensity of magnetization depending on the magnetic moment. The values G and δ stand for the universal gravitational constant and density, respectively. If the magnetic field is reduced to the pole, the factor P simplifies to

$$P = 2\pi M_o \qquad (6)$$

From the above equations it is evident that the spectrum may be grouped into the following factors: the frequency factor, depth factor, the thickness factor, the size factor which depends on the horizontal dimensions, and the physical factor. Both the depth and thickness factors depend on frequency and therefore control the shape of the power spectrum curve whereas the physical factor controls the magnitude of the amplitude and is independent of the frequency when the magnetic data is reduced to the pole. The size factor depends on the frequency and hence affects the shape of the spectrum. This effect must be removed from the amplitude spectrum in order to get accurate depth estimates to top and bottom of prisms causing the anomalies. In the method of Spector and Grant (1970), the size effect correction requires the estimate of the size of the prism which in practice is hard to determine. However, Ruotoistenmäki (1987) has shown that after correction of the frequency factor, the effect of the size factor can be assumed constant. The average depth to the top of prisms is then determined from the slope of a plot of the loga-

rithm of the amplitude spectrum against the angular frequency s. In cases where h_2 is much larger than h_1, the equation for corrected amplitude spectrum is then given by

$$\ln | (F/C) | = -sh_1 + \ln | (E) | \qquad (7)$$

and if the average depth to the bottoms is detected, the logarithmic plot will show a peak at frequency S_0 given by (Bhattacharyya, 1966);

$$S_0 = \{Ln \ (h_2/h_1)\}/(h_2-h_1) \qquad (8)$$

Connard et al. (1983), Okubo et al. (1984), and Bhattacharyya and Leu (1975) used equation (8) to determine the depths to the bottoms of magnetic sources. However, depths estimated using equation (8) and the radial averaged power spectrum as suggested by Spector and Grant (1970) have been reported to have several uncertainties

(Shuey et al., 1977, Mantovani & Shulowsky, 1982, and Ruotoistenmäki, 1987).

The method used in this study is that suggested by Ruotoistenmäki (1987) in which the spectrum is corrected for frequency, giving amplitude spectra which are free from size effect, and no reduction to the pole is required. The spectrum is obtained by plotting the natural logarithm of the frequency-corrected amplitude spectrum against the angular frequency in the form of a scatter diagram. The spectrum represented in the scatter diagram can be classified in subspectra whose slopes reflect depths to sources of magnetic anomalies as is shown in Figure 13. According to Ruotoistenmäki (1987a) spectra of this type can reflect also depths to the bottom of sources if they are vertically inhomogeneous: the directions of the upper and lower faces differ and
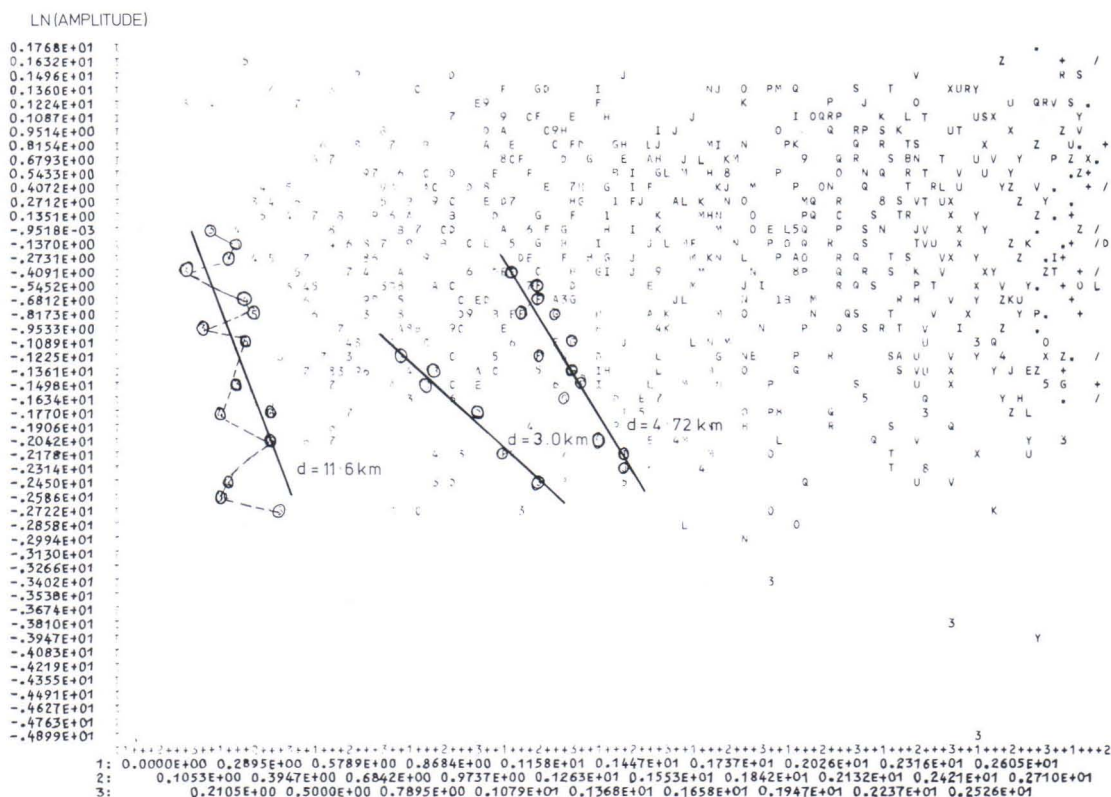

Fig. 13. The scatter diagram for Rukwa2 data window showing three spectras giving spectral depths of 3.0, 4.72 and 11.6 km. The depths are measured with respect to ground level.

physical parameter values increase downwards.

Both aeromagnetic and gravity data were analyzed at the Geological Survey of Finland using the routines developed by Ruotoistenmäki (1987). This method has been tested using theoretical data and observed data from Finland, where spectral depths obtained were found to be in agreement with the calculated depths, and depths obtained from seismic refraction studies (Ruotoistenmäki, 1987).

Analysis of aeromagnetic data

A total of 28 blocks of different size windows were analyzed. The data windows were chosen by considering the homogeneity of the anomaly patterns. The smallest window had dimensions of 55 by 52 covering an area of 54 km by 51 km and the largest window covered the whole study area with a data matrix of 164 by 330. The location of the data windows is shown in Figures 14 and 15.

The results of spectral depth determinations from the scatter diagrams are presented in Table 9, from which it was found that the depths range from 0.50 km to a maximum of 18 km. These results may be classified into shallow depths ranging from 0.50 to 4.0 km, intermediate depths lying between 4.0 km to 10 km, and spectral depths exceeding 10 km were classified as great depths.

These spectral depths are interpreted as depths to the top and bottom of magnetic bodies, caused by vertical variations in susceptibility, which form horizontal geological boundaries within the earth's crust. Comparison of the geology and spectral depths show some correlation as most shallow spectral depths are observed in blocks with mafic intrusives and high grade metamorphics, some of which are outcropping and give rise to high amplitude magnetic anomalies. Figure 16 shows the distribution of shallow depths from which it is observed that, the most shallow depths (< 1 km) are found in the southwestern and southern central data windows (Ufipa, Mbozi, Itumba, Mbalizi and Msangano). The spectra for blocks where the basement is covered with sediments or the exposed basement rocks are predominantly granitic in composition, generally show relatively higher shallow depths compared to areas covered with metamorphics and volcanics. Blocks where basement rocks are covered with sediments include Rukwa, Rukwa2, Mbeya, Buanji, and Ukinga. The shallow spectral depths observed in these windows range from 1.60 to 4.0 km.

The blocks of Chunya, Shoga and Buhoro with granitic basement rocks exposed to the surface, show shallow spectral depths in the order of 1.40 km to 3.0 km. The data windows covering the Rukwa trough (Rukwa2, Rukwa, and Galula) have shallow and intermediate depths ranging from 1.60 km to 8.0 km. The depth of 8.0 km corresponds to the depth of 7 km obtained by Peirce & Lipkov (1988) by gravity modelling as the maximum thickness of sediments in the Rukwa trough. In these blocks, the shallow and intermediate spectral depths may correspond to depths to the crystalline basement. In the southeast, the Buanji and Ukinga blocks, shallow and intermediate depths ranging from 2 km to 4.72 km were observed. The basement in these blocks is covered by the Ukingan metasediments whose thickness is unknown and the Buanji sediments with a thickness estimated at 1080 m (Harpum & Brown, 1958). The spectral depths in the two blocks may also be considered to represent the combined thickness of the Ukingan metasediments and the Buanji sediments and therefore the spectral depth of 4.7 km may be considered to be the maximum thickness of the combined two series.

The Ufipa block shows a different pattern from the rest of the blocks by giving a maximum depth of 2.1 km and minimum depth of 1.69 km.
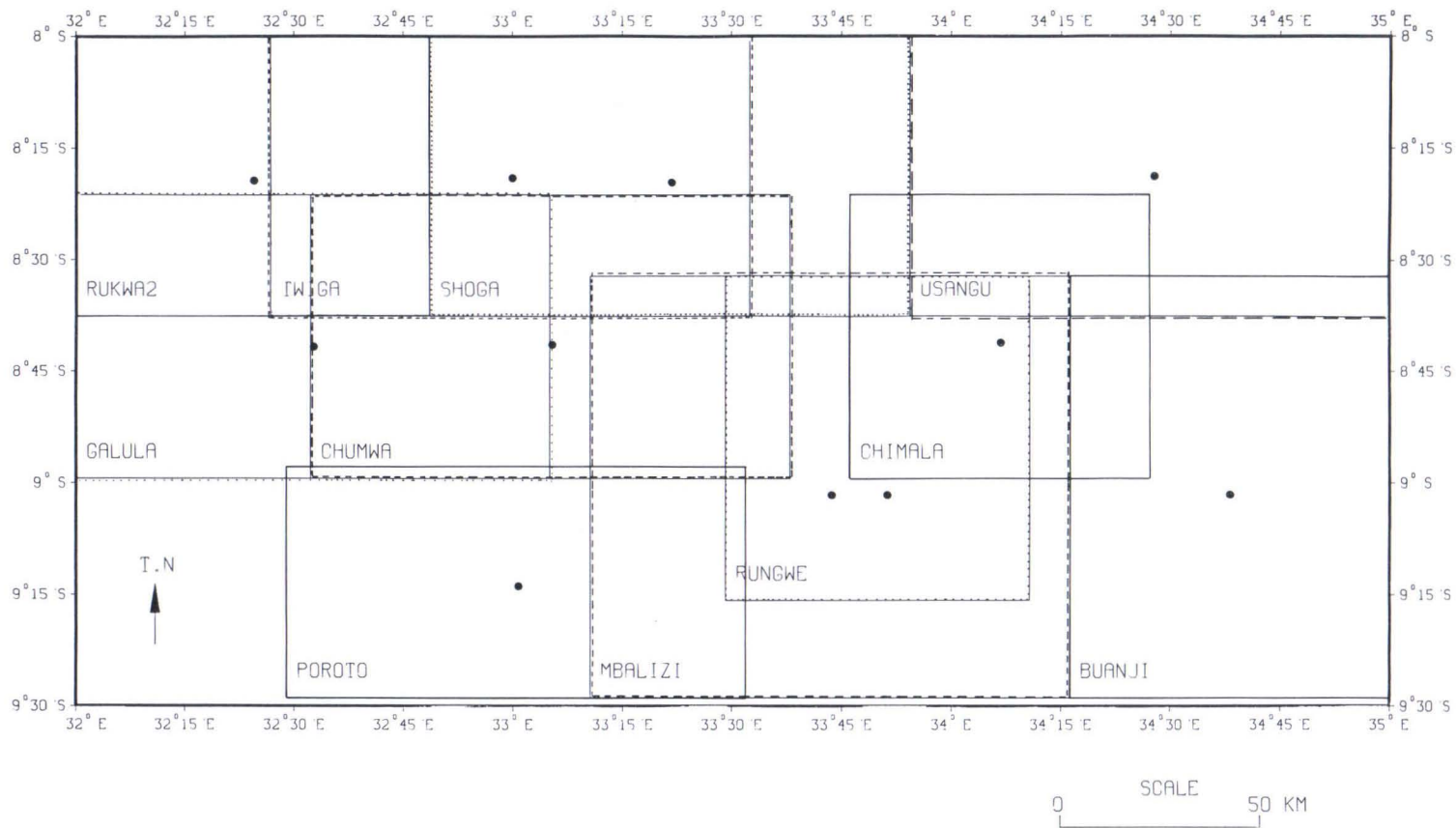
Fig. 14. Distribution of large data windows used in spectral analysis. The name of each window is written in the lower left corner.
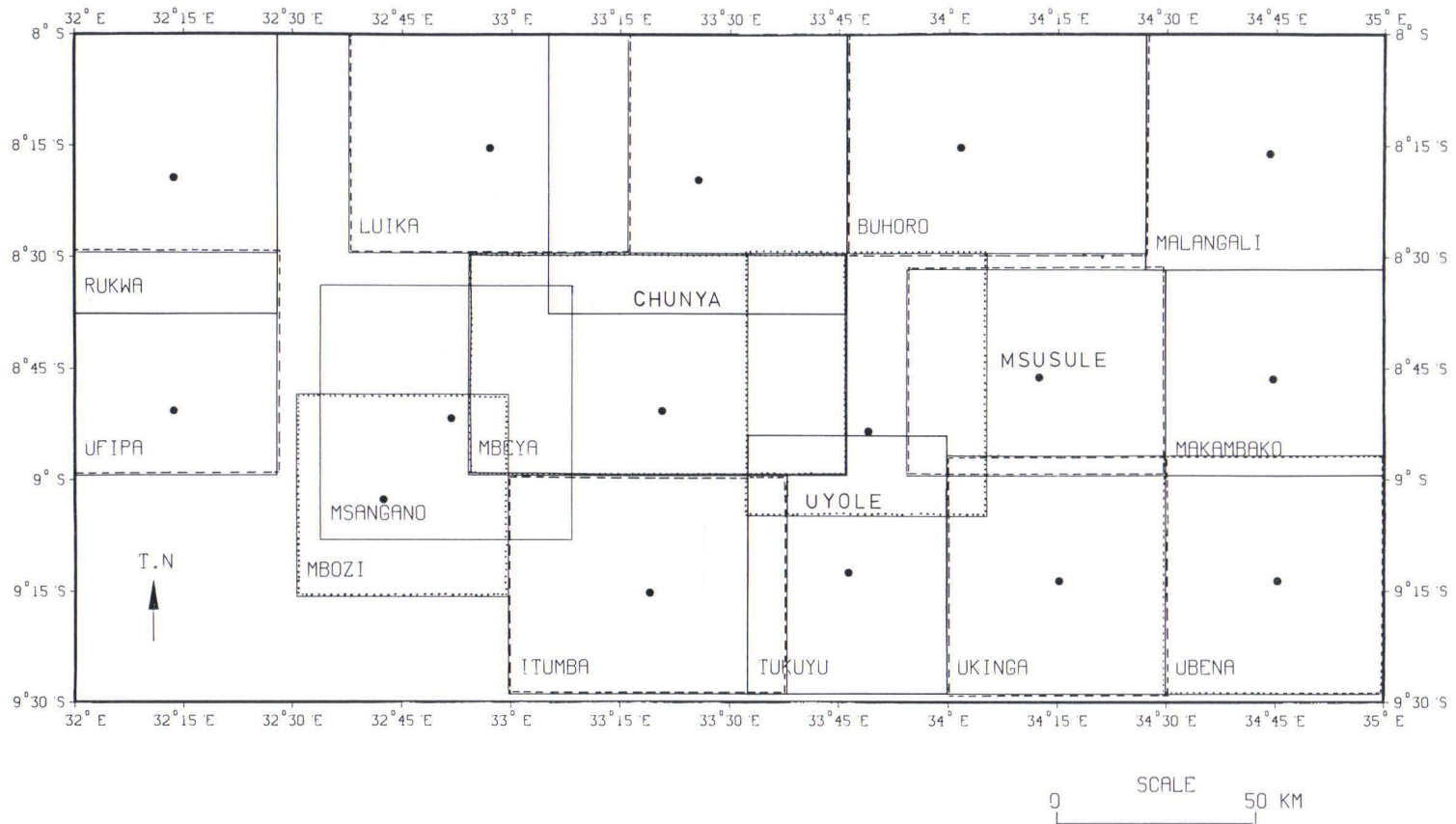
Fig. 15. Distribution of small data windows used in the spectral analysis. The name of the window is written in the lower left corner except Chunya, Msusule and Uyole.
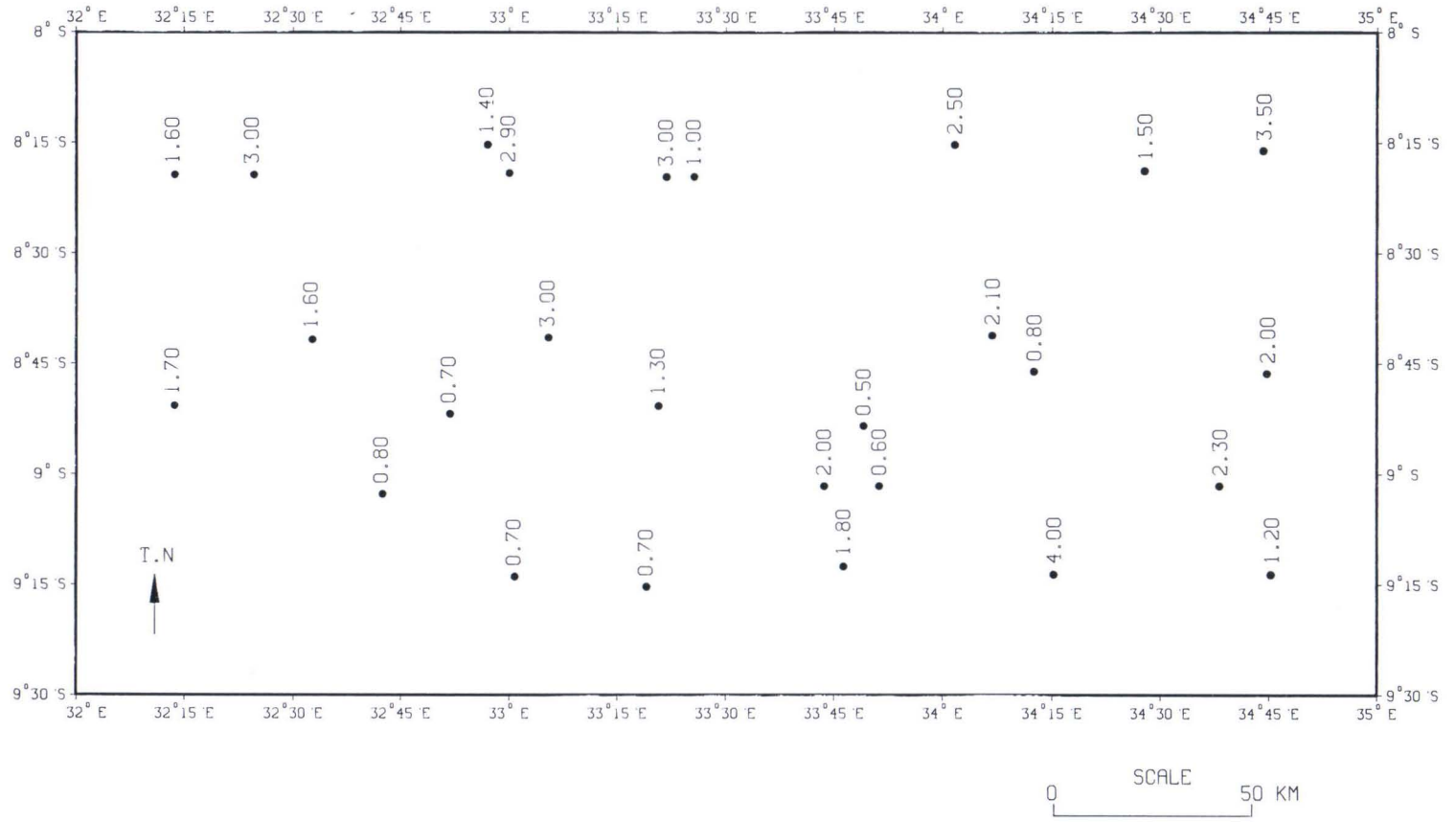
Fig. 16. The distribution of shallow spectral depths, showing a minimum of 0.50 km in Uyole data window and a maximum of 4.0 km over the Ukinga data window.
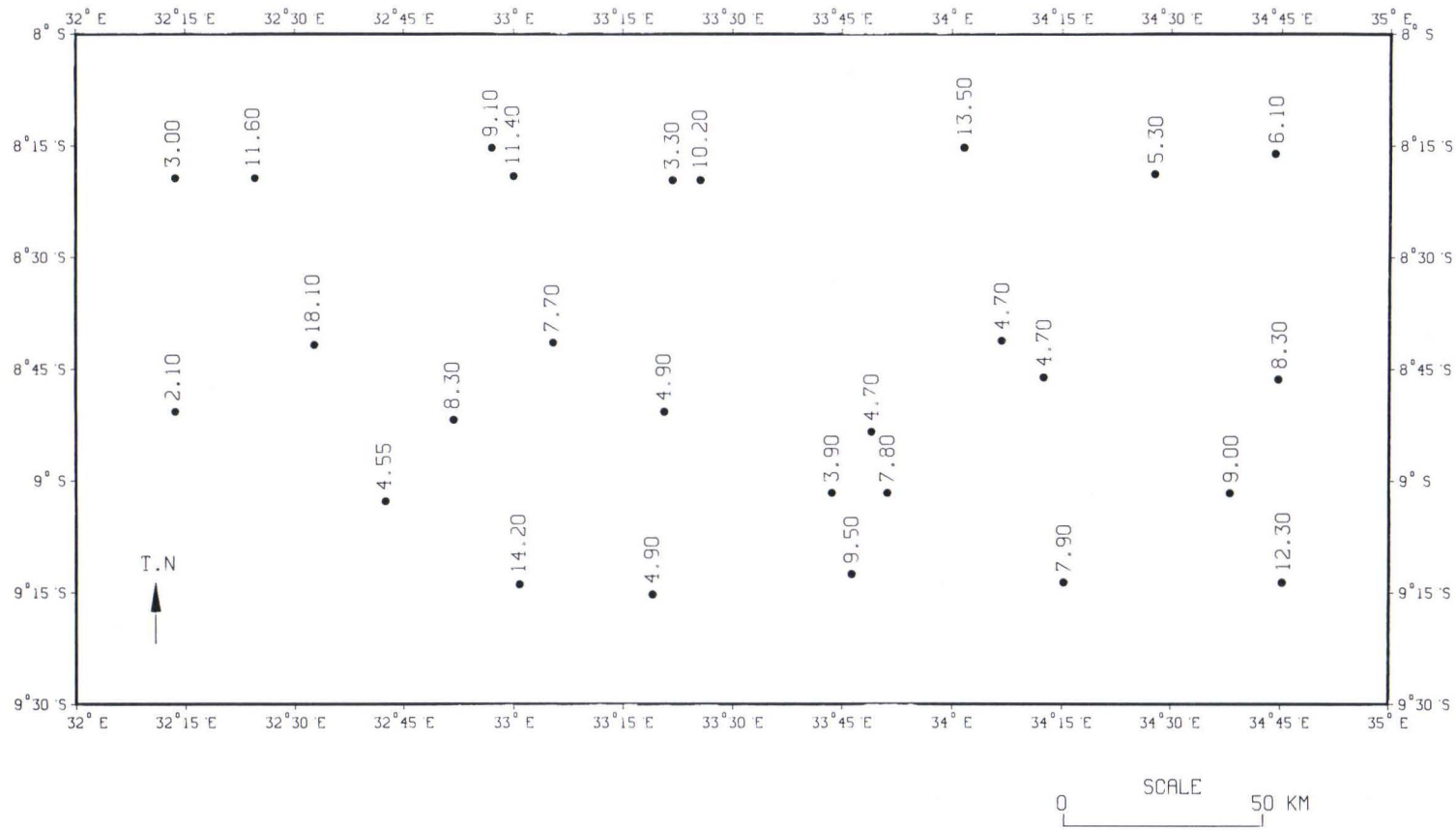
Fig. 17. The distribution of the deepest spectral depths obtained from each data window. A maximum depth of 18 km is observed in the spectrum of the Galula data window while a minimum of 2.10 km was obtained from the spectra of the Ufipa data window.

The spectral depths observed here reflect the top of the magnetic bodies with their bottoms extending at deeper depths which are not detected by the spectral analysis.

The spectral window (SWTAN) covering the whole area shows depths of 1.56 km to 5.4 km. The maximum spectral depths are given in Figure 17 where it is observed that the spectral win-

Table 9. Results of spectral depths.

name of window	dimensions				window size in km	depths (km)		
	N1	N2	M1	M2				
swtan	1	164	1	330	163 × 329	1.56	2.33	2.85
						4.53	5.40	
Rukwa2	1	70	1	90	69 × 89	3.00	4.72	8.08
						11.60		
Shoga	1	70	90	210	69 × 120	2.99	3.30	
Twiga	1	70	50	170	69 × 120	2.90	4.94	5.32
						11.40		
Usangu	1	70	210	330	69 × 120	1.50	2.08	3.0
						5.27		
Galula	40	110	1	120	70 × 119	1.63	2.50	6.20
						18.13		
Mbalizi	60	164	130	250	104 × 120	1.96	2.90	3.94
Chumwa	40	110	60	180	70 × 120	2.99	3.10	7.73
Chimala	40	110	195	270	70 × 75	2.10	4.32	4.74
Poroto	107	164	54	169	57 × 115	0.66	2.66	3.07
						11.06	14.15	
Buanji	60	164	250	330	104 × 80	2.30	3.00	8.94
Rungwe	60	140	164	240	80 × 80	0.57	2.58	3.08
						7.84		
Rukwa	1	70	1	52	69 × 51	1.58	2.32	2.99
Luika	1	55	70	140	54 × 70	1.44	3.28	6.98
						9.10		
Chunya	1	70	120	195	69 × 75	1.00	1.75	6.10
						7.99	10.22	
Buhoro	1	55	195	270	54 × 54	2.46	7.04	13.49
Malangali	1	59	270	330	58 × 59	3.48	3.56	6.07
Ufipa	55	110	1	52	55 × 51	1.69	1.73	1.90
						2.1		
Msangano	63	126	63	126	63 × 63	0.67	2.10	4.10
						6.90	8.25	
Mbeya	55	110	100	195	55 × 95	1.28	2.98	4.87
Uyole	55	120	170	230	65 × 60	0.51	0.97	1.10
						1.89	4.68	
Msusule	59	110	210	275	51 × 65	0.79	1.30	1.68
						2.36	4.72	
Makambako	59	110	275	330	51 × 55	1.98	2.57	3.23
						3.77	8.30	
Itumba	110	164	110	180	54 × 70	0.66	1.89	2.30
						4.49	4.92	
Mbozi	90	140	57	110	50 × 53	0.76	2.17	3.92
						4.54		
Tukuyu	100	164	170	220	64 × 50	1.80	2.30	9.40
						9.53		
Ukinga	105	164	220	275	59 × 55	3.97	4.32	5.12
						7.87		
Ubena	105	164	275	330	59 × 55	1.20	2.30	2.57
						12.28		

dows in the central part namely Chimala, Uyole, Mbeya, and Mbalizi show maximum depths of 4.74 km, 4.68 km, 4.87 km, and 3.9 km, respectively. This group of depths is also observed in other blocks adjacent to the central blocks (Table 9). The crystalline basement in this block is overlain by volcanics and lake sediments and therefore the spectral depths observed may indicate the average depth to the bottom of intrusive bodies in the area. The Rungwe and Tukuyu data windows covering areas overlain by volcanics show maximum spectral depths of 7.84 km and 9.53 km, respectively. The maximum spectral depth of 18 km is observed in the Galula data window which includes part of the Rukwa and Msangano troughs. The Itumba window in the south show a maximum spectral depth of 14 km. Both Galula and Itumba data windows lie within the uplifted Mbozi block.

The results also indicate a group of spectral depths ranging between 7.0 to 13.5 km and is observed in most spectral data windows. In the north this group of spectral depths is observed between 8.00 km in the Chunya block to 13.5 km in the Buhoro block in the northeast, as is shown in Figure 17 and Table 9 above. This depth group is also observed in some of the adjacent windows in the south. The Galula and Msangano blocks show depths between 8.25 to 12.40 km. In the southeastern data windows, this group of depths is observed between 7.84 and 12.28 km with the

Ubena showing the deepest. In many of the spectral windows this depth is the maximum spectral depth detected except for a few windows covering the Rukwa trough area.

Assuming that this method detects magnetic discontinuities within the crust, it can be concluded that spectral depths obtained correspond to discontinuities in the earth's crust brought about by changes in the chemical composition of rocks or physical changes due to high geothermal gradients in the crust. The shallow spectral depths in each of the data windows were interpreted as depths to top of the bodies causing the high frequency anomalies analyzed. Depending on the local geology, the depth to the top of the magnetic bodies may correspond to depth to crystalline basement or depths to top of intrusive bodies. The intermediate and maximum depths may represent lithological discontinuities within the crust. The interpretation of the spectral depths is complicated by the geology of the area and the big variations of thickness of sediments in the study area. In the Rukwa basin the sediments are thick and therefore the intermediate depths in this area correspond to the thickness of sediments whereas in areas with exposed basement rocks such depths of 7 km correspond to lithological discontinuities within the crust. The maximum depth of 18 km may correspond to the thickness of the crust.

Analysis of gravity data

The gravity data of the Rukwa basin, covering an area lying between 8° to 9° S and 32° to 33°30′ E was gridded at a spacing of 2.5 km using DISSPLA subroutines BGNMAT, GETMAT and ENDMAT (DISSPLA, 1985). The original data along profiles was first used to grid the data at a square grid of 5.0 km by 5.0 km. The newly interpolated data together with the original data were then used to produce data at a grid of 2.5 km by 2.5 km producing a data matrix of 47 rows

by 67 columns. The gravity data is presented in Figure 18 below in the form of a contour map, in which the major feature is the negative anomaly corresponding to the lake basin. The structural interpretation of gravity data along profiles has been covered by Peirce and Lipkov (1988).

The gravity data was analyzed using the method described above for aeromagnetic data. Due to small data matrix, the whole data was analyzed as a single data window. The scatter diagram ob-
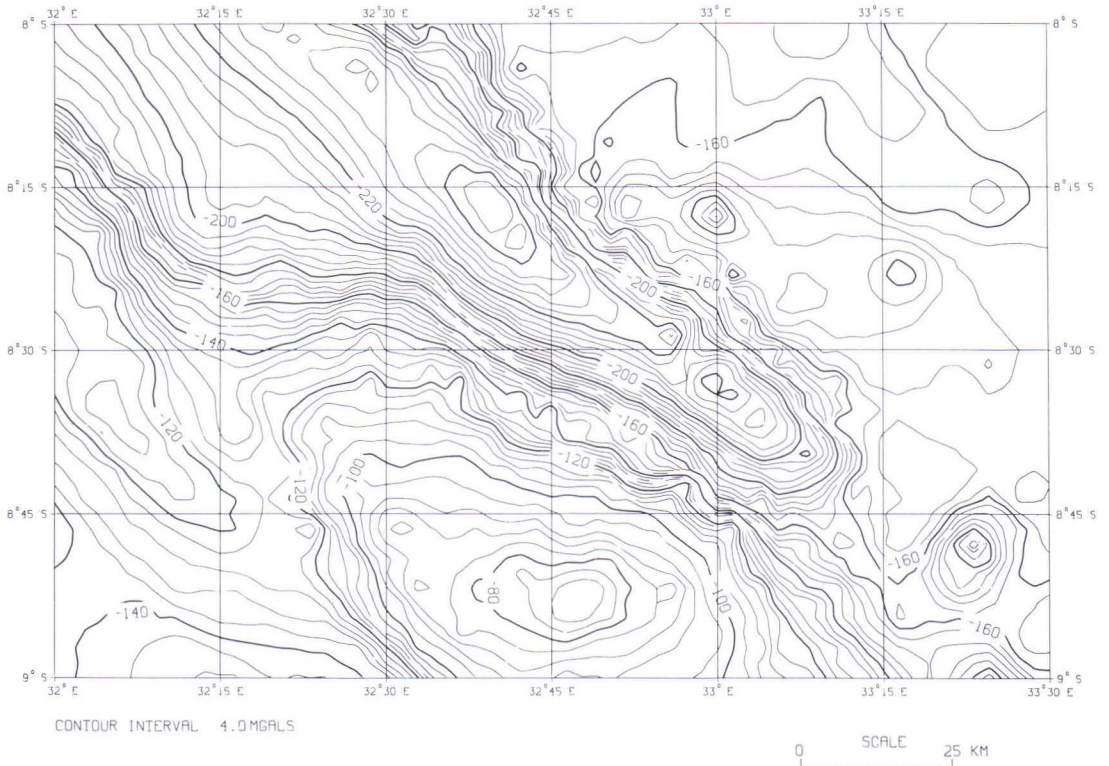
CONTOUR INTERVAL 4.0 MGALS

Fig. 18. The Bouguer gravity anomaly map of Rukwa basin presented in contours. The gravity data used to produce this map was used in the spectral analysis.
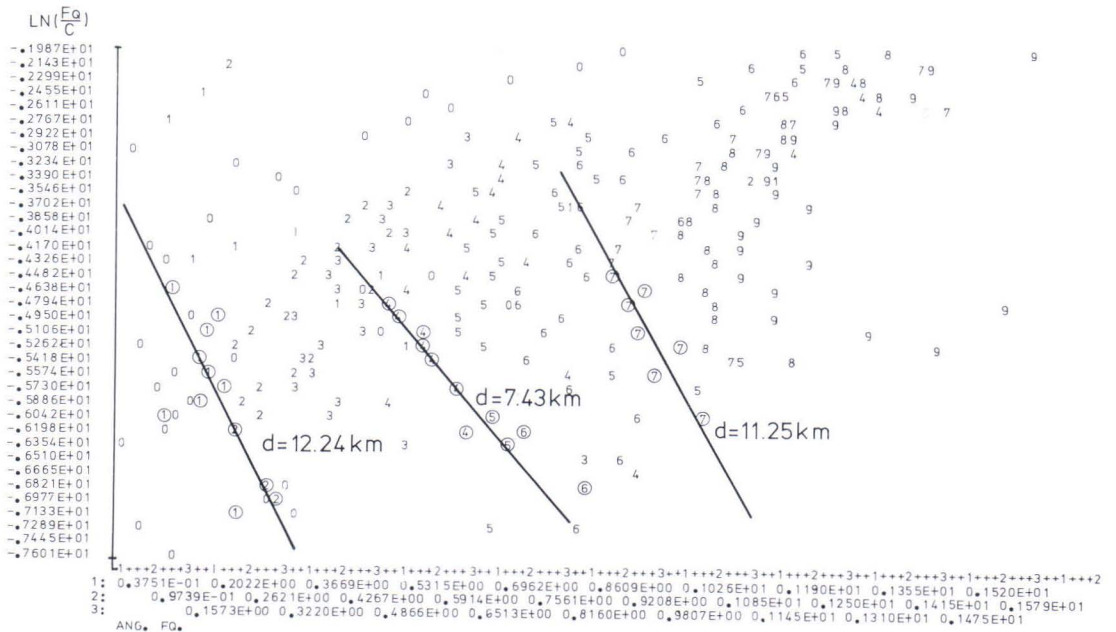

Fig. 19. The scatter diagram obtained in the spectral analysis of gravity data.

tained is presented in Figure 19 from which three spectra were detected. The depths calculated from the spectras are 7.43 km, 11.25 km, and 12.24 km. The middle spectra of depth 7.43 km as can be seen in Figure 19, is the best spectra as most of the points forming the spectra lie close to the fitted line and are composed of medium frequencies.

The spectral analysis has given depths which are assumed to reflect density discontinuities giving rise to gravity anomalies. The spectral depth of 7.43 km obtained from analysis of gravity data agree with the depth of 8.0 km obtained from spectral analysis of magnetic data of the Rukwa2 data window and with the maximum thickness of 7.0 km of sediments in the Rukwa trough obtained by 2-dimensional modelling using a sandstone model (Peirce & Lipkov, 1988). The deeper depths of 11.25 km and 12.24 km correlate with spectral depths ranging from 10.2 to 11.6 km obtained from analysis of magnetic data windows of Rukwa2, Twiga, and Chunya.

Summary and discussion

The gravity data covers only a small portion of the study area, from which depths determined from both two sets of data may be compared. In the northwestern magnetic data windows (Rukwa, Rukwa2, Galula, Luika, and Msangano) shallow and intermediate spectral depths ranging from 3 km to 9 km are observed. Some of these depths may be interpreted as depths to basement whereas others correspond to lithological boundaries within the basement rocks.

The spectral analysis of gravity data has demonstrated that spectral depths correspond to depths interpreted by modelling of gravity anomalies. Comparison of spectral depths determined from gravity and those from magnetics shows some correlation. Spectral depths of 8.08 km and 6.20 km determined from Rukwa2 and Galula magnetic windows respectively are comparable with a depth of 7.43 km determined from gravity. In addition the spectral depth of 11.6 km is also detected in the analysis of magnetic data of the Rukwa2 window which correspond to the depths of around 11 to 12 km obtained from gravity data.

The maximum spectral depths of 14 km and 18 km obtained from analysis of magnetic data are observed in the Mbozi block which is an up-lifted block between the Msangano and Songwe troughs. Such depths may suggest an anomalous material within the uplifted block of Mbozi. Seismic refraction and gravity studies done in the Gregory Rift Valley in northern Tanzania and Kenya have shown crustal discontinuities which are in the range of the spectral depths obtained here. The depth of 18 km is comparable to the thickness of 19 to 20 km of the crust in Gregory Rift in Kenya determined from gravity and seismic refraction studies (Searle, 1970, Griffiths et al., 1971). Rykonouv et al. (1972), using micro-earthquake studies, estimated the thickness of the upper crust to be 18 km in the Gregory Rift in northern Tanzania. Griffiths (1972) working in L. Baringo area in Kenya, observed seismic velocity discontinuities at a depth of 3 km and 10 km which were interpreted as depths to the bottom of volcanics and the top of an axial intrusion of basic magma respectively. The spectral analysis of data windows covering the Rungwe volcanic area (Tukuyu, Rungwe, and Uyole) show shallow spectral depths of 2 to 3 km and deeper depths ranging from 7 km to 9.5 km which show similarity with seismic velocity discontinuities observed in the L. Baringo area.

INTERPRETATION OF MAGNETIC ANOMALIES

The aeromagnetic map of the study area (Figure A2) shows several isolated magnetic anomalies which can be interpreted individually to determine the parameters of the causative bodies. Most of the magnetic anomalies observed in this area are related to mafic rocks intruding basement rocks. Other anomalies occur in areas where the basement rocks are overlain by sediments and the interpretation of such anomalies may indicate the thickness of sediments overlying the causative bodies. The anomalies covered in this section were interpreted using an optimization algorithm suggested by Marobhe (1989a) in which prism, dyke and buried slope models were used. The algorithm is briefly outlined below.

Optimization of magnetic anomalies

The optimization method was used for interpretation of magnetic anomalies using prism, dyke, and buried slope models. The total magnetic field anomaly caused by a uniformly magnetized dyke of infinite strike length or a buried step model of uniform thickness and magnetized by induced field has been given in general form (Gay, 1967) as

$$\Delta T = 2kTh^2 Sin\beta\{sin(2I-\beta)\Delta\phi - cos(2I-\beta)Ln\Delta R\} + T_o \qquad (9)$$
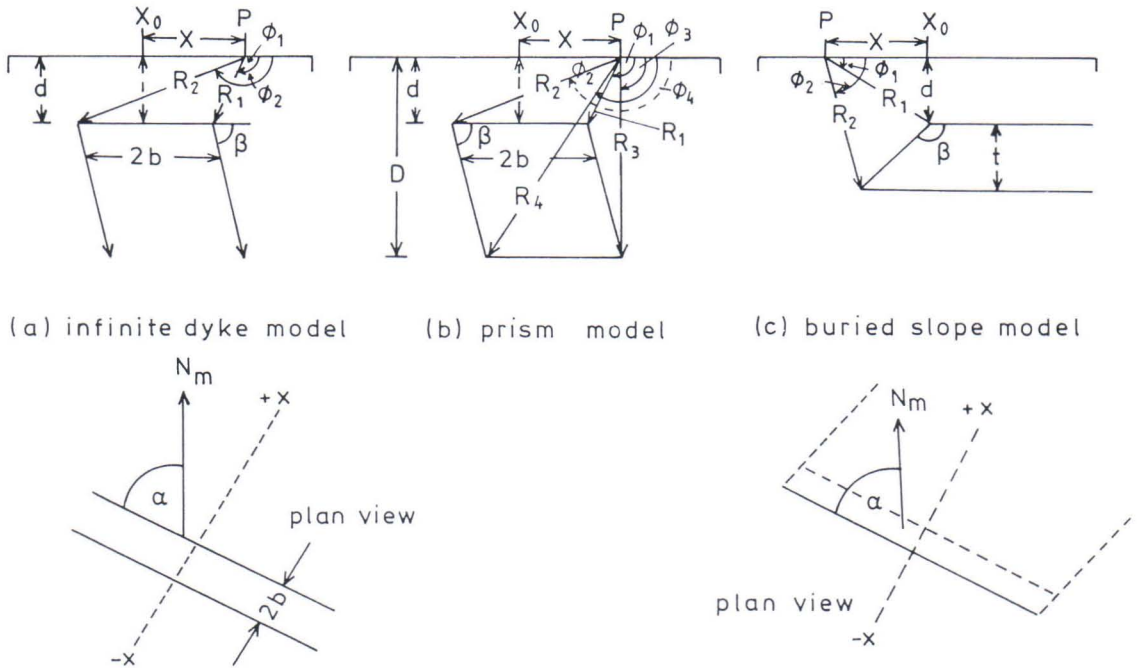
where some of the symbols are illustrated in Fig-

(a) infinite dyke model   (b) prism model   (c) buried slope model

Fig. 20. Geometry of models and nomenclature. N_m is the magnetic north and α is the strike angle measured anticlockwise from magnetic north.

ure 20 and some are explained in Table 10. The anomaly due to prism model is determined by calculating the anomalies of two similar dykes with tops lying at depth d and D below the plane of observation and D > d. The center of the deep seated dyke is given with respect to the center of the upper dyke as

$$x' = x_o + (D-d)\cot\beta \qquad (10)$$

The parameters to be optimized include the depth d to the top of the model, the half width b of dyke or prism model or thickness t of the step model and the horizontal location x_o of the center of the dyke and prism or the top of the upper corner of the step model. Other parameters are intensity of magnetization, the angle of dip β, the datum level T_o, and in the case of the prism model the depth to the bottom of the prism D measured from the plane of observation.

The algorithm used to determine the parameter vector change combines singular value decomposition and least squares solution (Marobhe, 1989a). The inversion process is started by giving the initial estimate of the parameters to be optimized from which the model response is calculated using equation (9). The sum of squares of the residual between the observed and the calculated anomalies is then minimized by changing the parameters of the model. The change in the parameter vector is determined from the residual vector and partial derivatives of the function with respect to the parameters to be optimized. If the model response is a linear function of the parameters, the relationship between the observed F_o, the calculated F_c, and the parameter vector change ΔP is given by

$$F_o(x_i) \approx F_c(x_i) + \sum_{j=1}^{n}(\frac{\partial F_c(x_i)}{\partial P_j}) (P_j^o - P_j) \qquad (11)$$

the second term on the right represents partial derivatives with respect to the j-th body parameter of the n parameters making the vector parameter P. The vector P_o contains the initial model parameter estimate and P is the parameter vector required to minimise the residual. In this particular case the model response is a nonlinear function of some of the body parameters and therefore equation (11) will hold only if high orders including second order derivatives are neglected. Using matrix notation the parameter vector change ΔP is given by

$$\Delta P = A^+ Y \qquad (12)$$

where A^+ is a generalized inverse of a rectangular matrix A with m rows and n columns containing partial derivatives of the model response with respect to parameters to be optimized. The vector Y is a column vector containing the residual between the observed and calculated anomalies. The generalized inverse (Lines & Treitel, 1984) of a rectangular matrix A is given by

$$A^+ = (A^T A)^{-1} A^T \qquad (13)$$

or alternatively the inverse may be accomplished by using singular value decomposition (Golub & Reinsch, 1970, Nash, 1979, Lines & Treitel, 1984) by which the matrix A is factorized into three matrices given by

Table 10. List of symbols.

I	= arctan(tani/sinα).
i	= inclination of earth's field (—90° to + 90°).
β	= dip of dike or slope measured from positive x-axis in degrees (0° to 180°).
α	= angle of strike in degrees measured anticlockwise from magnetic north.
T	= earth's magnetic field strength in nT
T_o	= datum level in nT
Nm	= Magnetic North
k	= susceptibility contrast (SI)
h^2	= $1-\cos^2\alpha\cos^2 i$
$\Delta\phi$	= $\phi_1 - \phi_2$
ΔR	= R_1/R_2

for dyke model

ϕ_1	= arctan((x-b)/d)
ϕ_2	= arctan((x+b)/d)
R_1	= $\sqrt{(d^2 + (x-b)^2)}$
R_2	= $\sqrt{(d^2 + (x+b)_2}$

for slope model

ϕ_1	= arctan(x/d)
ϕ_2	= arctan([x-t cotβ]/(d + t))
R_1	= $\sqrt{(x^2 + d^2)}$
R_2	= $\sqrt{([x-t cotβ]^2 + (d + t)^2)}$

$$A = VSU^T \tag{14}$$

where the matrices V, S, and U have been defined (Lines & Treitel, 1984) as follows: V is n by n matrix consisting of orthonormal eigenvectors of $A^T A$ as columns so that $VV^T = V^T V = I$, and where I is the identity matrix of n by n. U is m by m matrix containing orthonormal eigenvectors associated with the largest eigenvectors of matrix AA^T which can be chosen to be of unit length, so that $UU^T = U^T U = I$ where I is the identity matrix of dimension m by m. S is m by n diagonal matrix with non negative elements along the diagonal, which are called singular values. Using this approach the generalized inverse of matrix A is given by

$$A^+ = VS^+ U^T \tag{15}$$

which has been shown by Lines and Treitel (1984) to be equivalent to equation (13).

Lines and Treitel (1984) suggested the addition of Marquardt's damping factor on the diagonal matrix, thus giving the modified matrix S^{++} as

$$S_{jj}^{++} = \tau_j / (\tau_j^2 + \sigma) \tag{16}$$

where τ_j is the j-th diagonal element of matrix S and σ is the Marquardt's damping factor.

The compact algorithm suggested by Nash (1979) was used in this study to decompose the matrix of partial derivatives into singular values which are used to determine the parameter vector change.

The partial derivatives for slope and dyke models used in the algorithm were derived from equation (9) with respect to model parameters to be optimized and those of prism model were obtained from the derivatives of two similar dykes with tops lying at depth d and D.

In applying the algorithm it was found that the solution ΔP so obtained has to be smoothed to avoid divergence and the change in parameters must be constrained (Marobhe, 1989a). The interpreter is required to give the minimum and maximum of each parameter within which the parameter is allowed to vary.

The algorithm which incorporates Marquardt's damping factor into singular values and smoothing factors was programmed in Turbo-Pascal (Marobhe, 1989b) in which the parameter vector change required to minimize the sum of squares of the residual was determined iteratively.

The program was used in this study to interpret some of the anomalies assumed to be caused by dyke, prism or buried slope models. In addition a similar algorithm for a vertical prism model of finite strike length was also programmed to interpret anomalies of limited strike length.

The interpretation of anomalies using a two-dimensional polygon model was done using trial and error methods. The algorithm used to calculate the total magnetic field using such polygon model was that suggested by Won and Bevis (1987). The algorithm was programmed in Turbo-Pascal and its accuracy was checked using the polygon model example given by Johnson (1969).

Interpretation of individual anomalies

Most of the anomalies interpreted in this study are caused by deep seated bodies and therefore their susceptibility and nature of remanent magnetization are not known. In addition the anomaly shapes shown by most of the anomalies conform to anomaly shapes caused by induction by earths magnetic field in the southern hemisphere.

The ambient magnetic field in the area is around 33500 nT and the angle of inclination is estimated at —35°, whereas the declination in 1980 was 3°26' west of grid north. The angle of strikes measured from the grid north were corrected for the declination prior to interpretation.

The Kipengere anomaly

The Kipengere anomaly shown in Figure 21, is a high amplitude negative anomaly trending NW-SE with a strike angle varying from N54°W in the northwest to N31°W in the southeast. In the NW the amplitude is about 230 nT and the main anomaly has an amplitude of the order of 900 to 1000 nT. The basement rocks in this area are known to be overlain by both the metasedi-

ments of the Ukingan orogeny and the Buanji continental sediments. These rocks have been so intensely folded that they form overfolds and thrusts. The sediments have been intruded by dolerite dykes trending NNE-SSW (Harpum & Harris, 1958). The anomaly lies along a north-westerly lineament which partially corresponds to the Gofio thrust.

The Kipengere anomaly is interpreted here with the assumption that it is caused by a thick intru-
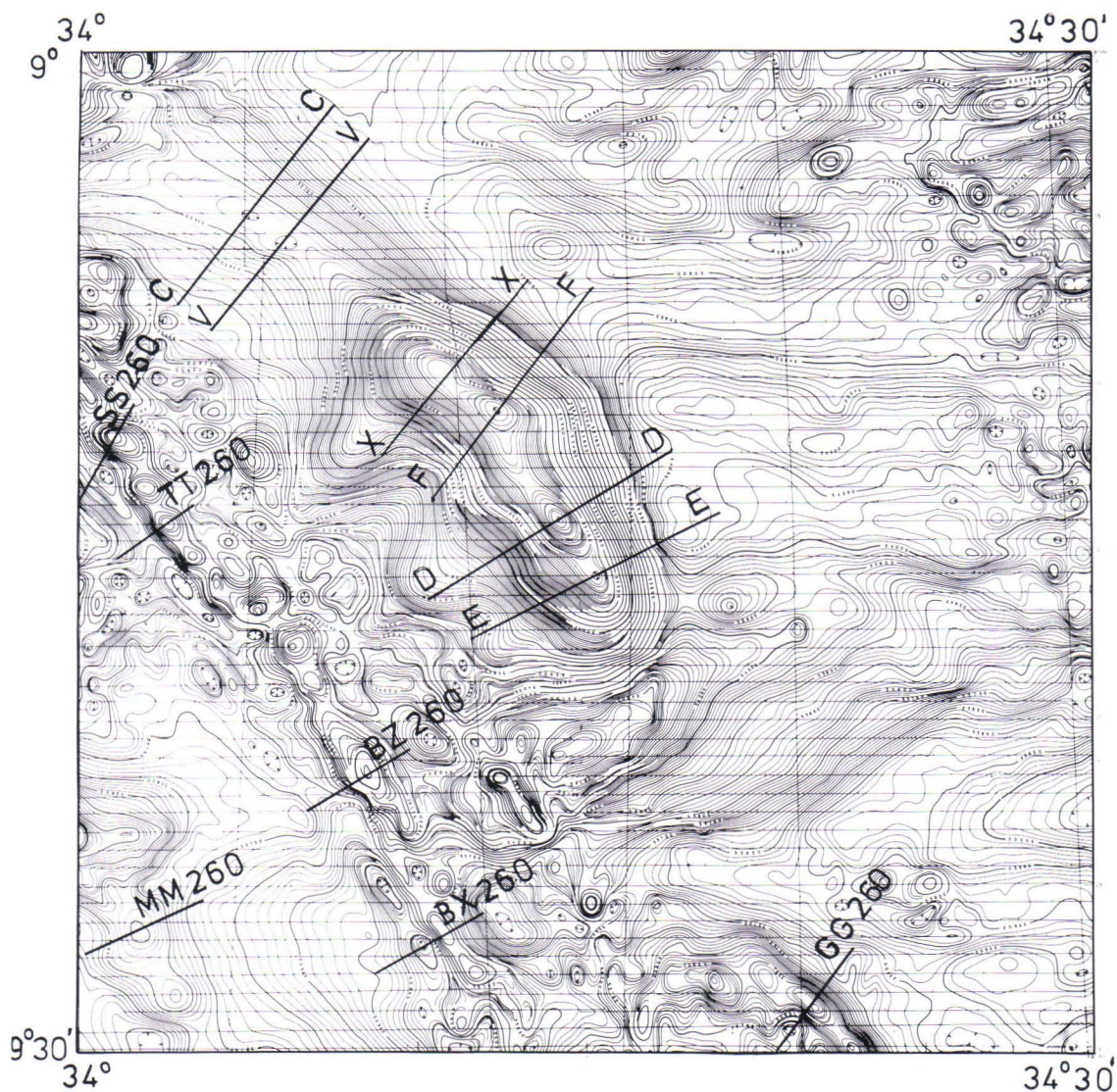
Fig. 21. Aeromagnetic map of QDS260 showing profiles across Kipengere and Upangwa anomalies.
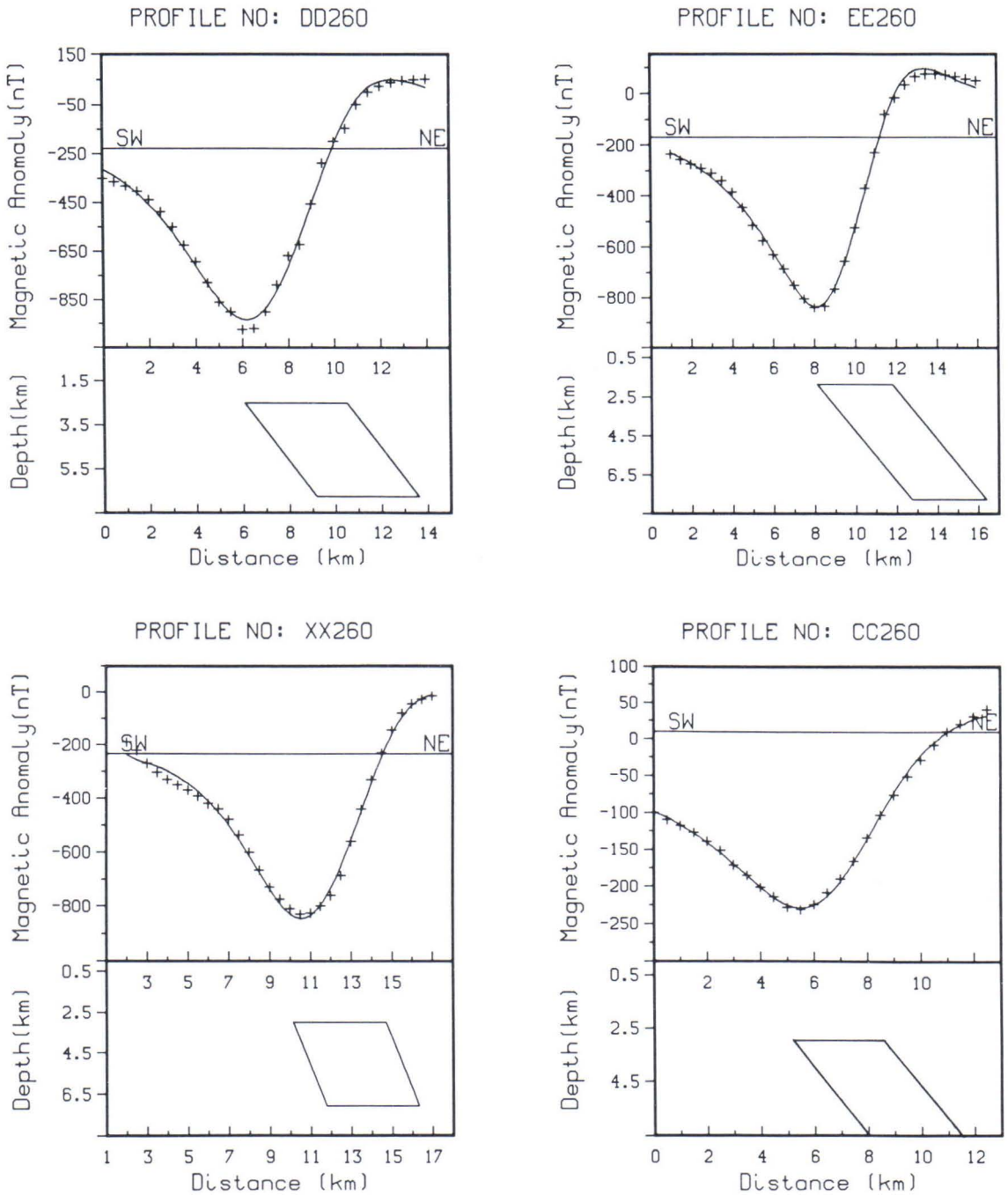
Fig. 22. Showing calculated and observed profiles of optimum models of some of the profiles across the Kipengere Anomaly. The observed values are represented by the (+) and solid line represent the calculated curves.

sive body within the basement rocks. However, it is also possible that this body intrudes the overlying sediments as there is evidence of gabbro and dolerite dykes intruding the Buanji sediments.

A total of six profiles, shown on the anomaly map Figure 21, perpendicular to the strike, were manually digitized from the original aeromagnetic map. The two profiles, CC260 and VV260 were interpreted using dyke model, whereas for the rest of the profiles, the prism model was used in the interpretation. The shapes of the anomaly profiles suggest that a body causing the anomaly is dipping towards the NE. The results of the interpretation are summarized in Table 11 where the parameters giving the best models for each profile are tabulated. Four of the profiles interpreted with the optimum models are shown in Figure 22.

The top of the body causing the anomaly lies between 1.85 to 3.30 km below the ground surface. The depths may reflect the maximum total thickness of the Ukingan metasediments and the Buanji sediments, if it is assumed that the body causing the anomaly is intrabasement or minimum thickness if the body intrudes the sediments. The estimate of the thickness of sediments is complicated by the folding and overthrust they have suffered and therefore the depths obtained above may not reflect the exact thickness of the sediments overlying the intrusive body. The depth to bottom ranges from 6.78 km to 8.58 km which correlate with deeper depths obtained from spectral analysis of the Ukinga data window (Table 9). The body dips towards the northeast with dip

angles ranging from 51° to 65°. The intensity of magnetization ranges from 175 nT to 1010 nT. Considering the ambient field in the area to be 33800 nT, the effective susceptibility contrast calculated from the intensity of magnetization obtained ranges from 5.1×10^{-3} SI to 30.0×10^{-3} SI units. The high susceptibility contrast suggests that, the cause of the anomaly may be an intrusive rock, probably of mafic to ultramafic composition.

The Upangwa anomalies

The Upangwa anomalies lie west of the Kipengere anomaly and strikes in the NW-SE. The anomalies are observed in an area where ultramafic to mafic intrusives and meta-anorthosites have been mapped. Some of the mafic rocks consist of lenses of magnetite, and geochemical anomalies of nickel, cobalt, and copper have been reported in the area (Harpum & Harris 1958). Some anomalies are observed in areas covered with mylonites of the Nyasa shear zone, but these occur as smooth anomalies which suggest deep-seated bodies as sources of the anomalies.

Quantitative interpretation of some profiles digitized across the anomalies were done using optimization methods in which the prism model was used. The results of the interpretations of profiles shown in Figure 21 above, are given in Table 12. The high magnetization ranging from 129 nT to 599 nT suggest bodies of high effective susceptibility.

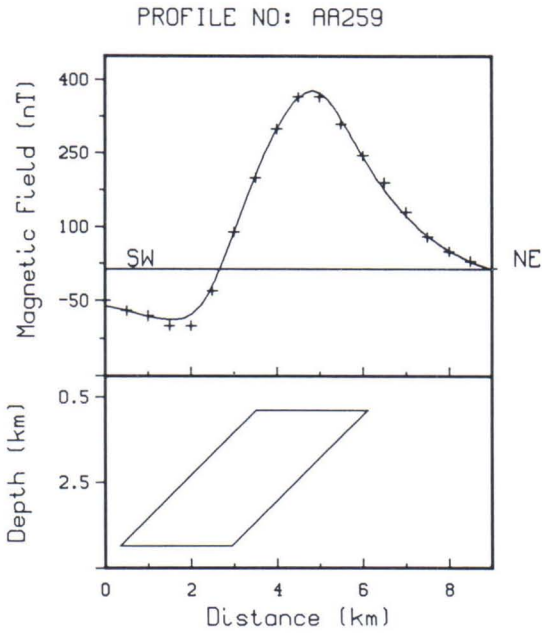Table 11. Interpretation results of the Kipengere anomaly.

profile	d(km)	D(km)	W(km)	Dip	KT(nT)
CC260	2.71	—	3.72	51°	183.5
VV260	2.41	—	3.37	53°	173.5
XX260	2.95	7.24	4.77	65°	628.6
FF260	3.15	8.58	4.04	53°	883.8
DD260	2.49	6.79	4.48	53°	1012.0
EE260	1.85	7.76	3.67	52°	784.5

note: d = depth to top, D = depth to bottom, W = width, KT = intensity of magnetization, dips are towards southeast.

Table 12. Interpretation results of the Upangwa anomalies.

profile	dip	W(km)	d(km)	D(km)	KT(nT)
SS260	127°	1.56	0.47	2.91	537
TT260	110°	1.34	0.28	3.24	276
BZ260	126°	1.36	0.38	5.50	599
BX260	116°	1.14	0.09	2.38	129
MM260	69°	1.35	1.22	—	226
GG260	138°	0.85	1.00	2.41	314

note: W = width, d = depth to top D = depth to bottom of prism, KT = magnetic polarization. Dips are measured clockwise from positive x axis.

PROFILE NO: AA259

Fig. 23. Anomaly profile across anomaly marked L3 in map shown in Appendix 2. The profile direction is NE-SW.

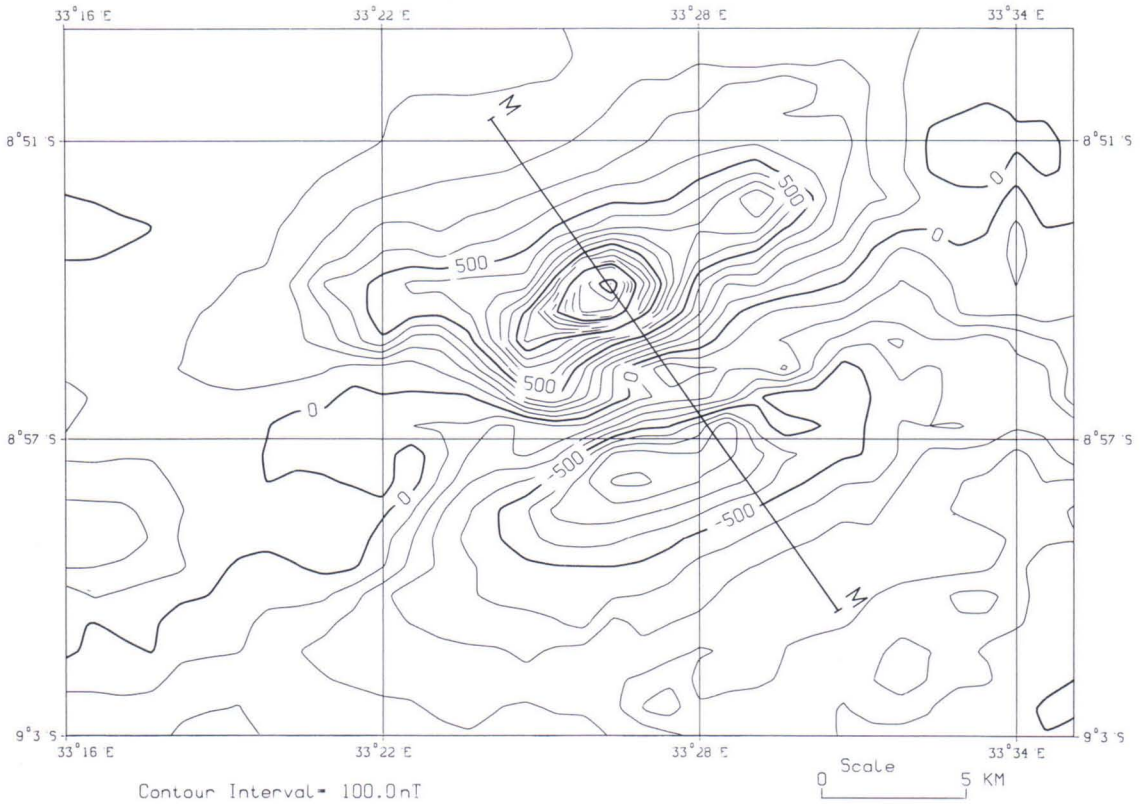The interpretation of the anomalies show that the Upangwa rocks dip southwest at angles ranging from 54° to 70°. The bodies have a shallow depth of burial, with the top of the body lying from 90 m to 470 m and with the depth to bottom reaching a maximum of 5.50 km below the ground level.

The profile MM260 is across a smooth anomaly observed where mylonites have been mapped. The profile was interpreted using a buried slab model whose top lie at a depth of 1.22 km and thickness of 1.35 km. The dip is towards the northeast at an angle of 69°.

The profile AA259 whose interpretation is shown in Figure 23 was taken from an anomaly

Contour Interval = 100.0 nT

Fig. 24. Showing residual and regional anomalies of Mbeya Magnetic Anomaly. The regional anomaly trends in the NW-SE direction.

marked L3 in the map of Figure A2. The profile runs through the center of the anomaly in a northeasterly trend. The anomaly lies within the Nyasa trough where lake sediments overlie the basement rocks. The depth of 0.82 km to the top of the body may indicate the thickness of the sediments overlying the basement rocks. This estimate is of the same order as the thickness of 810 m of sediments estimated by Harkin (1955) from rock outcrops.

The Mbeya Anomaly

The Mbeya anomaly is centered around the town of Mbeya and lies between 33°16′ E to 33°35′ E and 8°48′ S to 9°03′ S. The anomaly trends N122°W but the separation of regional and residual anomalies by upward continuation has shown that the residual anomaly is superimposed on a NW-SE trending regional anomaly. The regional and residual anomalies are shown in Figure 24 below, where the regional anomaly trends N63°W parallel to the rift structures defining the Songwe trough.

Some profiles were digitized from the original contour maps and quantitatively interpreted. The shape of the anomaly profile shown in Figure 25, which passes through the center clearly suggests that the anomaly is caused by more than one disturbing body. The principal profile through the center shows a strong positive anomaly with an amplitude of about 2330 nT and a negative anomaly in the southeast with an amplitude of 1090 nT.

The profile was first interpreted using prism models, but these could not give satisfactory fit. The combination of vertical prism models and polygon models as shown in Figure 25 was found

Contour Interval = 20.0 nT

Scale
0 ___ 5 KM
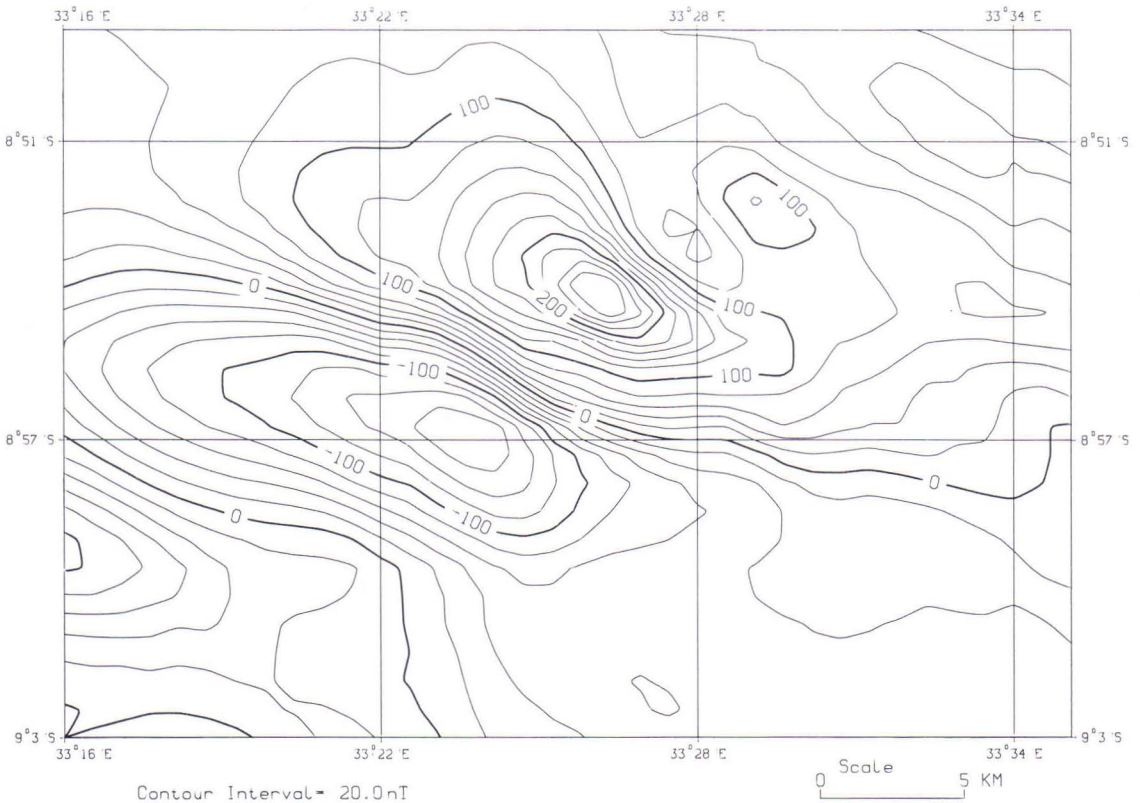
to best account for the observed anomaly. This model is found to be geologically feasible as the area has been a center of volcanic activities. The model approximates a volcanic plug with an offshoot which partly accounts for the positive anomaly. The top of the offshoot lies at a depth of 0.8 km below the ground surface. The vertical prisms have tops lying at the depth of 1.0 km. The intensity of magnetization of the bodies are 566 nT, 704 nT, and —805 nT from which the effective susceptibility values calculated using ambient field of 33800 nT are 1.67×10^{-2}, 2.08×10^{-2}, and 2.38×10^{-2} SI respectively. The negative magnetization was interpreted here as due to reverse magnetization. The susceptibility values are comparable to the values measured from basalt samples 24451 to 24459 in Table 3, collected from the area.

The high amplitude of the anomaly is unusual when compared to other anomalies observed in the Rungwe volcanic province. However, the anomaly lies very close to the Panda Hill and Mbalizi carbonatites where veins of iron ore have been observed within the body. It is therefore possible that the anomaly is caused by a body rich in magnetite.

The Chunya Linear anomaly

The linear anomaly observed in Chunya block, striking between N-S and NNE-SSW was also interpreted. The anomaly does not match any observed geologic structure and therefore it was interpreted with the assumption that it is caused by a subsurface structure. The anomaly is displaced by NW-SE and E-W trending lineaments at several places along its length and changes direction where it is crossed by lineaments.

The profiles across the anomaly shown on the aeromagnetic contour map presented as Figure A2 were interpreted using the prism model and the dyke model for two profiles where the prism model could not give satisfactory results. The results of the interpretation are tabulated in Table 13 below. The interpretation of the profiles show a prismatic body dipping at different angles towards the southeast. The intensity of magnetization increases towards the south from 107 nT to 450 nT. The interpretation also indicates an increase in depth to the top towards the south and ranges from 90 m to a maximum of 380 m
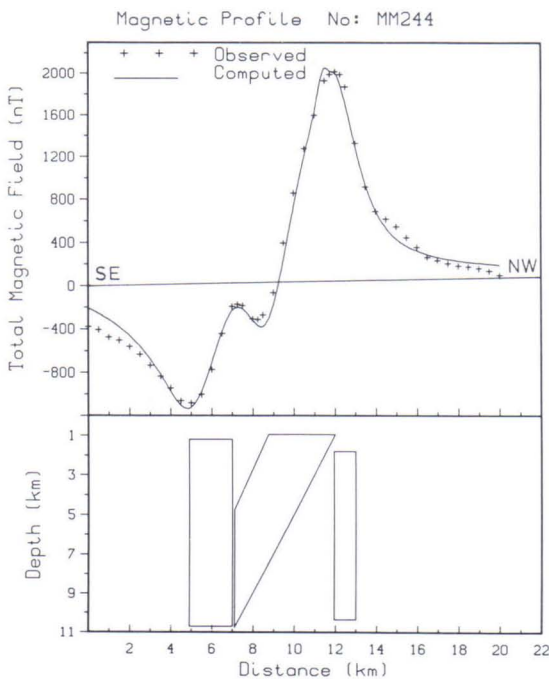

Fig. 25. The interpretation model of the Mbeya anomaly. The profile was digitized from the original contour map along profile MM shown on the residual map.

Table 13. Interpretation results of the Chunya linear anomaly.

profile	dip	W(m)	d(m)	D(m)	KT(nT)
AA229	77°	759	90	—	107
CC229	86°	756	112	2415	134
DD229	61°	572	262	—	173
EE229	59°	606	223	2160	249
AA244	89°	459	310	2877	451
AE244	64°	702	379	2695	353

note: W = width, d = depth to top, D = depth to bottom, KT = magnetization intensity, dip direction towards the southeast.
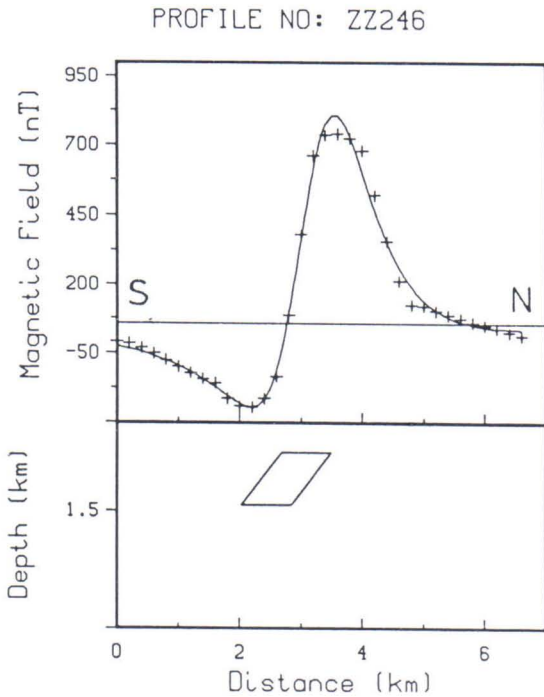
Fig. 26. Summary of interpretation of anomalies of Buhoro trough and adjacent areas. The dip, depths and width bodies are shown.

in the south. The depth to the bottom varies between 2.1 km to 2.9 km.

Anomalies in the Buhoro trough and adjacent areas

The Buhoro magnetic province has been described before under section of magnetic provinces and is composed of several isolated anomalies which can be analyzed individually. The anomalies in the south are related to intrabasement rocks overlain by the sediments of Buhoro flats. The anomalies in the northeast are mainly due to structures within the granitoids and most of them are linear anomalies. The anomalies were interpreted with a purpose of estimating the depth to the basement, assuming that the structures causing the anomalies are older than

the overlying sediments. A few conspicuous anomalies are described below and Figure 26 summarises the results of the quantitative interpretation of both circular and linear anomalies characterizing the Buhoro trough.

The circular anomaly located (Figure A2) at 8°29' S and 33°51' E is predominantly positive with a small negative part in the south. The anomaly was interpreted using a vertical prism model with negligible remanent magnetization. The depth to the top of the body was found to be 1170 m below the ground surface and to have an intensity of magnetization of 319 nT.

Anomaly Z246

This anomaly is located at 8°50' S and 34°12' E and occurs as a circular anomaly with an am-

PROFILE NO: ZZ246

Fig. 27. Shows the observed (+) and calculated (solid line) curves for the principal profile across anomaly Z246.

plitude of about 1000 nT. The anomaly is found in an area overlain by lower series of the Buanji sediments. The anomaly profile digitized was interpreted using a prism model and the result of this interpretation is given in Figure 27 where the prism is seen to have a width of 810 m, depth to top of 520 m, depth extent of 1410 m below the ground surface,and dip angle of 54° towards the south. The intensity of magnetization in the plane of the profile was estimated at 710 nT which give effective susceptibility of 2.14×10^{-2} SI.

The depth to top of the prism gives an estimate of the thickness of the lower series of Buanji sediments overlying the intrusive body that gives rise to the anomaly. The nearest basement rocks are meta-anorthosites and meta-anorthositic gabbros which extend underneath the sediments. The source of the anomaly may be related to intrusives within the meta-anorthosite body. It is sug-

gested here that this anomaly should be further investigated due to its high susceptibility, to find if it may be mineralized.

Anomaly P246

The negative anomaly (Figure A2) marked P246, located at 8°55′ S and 34°07′ E is found in an area overlain by the middle series of Buanji sediments. The anomaly is elongated in the WNW with an amplitude of 900 nT along the profile P246. The anomaly was analyzed using the prism model which gave the best fit with the following parameters: width of 2.45 km, depth to top of 0.68 km, depth to bottom of 2.90 km measured from the ground level, dip of 34° towards the northeast. The intensity of magnetization giving the optimum model is 456 nT which gives the effective susceptibility of 13.5×10^{-3} SI. The calculated and observed anomalies are presented in Figure 28.

PROFILE NO: PP246
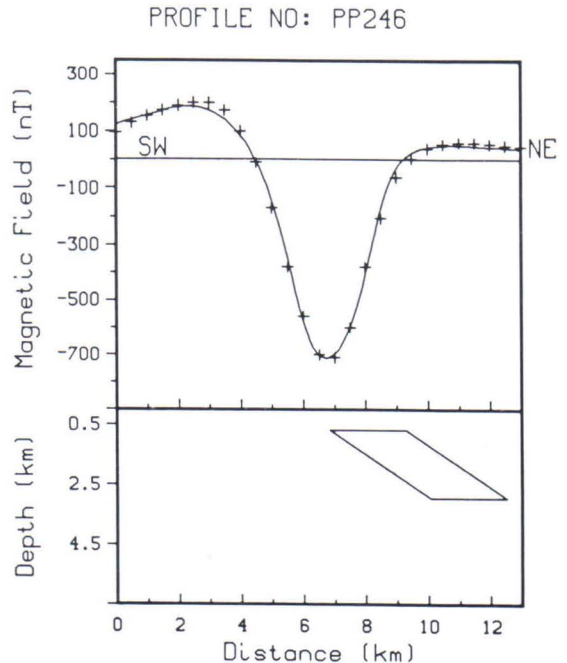
Fig. 28. Shows the observed (+) and calculated (solid line) curves across anomaly P246.

The location of the anomaly is very near to the gabbroic intrusives of Chimala, which were emplaced during the Buanji orogenic episode. The anomaly may therefore be related to gabbroic intrusives overlain by the Buanji sediments and the depth to top of the body causing the anomaly indicate the minimum thickness of the Buanji sediments.

The results of interpretation presented in Figure 26 indicate that the maximum depth to basement rocks in the Buhoro Trough is 1.6 km. The deepest part lies between the Njombe lineament and the lineament marked BB' (Figure 7). The later lineament was interpreted as due to a contact between the crystalline basement in the south and the granitoids in the north. A buried step

model was used in modelling the body causing the anomaly. The interpretation of anomaly profiles across the structure revealed a depth to the basement of the order of 1.14 to 1.5 km. The thickness of a step giving optimum model was found to be so large that, it was reasonable to consider it as a contact dipping towards the northeast at an average angle of 28°. The magnetic polarization contrast is 327 nT with low susceptibility rocks lying in the northeast of the contact. The difference in depths to top obtained by the modelling of the Nsamya Hills Anomaly (NH) and depths obtained from adjacent anomalies in the trough, suggest a throw of about 400 m along the Usangu Fault. The depths in the northeast of the trough interpreted from E-W
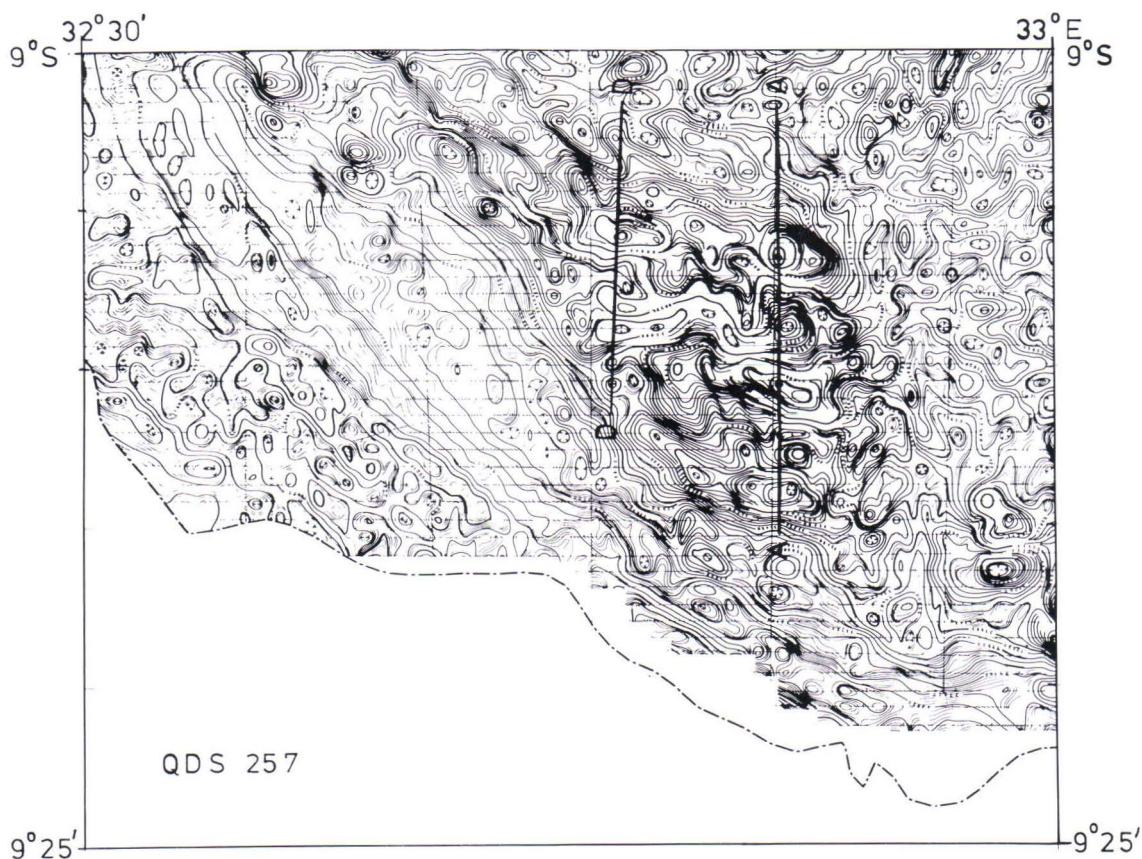
Fig. 29. The aeromagnetic anomaly map, showing location of Profiles AA257 and DD257 across the anomaly due to the Mbozi gabbro syenite complex.

trending anomalies are shallow and some of the bodies causing the anomalies dip south while others dip towards the north.

Mbozi and Msangano Trough Anomalies

The group of high amplitude magnetic anomalies in Mbozi and Msangano trough are due to intrusives of mafic alkaline composition. The major anomaly is one due to Mbozi gabbro syenite complex intrusives. The main anomaly in the center trends E-W with anomaly amplitudes reaching 1700 nT. The anomaly extends further northwest where individual anomalies trend NW-SE while the southeastern end is marked by a northeasterly trending anomaly. Several profiles trending N-S were digitized across the anomaly shown in Figure 29. The profiles were interpreted using 2-D polygonal models and others were interpreted using prism models. Other isolated anomalies were also interpreted using optimization

methods. The petrophysical studies done on samples collected from outcrops show high remanent magnetization over induced as expressed by high Q-values (Table 4). However, the high remanence observed may be a surface phenomenon as that observed in Zanzui ring complex in northern Tanzania (Krs, et al., 1987). In the Zanzui structure high Q-values in the order of 100 and above were observed from rock samples collected from outcrops whereas samples collected from drill cores exhibited low Q-values with half of the samples having Q-values of less than 1 and the highest value observed was 23. The data for subsurface samples is not available and therefore using high Q-values in the interpretation may result in underestimating the size of the body causing the anomaly and also errors in the estimation of dip if the remanence has different direction from the induced magnetization. The interpretation was however done assuming presence of normal remanent magnetization and therefore the intens-
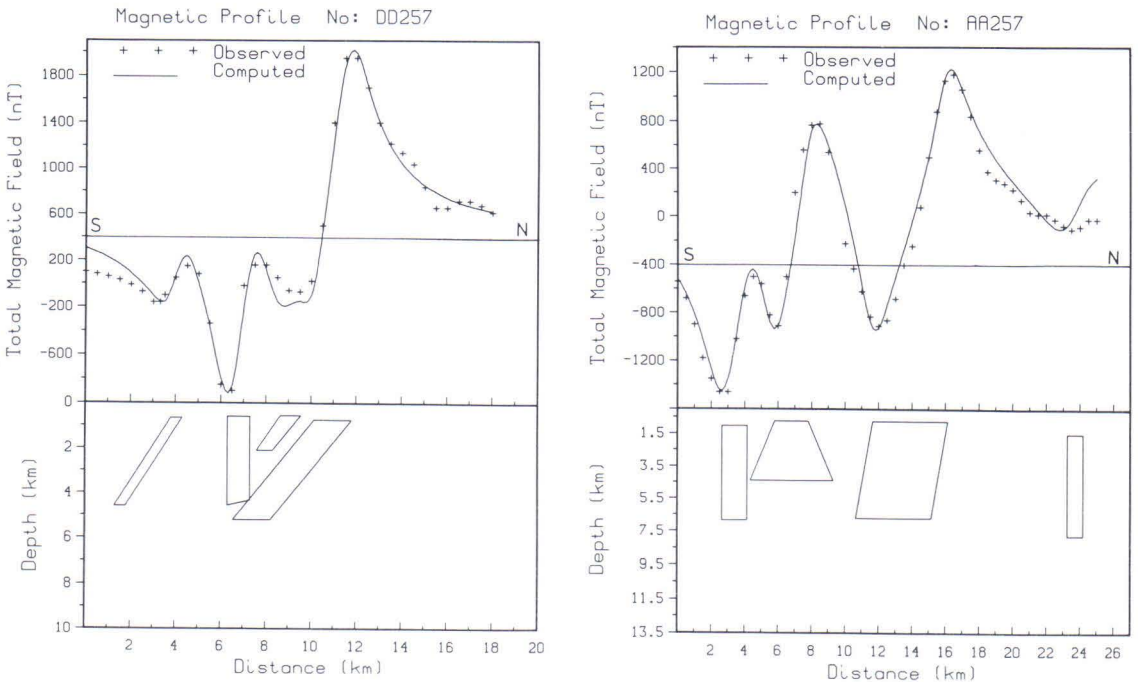
Fig. 30. The observed and calculated curves for profiles AA257 and DD257 across Mbozi anomaly.

ity of magnetization used in the interpretation was made higher than that calculated using measured susceptibility.

Fig. 31. The location of anomaly profiles across Ilunga Hills magnetic anomaly.

The profiles crossing the complex have amplitudes in the order of 1700 nT. The results of the interpretation of the two profiles crossing the center are presented in Figure 30 below from which it is observed that, the main anomaly is caused by a body which dips towards the south and extends to a depth of around 5.0 km below the observation plane. The spectral data window of Mbozi in which the anomalies lie gave spectral depths of 3.92 to 4.54 km which agree with depths calculated using modelling along the profiles. The intensity of magnetization giving the best model were found to range from 220 nT to 845 nT. The intensity is higher than that calculated from susceptibilities measured from rock samples (Table 4). The interpretation of anomalies further north reveal that the bodies causing the anomalies are steeply dipping towards the southwest. The occurrence of intrusive rocks exclusively in the Mbozi block and the dipping of bodies towards the Ufipa shear zone support the theory of collision of Ufipa and Mbozi block as suggested by Nanyaro (1984).

The Ilunga Hills anomaly

The Ilunga Hills anomaly occurs as an E-W trending anomaly south of the Mkondo lineament. The anomaly extends over a strike distance of over 40 km with amplitudes reaching 900 nT. The anomaly correlates with ultramafic and mafic

Table 14. Interpretation results of the Ilunga Hills anomaly.

Profile	Dip	d(km)	D(km)	W(km)	KT(nT)
I1227	52°	0.17	1.40	1.23	204.4
KK227	62°	0.16	2.03	1.00	156.0
AA228	52°	0.30	1.88	2.05	468.0
CC228	42°	0.53	3.06	2.05	490.3
XX228	43°	0.23	1.14	1.42	402.3
BB228	49°	0.24	2.40	1.79	357.0
FF228	43°	0.20	1.11	1.37	367.0
JJ228	52°	0.14	1.21	1.23	167.0

note: d = depth to top, W = width of prism, D = depth to bottom, KT = intensity of magnetization, dip direction is towards the south.

3

intrusives. The rocks have undergone intense shearing along the Mkondo shear zone (McFarlane et al., 1963).

The shape of the anomaly profiles across the body has a strong positive part in the north and a weak negative part in the south. This kind of shape suggests that the anomaly is caused by magnetic body dipping towards the south and of finite depth extent. The interpretation of the anomaly profiles, whose positions are shown in Figure 31, were done using the prism model. The results of the interpretation are presented in Table 14.

The interpretation results show that the body causing the anomaly has its top lying at depths of 140 m to 530 m below ground surface. The width of the body varies from 1.0 km to a maximum of 2.05 km in the center while the depth to the bottom varies from 1.11 km to 3.06 km which correlate with the shallow spectral depths of 1.4 to 3.3 km obtained from the Luika magnetic data window. The finite depth extent of the model suggests that the body causing the anomaly is embedded in a relatively young granitic intrusives. The effective susceptibility calculated from the intensity of magnetization using ambient field of 33500 nT ranges from 4.66×10^{-3} to 1.46×10^{-2} IS. The susceptibility is higher than that observed for diorite and granodiorite rocks of Lupa (Table 6).

SUMMARY AND CONCLUSIONS

The study of aeromagnetic and gravity data of Southwest Tanzania reveals the presence of anomalies which are related to both basement geologic structures underlying sediments and surface rocks. The geologic features distinguished are presented in Figure 32 and briefly explained
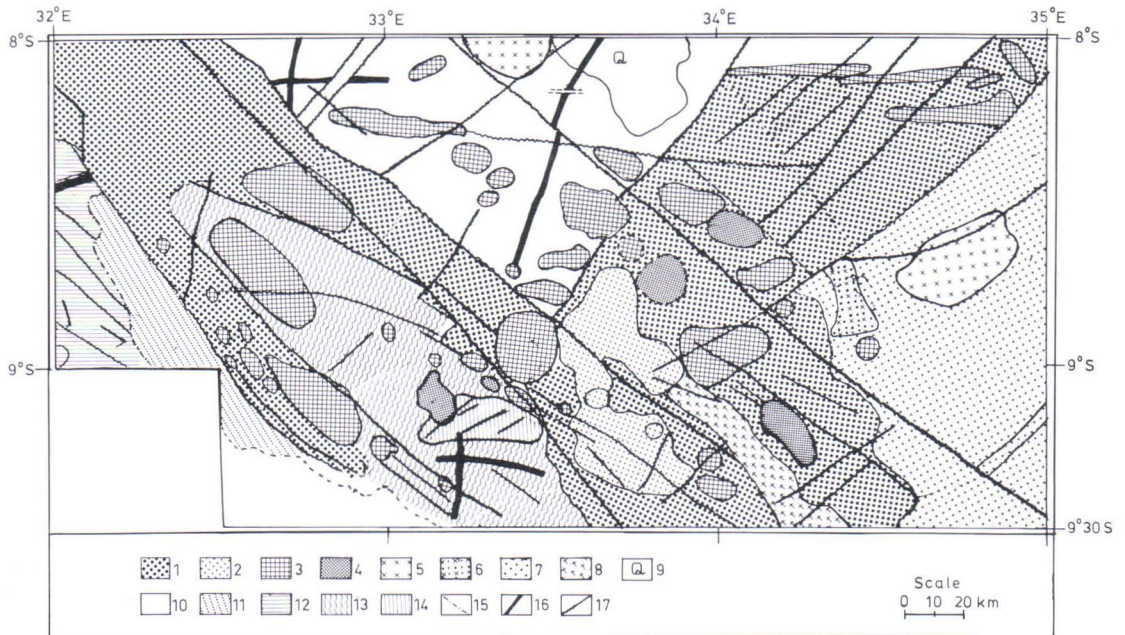
Fig. 32. The interpretation map showing major magnetic anomalies due to subsurface and surface geologic structures. The explanation of map units is given in Table 15 below.

in Table 15. The main units interpreted include anomalies which indicate the presence of volcanics, sedimentary rocks, metamorphics, mafic and felsic intrusives, and lineaments due to faults.

The use of stacked and greytone image maps helped to distinguish anomalies according to their field intensity. The low intensity anomalies were observed in areas with granitic rocks or negative parts associated with high amplitude anomalies caused by mafic intrusives. The aeromagnetic map of the study area was classified into eight provinces characterized by different anomaly patterns and each province was found to be indica-

tive of the rock types. The high frequency anomalies forming a complex pattern in the Rungwe area were found to be indicative of the volcanic rocks. Areas covered with metasediments and sediments were characterized by smooth anomalies which form distinct zones of simple linear anomaly patterns. The troughs of Rukwa, Msangano, and Buhoro, covered with lake sediments, and the Kipengere area with thick cover of Proterozoic sediments were found to be characterized by smooth anomalies. The high grade metamorphics of Ufipa and Mbozi block show different high relief magnetic anomaly patterns of

Table 15. Brief Explanation of Map Units of Figure 32.

Map Unit	Nature of Anomalies	Rock Units/Geologic Feature
1	Smooth anomalies	Lake sediments, Buanji Sediments and Ukingan Metasediments or mylonites.
2	High frequency anomalies	Rungwe volcanics (basalts, trachytes and phonolite)
3	Predominantly positive anomalies	Ultramafics, mafics and their metamorphosed equivalents, carbonatites.
4	Negative anomalies	Ultramafic and mafic intrusives overlain by sediments
5	Positive Anomalies	Magnetic granites, someintruded by iron reefs.
6	Positive anomalies trending N/S.	Igawa crystalline rocks with ferruginous quartzites.
7	Magnetic anomalies with NE trending grain	Ubena granitoids, Usagaran gneisses.
8	NW trending Positive anomalies	Granitic rocks, gabbros and ultramafics of Upangwa.
9	Magnetic Quiet Zone	Muscovite biotite granite of Kinguamuma
10	No defined trends	Chunya granitoids and gneisses
11	NW trending anomalies	Ufipa gneisses and schists
12	NW trending anomalies with strong lineaments	Possible ferruginous quartzites underlying thick soils.
13	NW trending anomalies	Mbozi gneisses and granulites
14	E/W trending anomaly with NE trending lineaments	Quartzite Formations
15		Contact zone in Buhoro
16	Positive linear anomalies	Dolerite dykes
17	Magnetic lineaments	Faults, shear zones

which the latter was characterized by oval to circular shaped anomalies indicative of intrusive rocks. These anomalies including that caused by the Mbozi ring complex, were found to lie along a linear belt parallel to the Ufipa shear zone and several bodies were revealed under the sediments of the Msangano trough. The Ubena area in the east and the Chunya-Usangu block were also found to have different anomaly patterns.

The lineaments were delineated from contour maps, stacked profile maps, and the stereographic projection map. The study of magnetic lineaments revealed long lineaments trending NW-SE, E-W, and NE-SW which are considered to be related to subsurface crustal structures. Several lineaments not mapped before were revealed by aeromagnetic data interpreted in this study. Such lineaments include the Njombe lineament which crosses the Buhoro Trough and extends on both sides beyond the study area. The lineament is parallel to the lineament marking the Rukwa fault. The Songwe lineament partly correlated with faults southwest of Mbeya, has been shown to continue in areas covered by sediments and volcanics. In the Rukwa Trough the Songwe lineament forms a narrow graben with the Rukwa fault and is well defined from the gravity anomaly map (Figure 18). The N-S and E-W trending positive anomalies in the Chunya-Usangu and Mbozi blocks have been revealed by the magnetic data. Other lineaments trending E-W were detected in the Buhoro trough and may be of the same origin with the Mkondo shear zone observed in Chunya-Usangu block. Another significant lineament revealed by the study is that marked LL' south of Galula lineament (Fig. 7). This lineament is associated with high amplitude anomalies in the NW end of the Mbozi block and extends into Songwe trough in the east, whereas in the west it crosses the Msangano trough into Ufipa block.

Most of the magnetic lineaments were found to correlate partially with known geological faults or shear zones. Such magnetic lineaments were found to be continuous in areas where the base-

ment structures are obscured by overlying sediments and volcanics, suggesting the continuity of faults mapped in the exposed basement.

The Kipengere, Chimala, Nsamya Hills, and some anomalies in Buhoro trough form a linear northwesterly trend which suggests the presence of a weak zone within the crust, along which these intrusives penetrated the crust. The Chimala anomaly is due to gabbroic intrusives related to the Buanji tectonic episode and the Nsamya Hills anomaly is due to the Ubendian metamorphosed mafics and ultramafics.

Several prominent anomalies were interpreted using prism, dyke, and slope models and the combination of polygon and prism models. The Ilunga Hills Anomaly south of the Mkondo shear zone was found to be caused by a body of limited depth extent. The Mbeya Anomaly was found to be caused by three bodies of which two are dipping vertically and the third is inclined. The anomaly occurs in an area where the basement rocks are overlain by basalt belonging to the old volcanics. The Upangwa anomalies north of Lake Nyasa were interpreted as caused by prismatic bodies dipping towards the southwest. The magnetic data has shown a number of anomalies in the Msangano trough which are related to the gabbro syenite complex and which occur exclusively on the eastern side of the Ufipa shear zone. Modelling of the anomalies show causative bodies either dipping vertically or at sharp angles towards the Ufipa shear zone and having limited depth extent.

The Upangwa anomaly, which occurs as a string of isolated anomalies, is caused by intrusive bodies, which dip towards the southwest. The interpretation has revealed that these bodies are of limited depth extent and show high magnetization levels.

The maximum depth to the basement calculated from anomalies observed in the Buhoro trough is around 1.6 km with the deepest part found between the Njombe Lineament and the lineament marked BB' (Figure 26).

The rock samples collected from outcrops rep-

resent a few rocks found in the area. However the results have shown the nature of magnetization for some important intrusives in the area. The ultramafics, mafics, and dolerite dykes were found to have high remanence magnetization, high susceptibilities and also high densities. The carbonatite body of Panda Hill was found to have low susceptibility, and remanence magnetization was high in samples with a high content of oxide minerals and specifically magnetite, ilmenite and haematite. The volcanics collected from the Rungwe volcanics were found to have low Q-values. The rocks of the Mbozi ring structure were found to have high Q-values and petrographical studies found high amounts of magnetite, ilmenite and pyrrhotite in gabbros and pyroxenites compared to alkali rocks.

The ferruginous quartzites of the Itewe Hills near Chunya were found to have both high susceptibility and remanent magnetization. However, no pronounced magnetic anomaly was observed in the Itewe area despite the fact that the hills trend NNE-SSW over a distance of 3 km.

The statistical analysis of magnetic and gravity data using spectral analysis gave depths which were interpreted as due to lithological discontinuities within the crust. Some spectral depths were interpreted as thickness of sediments overlying the crystalline basement. A specific example is the spectral depth of 7.43 km determined from the spectra of gravity data of the Rukwa trough, which was found to be in agreement with the depth of 7 km interpreted from gravity data profiles using a two dimensional polygon model. In the southwest of the study area where the basement is overlain by metasediments of the Ukingan orogeny and Buanji sediments, shallow spectral depths of 1.2 to 4.0 km were observed and interpreted as depths to the top of the basement. This may suggest that the maximum combined thickness of Ukingan metasediments and Buanji sediments is about 4 km. The interpretation of the Kipengere Anomaly (Fig. 21) gave a maximum depth of 3.2 km to top of the body causing the anomaly. Assuming that the body causing the Kipengere Anomaly intrudes the sediments, the depth of 3.2 km should be less than the true thickness of the sediments. Therefore the depth of 4 km obtained from spectral analysis may be closer to the true maximum thickness.

The spectral depths of 14 km and 18 km obtained from the spectra of data windows covering the Mbozi block suggest the presence of subsurface anomalous materials. The Mbozi block however, occurs as an uplifted block between Rukwa and Msangano troughs and therefore the crust in the block is expected to be shallow compared to adjacent downfaulted blocks.

REFERENCES

Aoki, H., 1969. Gravity measurements of Rift Valleys. Nagoya University Journal of Earth Sciences, 17, 169 —187.

Bates, C.C., Gaskell, T.F. & Rice, R.B., 1982. Geophysics in the affairs of man. Pergamon Press, Oxford. 492 p.

Båth, M.W., 1975. Seismicity of Tanzania Region. Tectonophysics, 24, 353—379.

Batterham, P.M., Bullock, S.J. & Hopgood, D.N., 1983. Tanzania: integrated interpretation of aeromagnetic and radiometric maps for mineral exploration. Transaction of Institute of Mining and Metallurgy, (Sect.B: Applied Earth Sciences.), 92, B83—92.

Bhattacharyya, B.K., 1966. Continuous spectrum of the total magnetic-field anomaly due to a rectangular prismatic body. Geophysics, 31, 97—121.

Bhattacharyya, B.K. & Lue, L.K., 1975. Analysis of magnetic anomalies over Yellowstone national Park: Mapping of curie point isothermal surface for geothermal reconnaissance. Journal of Geophysical Research, 80 (32), 4461—4465.

Bhattacharyya, B.K. & Navolio, M.E., 1976. A fast Fourier Transform method for rapid computation of gravity and magnetic anomalies due to arbitrary bodies. Geophysical Prospecting, 24, 663—649.

Brinckman, J., 1964. Brief explanation of the geology of Malangali, QDS247. German Geological Mission in Tanzania. 1 p.

Brock, P.W.G., 1968. Metasomatic and intrusive nepheline bearing intrusive rocks from the Mbozi syenite gabbro complex. Canadian Journal of Earth Sciences, 5, 387—419.

Brown, P.E., 1962. The tectonic and metamorphic history of the Precambrian rocks of the Mbeya Region, Southwest Tanganyika. Quarterly Journal of Geological Society of London, 118, 295—314.

Collison, D.W., 1983. Methods in rock magnetism and paleomagnetism. Chapman and Hall, London. 503 p.

Connard, G., Couch, R. & Gemperle, M., 1983. Analysis of aeromagnetic measurements from Cascade Range in Central Oregon. Geophysics, 48, 376—390.

DISSPLA, 1985. User's manual, Display Integrated Software System and Plotting Language, Version 10.0., ISSCO, San Diego.

Ebinger, C.J., Deino, A.L. & Drake, R.E. Chronology of volcanism and Rift Basin propagation: Rungwe Volcanic Province, East Africa. Journal of Geophysical Research (manuscript submitted 1988)

Fawley, A.P. & James, T.C., 1955. A pyrochlore carbonatite, Southern Tanganyika. Economic Geology, 50, 571—585.

Fesefeldt, K., 1964. Brief explanation of the geology of Njombe, QDS261. Germany Geological Mission in Tanzania. 1 p.

Fick, L.J. & Van Der Heyde, C., 1959. Additional data on the geology of Mbeya carbonatite. Economic Geology, 54, 842—872.

Gay, P. S. Jr., 1967. Curves for interpretation of magnetic anomalies caused by two dimensional structures. In Mining Geophysics II, SEG., Tulsa Ok., 512—548.

Gay, P. S. Jr., 1972. Fundamental characteristics of aeromagnetic lineaments, their geological significance and their significance to geology. Stereo Map Co. Utah, 90 p.

Golub, G.H. & Reinsch, C., 1970. Singular value decomposition and least squares solution. Numerical Mathematics, 14, 403—420.

Grantham, D.R., Teale, E.O, Spurr, A.M.M., Harkin, D.A. & Brown, P.E., 1958. Brief explanation of the geology of Mbeya, QDS244. Geological Survey of Tanganyika. 1 p.

Griffiths, D.H., King, R.F., Khan, M.A. & Blundell, D.J., 1971. Seismic refraction line in the Gregory Rift. Nature Physical Sciences, 229, 69—71.

Hahn, A., Kind, E.G. & Mishra, D.C., 1976. Depth estimation of magnetic sources by means of Fourier amplitude spectrum. Geophysical Prospecting, 24, 287—308.

Harkin, D.A., 1955. The geology of the Songwe-Kiwira Coalfield, Rungwe District. Geological Survey of Tanganyika Bulletin, 27. 33p.

Harkin, D.A. & Harpum, J.R., 1957. Brief explanation of the geology of Tukuyu, QDS259, Geological Survey of Tanganyika. 1 p.

Harkin, D.A., 1960. The Rungwe volcanics at the northern end of L. Nyasa. Geological Survey of Tanganyika. Mem. II. 172 p.

Harpum, J.R. & Harris, J.F., 1958. Brief explanation of the geology of Kipengere, QDS260. Geological Survey of Tanganyika. 1 p.

Harpum, J.R. & Brown, P.E., 1958. The Brief explanation of the geology of Chimala, QDS246. Geological Survey of Tanganyika. 1 p.

Hood, P. & Ward, S.H., 1969. Airborne geophysical methods. In Advances in Geophysics, 13, 2—112. ed. by H.Landberg and J.Van Miegehm. Academic Press. New York. 267 p.

Hunting Geology & Geophysics, 1983. African Resources mapping and development chart.

IMSL, 1984. Reference Manual. International Mathematical and Statistical Libraries. Inc.

Johnson, W.W.,1969. A least squares method of interpreting magnetic anomalies caused by two-dimensional structures. Geophysics, 34, 65—74.

Kent, P.E., Hunt, J.A. & Johnstone, D.W., 1971. The geology and geophysics of coastal Tanzania. Geophys. Paper, 6 Institute of Geological sciences. London, 101 p.

Kernerly, J.B., Teale, E.O. & Eades, N.W., 1962. Brief explanation of the geology of Shoga, QDS229. Geological Survey of Tanganyika. 1 p.

Kernerly, J.B., Spence, J. & Spurr, A.M.M., 1963. Brief explanation of the geology of Itaka, QDS243. Geological Survey of Tanganyika. 1 p.

Krs, M., Pondaga, M.M., & Savary, B.P., 1987. Geophysical investigation of the ring structure at Zanzui, North-

ern Tanzania. Physics of the Earth and Planetary interiors, 45, 294—303.

Kursten, M., 1964. Brief explanation of the geology of Madibira,QDS231. Germany Geological Mission in Tanzania. 1 p.

Leonen, R., Kernerly, J.B. & Spurr, A.M.M., 1964. Brief explanation of the geology of Kamsamba. QDS226. Geological Survey of Tanganyika. 1 p.

Leonen, R., Kernerly, J.B. & Spurr, A.M.M., 1965. Brief explanation of the geology of Mkulwe QDS242 and 242S. Geological Survey of Tanganyika. 1 p.

Lines, L.R. & Treitel, S., 1984. Tutorial: A review of least squares inversion and its application to geophysical problems. Geophysical Prospecting, 32, 159—186.

Makowiecki, L.Z., King, A.J. & Cratchley, C.R., 1971. A comparison of selected geophysical methods in mineral exploration. Institute of Geological Science, Geophysical paper 3, London.

Mantovani, M.S.M.& Shulowsky, W., 1982. Analysis of a large extent aeromagnetic survey near the geomagnetic equator (Minas Gerais, Brazil). Pure & Applied Geophysics, 120, 784—794.

Marobhe, I. M., 1989a. Optimisation of magnetic anomalies via singular value decomposition. Theory and Practice of Applied Geophysics, 4, (in print).

Marobhe, I.M., 1989b. A versatile TurboPascal program for optimisation of magnetic anomalies caused by two-dimensional dyke, prism or slope models. (accepted for publication in Computers & Geosciences).

McConnel, R. B., 1972. Geological development of the Rift System of Eastern Africa. Geological Society of America Bulletin, 83, 2549—2572.

McFarlane A., 1963. Brief explanation of the geology of Itumba, QDS258. Mineral Resources Division, Tanzania. 1 p.

McFarlane A.; Mudd G.C. & Orridge, G.R., 1963. Brief explanation of the geology of Makongolosi, QDS228. Geological Survey of Tanganyika. 1 p.

McFarlane, A. & MacDonald, 1964. Brief explanation of Geology of Luika, QDS227. Geological Survey of Tanganyika. 1 p.

McFarlane, A. & Brock, P.W.G., 1966. Brief explanation of the geology of Tunduma, QDS257. Mineral Resources Division Tanzania. 1 p.

McKinlay, A.C.M., 1965. The coalfields and the coal resources of Tanzania. Geological Survey Tanzania. Bull. 38. 82 p.

Nagy, D., 1988. Fast Fourier transform in gravity interpretation. Acta Geod. Geoph. Mont. Hung., 23, 97—115.

Naidu, P.S., 1969. Estimation of spectrum and cross-spectrum of aeromagnetic field using fast digital Fourier transform

(FDFT) techniques. Geophysical prospecting, 17, 345—361.

Nanyaro, J.T., 1984. Technical report on the Geotraverse across the Ukingan and Ubendian fold belts in S.W. Tanzania. unpublished report, University of Dar-es-Salaam, 20 p.

Nash, J.C., 1979. Compact numerical methods for computers: linear algebra and function minimisation. Adam Hilger Ltd Bristol 226 p.

Okubo, Y., Graf, R.J., Hansen, R.O., Ogawa ,K. & Tsu, H., 1985. Curie point depths of the island of Kyushu and surrounding areas, Japan. Geophysics, 50, 481—494.

Peirce, J.W. & Lipkov, L., 1988. The structural interpretation of Rukwa Rift, Tanzania. Geophysics, 53, 824—836.

Pentel'kov, V.G., 1981. Mesozoic rifting and volcanism in the Rungwe Region, South border of the Tanganyika Shield. Geotectonics, 15, 379—387.

Ruotoistenmäki, T., 1987. Estimation of depth to potential field sources using the Fourier amplitude spectrum. Geological Survey of Finland, Bulletin 340, 84 p.

Ruotoistenmäki, T., 1987a. Depth estimation from potential field data using the Fourier amplitude spectrum. Poster in Exploration '87, Toronto 27.9.—1.10.

Searle, R.C., 1970. Evidence from gravity anomalies for thinning of the lithosphere beneath the rift valley in Kenya. Geophysical Journal of the Royal Astronomical Society, 21, 13—31.

Shuey, R.T., Schelinger, D.K., Tripp, A.C.& Alley, L.B., 1977. Curie depth determination from aeromagnetic spectra. Geophysical Journal of the Royal Astronomical Society, 50, 75—101.

Spector, A. & Grant, F.S., 1970. Statistical models for interpreting aeromagnetic data. Geophysics, 35, 293—302.

Spence, J., 1954. The geology of Galula Coalfield, Mbeya District. Geological Survey of Tanganyika. Bull. 25, 34 p.

Suwa, K., Osaki, S., Oana, S., Shiida, I. & Miyakawa, K., 1969. Isotope geochemistry and petrology of Mbeya carbonatites, South-west Tanzania. Journal of Earth Sciences Nagoya University, 17, 125—168.

Teale, E.O., Eades, N.W., Harkin, D.A, Harpum, J.R. & Horne R.F.G., 1962. Brief explanation of the geology of Irambo, QDS245. Geological Survey of Tanganyika. 1 p.

Tiercelin, J.J., Chorowicz, J., Bellon, H., Richert, J.P., Mwanbene, J.T. & Walgenwitz,F., 1988. East African System: offset, age and tectonic significance of the Tanganyika-Rukwa-Malawi intracontinental transcurrent fault zones. Tectonophysics, 148, 241—252.

Won, I.J. & Bevis, M., 1987. Computing the gravitational and magnetic anomalies due to polygon: Algorithms and Fortran subroutines. Geophysics, 52, 232—238.
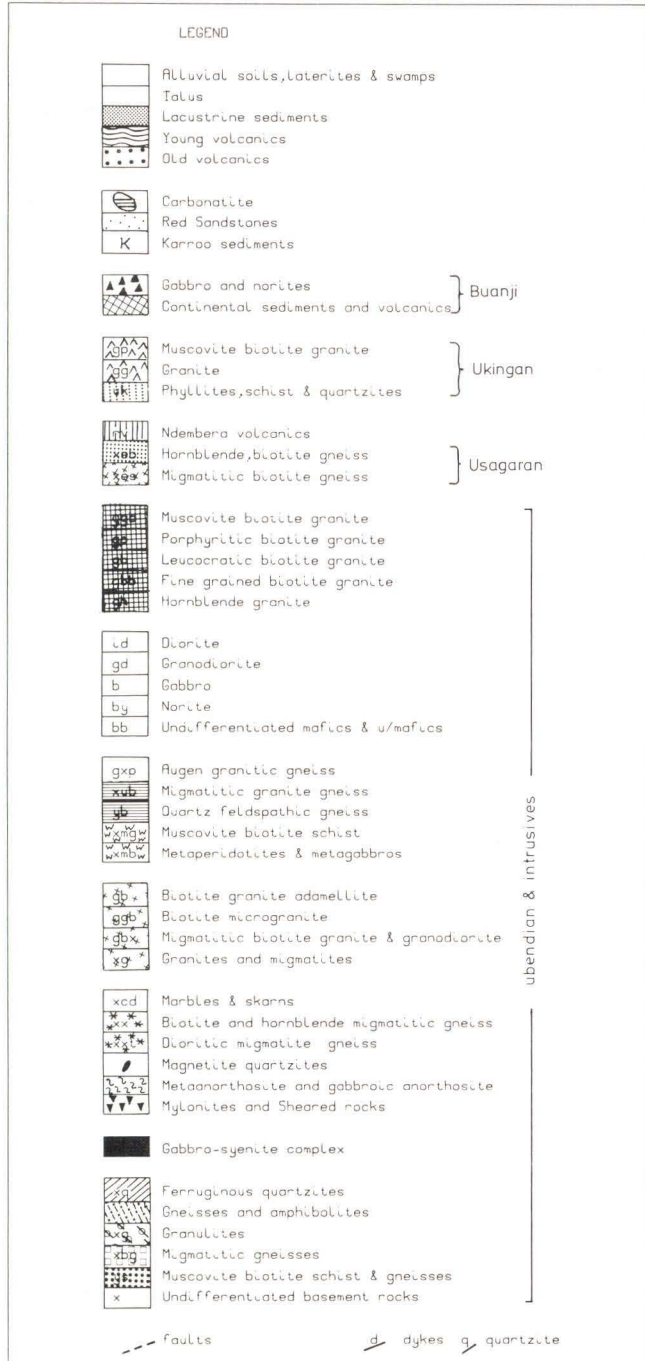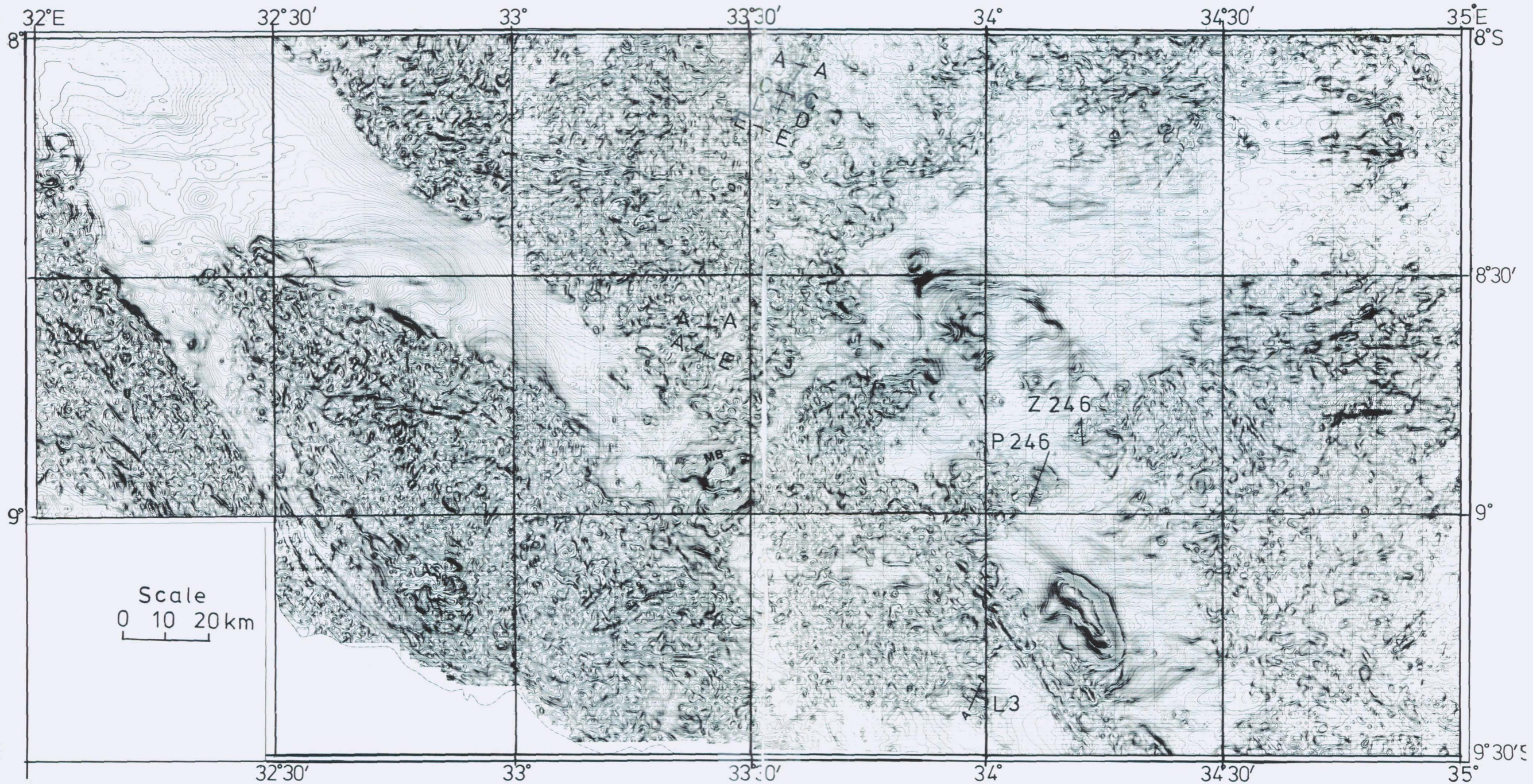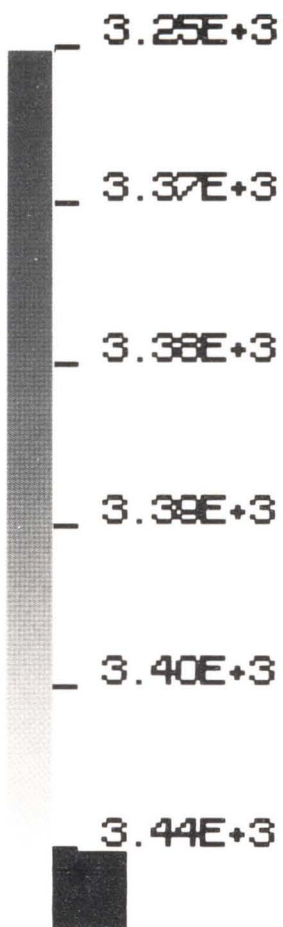
Legend to figure A1

LEGEND

- Alluvial soils, laterites & swamps
- Talus
- Lacustrine sediments
- Young volcanics
- Old volcanics

- Carbonatite
- Red Sandstones
- Karroo sediments

- Gabbro and norites
- Continental sediments and volcanics } Buanji

- Muscovite biotite granite
- Granite } Ukingan
- Phyllites, schist & quartzites

- Ndembera volcanics
- Hornblende, biotite gneiss
- Migmatitic biotite gneiss } Usagaran

- Muscovite biotite granite
- Porphyritic biotite granite
- Leucocratic biotite granite
- Fine grained biotite granite
- Hornblende granite

- d — Diorite
- gd — Granodiorite
- b — Gabbro
- by — Norite
- bb — Undifferentiated mafics & u/mafics

- gxp — Augen granitic gneiss
- xub — Migmatitic granite gneiss
- yb — Quartz feldspathic gneiss
- wxmgw — Muscovite biotite schist
- wxmbw — Metaperidotites & metagabbros

- db — Biotite granite adamellite
- ggb — Biotite microgranite
- gbx — Migmatitic biotite granite & granodiorite
- xg — Granites and migmatites

- xcd — Marbles & skarns
- Biotite and hornblende migmatitic gneiss
- Dioritic migmatite gneiss
- Magnetite quartzites
- Metaanorthosite and gabbroic anorthosite
- Mylonites and Sheared rocks

- Gabbro-syenite complex

- xg — Ferruginous quartzites
- Gneisses and amphibolites
- xg — Granulites
- xbg — Migmatitic gneisses
- Muscovite biotite schist & gneisses
- x — Undifferentiated basement rocks

Ubendian & intrusives

- - - - faults   d, dykes   q, quartzite

Rukwa Trough

L. Rukwa

L. Rukwa

Kwimba

Kinguamuma

Madibira

MKONDO

SHEER

Mkutano

Saza

Makongolosi

Chunya

Itewe Hills

Nsamya Hills

BUHORO FLATS

MALANGALI

HOLI HILLS

Msusule

Chimala

Ivuna

Gatula

Songwe Trough

UFIPA

Kanda fault

Itaka

Makambako

MBOZI

Msangano Trough

Ufipa fault

Musensi

MBEYA

Uyole

Panda

GOLF PLATEAU

KIPENGERE RANGE

Kidugala

Miamba Hills

S.Mbozi

Kiejo

Tukuyu

Njombe

ZAMBIA

Tunduma

BUNDALI HILLS

NKENZA fault

Nyasa fault

Upangwa

Hagafiro valley

0 10 20km

Scale

Scale

0 10 20 km